SYMPOSIUM ON SURFACE SCIENCE 2020

St. Christoph am Arlberg, Austria
March 1 - 7, 2020

CONTRIBUTIONS

EDITORS
Friedrich Aumayr, Ulrike Diebold and Christoph Lemell
TU Wien

ASTRAIOS 190

2D MOMENTUM MAPPING ELECTRON ANALYZER FOR UNRIVALED ARPES PERFORMANCE

KEY FEATURES

- Single spot parallel shifting lens (patent applied)
- ± 30° acceptance angle (± 1 $Å^{-1}$ k-range for He I, ± 2.5 $Å^{-1}$ k-range for (S)XPS)
- k-resolution < 0.003 $Å^{-1}$
- Energy resolution < 1.5 meV
- Motorized virtual analyzer entrance slit

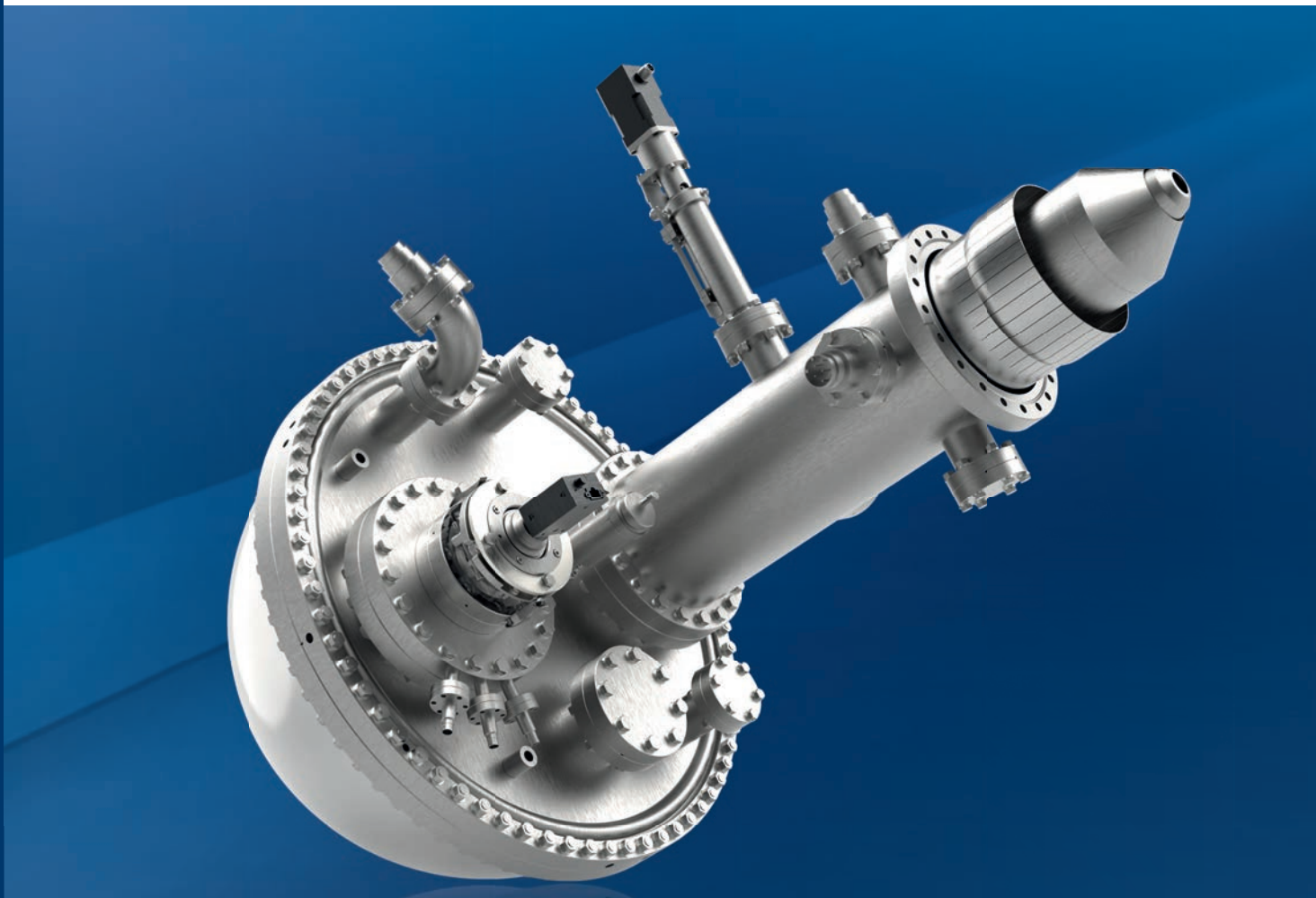

SPECS Surface Nano Analysis GmbH

T +49 30 46 78 24 0
E info@specs.com
H www.specs-group.com

SPECS™

A member of SPECSGROUP

The Optical Low Temperature UHV STM

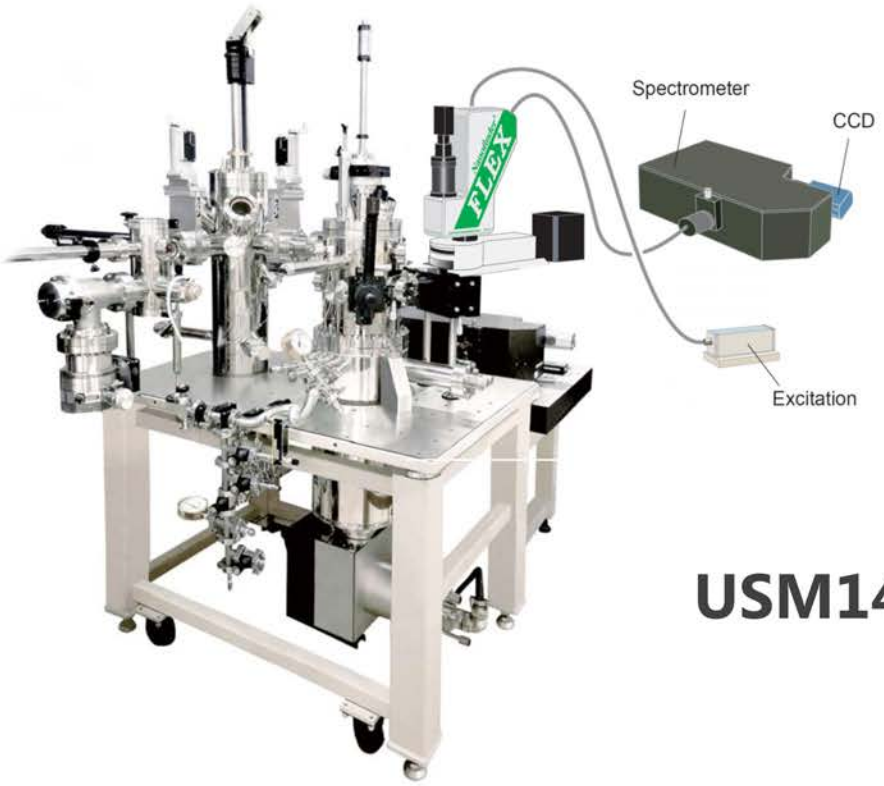

UNISOKU

USM1400-TERS

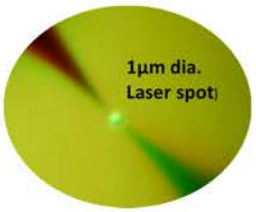

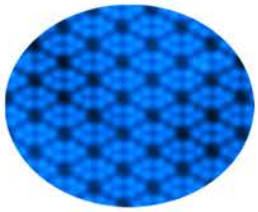

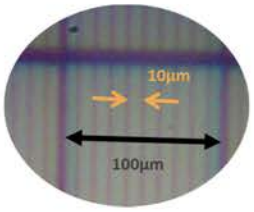

- **High Resolution STM**
- **Low & Variable Temperature Operation**
- **Precise Tip Navigation under Optical Control**
- **Optical Spectroscopies in UV, vis, IR & FIR**
- **High N_A Detection**
- **Perfect Focusing with Close Up Lenses**
- **TERS with Single Molecule Resolution**
- **Parabolic Mirrors available for THz Range and sub-fs Time Resolution**

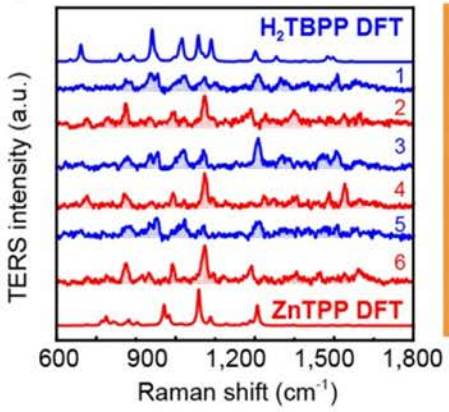

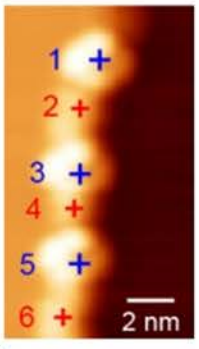

ZnTPP+H2TBPP on Ag,
Z.Dong + et al. Nature Nanotechnology 10, 865–869 (2015)

NANOSCORE nanoscore

nanoscore gmbh Distributor for UNISOKU and BihurCrystal in Europe

Maisebachstr. 3
61479 Glashütten
Germany

www.nanoscore.de

SYMPOSIUM ON SURFACE SCIENCE 2020

St. Christoph am Arlberg, Austria
March 1 - 7, 2020

CONTRIBUTIONS

EDITORS
Friedrich Aumayr, Ulrike Diebold and Christoph Lemell
TU Wien

This symposium is organized by

Friedrich Aumayr and Ulrike Diebold
TU Wien, Institute of Applied Physics (IAP)
Wiedner Hauptstr. 8-10/E134
1040 Vienna, Austria
http://www.iap.tuwien.ac.at/www/3s20/

Venue
Ski Austria Academy, St. Christoph 10,
6580 St. Anton a. Arlberg, Austria
www.skiakademie.at

Medieninhaber: F. Aumayr und U. Diebold, Institut für Angewandte Physik, Technische Universität Wien, Adresse: Wiedner Hauptstr. 8-10/E134, A-1040 Wien
Druck: R. & W. Smutny OEG, A-1110 Wien

PREFACE

We welcome all participants and accompanying persons to the 33st Symposium on Surface Science (3S). The 3S was founded as a winter school by members of the Institute of Applied Physics of the Vienna University of Technology (TU Wien) in 1983. The conference seeks to promote the growth of scientific knowledge and its effective exchange among scientists in the field of surface physics and chemistry and related areas, including applied topics. Its format is similar to that of Gordon Conferences, with ample time for discussions and joint outdoor activities. The number of participants is kept below 100 in order to guarantee active communication between all attendees.
Initially the 3S was held exclusively in Austria and took place every other year. It became an annual event in 1990, and the site started to alternate between locations in France and Austria. In 1998 the 3S evolved into a truly global conference, with venues in the US, Canada, Bulgaria, Japan, Switzerland, Spain, France and Sweden, always returning to Austria in alternate years. This year we are again happy to host the 3S in Austria; for the 10th time in the Arlberg area.

We hope that all participants will experience a lively and successful meeting while enjoying the surroundings in this beautiful mountain region in Austria.

Fritz Aumayr Ulrike Diebold

Dates and locations of 3S conferences:

1983	(31.01.-04.02.)	Obertraun	AT
1985	(27.01.-02.02.)	Obertraun	AT
1988	(22.05.-28.05.)	Kaprun	AT
1990	(11.03.-17.03.)	La Plagne	FR
1991	(10.02.-16.02.)	Obertraun	AT
1992	(15.03.-21.03.)	La Plagne	FR
1993	(09.05.-15.05.)	Kaprun	AT
1994	(06.03.-12.03.)	Les Arcs	FR
1995	(23.04.-29.04.)	Kaprun	AT
1997	(26.01.-31.01.)	Aussois	FR
1998	(29.03.-04.04.)	Park City	US
1999	(21.02.-27.02)	Pamporova	BG
2000	(15.02.-18.02.)	Kananaskis	CA
2001	(07.01.-13.01.)	Furano	JP
2002	(03.03.-09.03.)	St.Christoph/Arlberg	AT
2003	(30.03.-05.04.)	La Plagne	FR
2004	(29.02.-06.03.)	St.Christoph/Arlberg	AT
2005	(13.03.-19.03.)	Les Arcs 1800	FR
2006	(05.03.-11.03.)	St. Christoph/Arlberg	AT
2007	(11.03.-17.03.)	Les Arcs 2000	FR
2008	(02.03.-08.03.)	St. Christoph/Arlberg	AT
2009	(08.03.-14.03.)	St. Moritz	CH
2010	(07.03.-13.03.)	St. Christoph/Arlberg	AT
2011	(06.03.-12.03.)	Baqueira Beret	ES
2012	(11.03.-17.03.)	St. Christoph/Arlberg	AT
2013	(03.03.-09.03.)	Åre	SE
2014	(09.03.-15.03.)	St. Christoph/Arlberg	AT
2015	(22.03.-28.03.)	Les Arcs 1800	FR
2016	(21.02.-27.02.)	St. Christoph/Arlberg	AT
2017	(05.03.-10.03.)	St. Moritz	CH
2018	(25.02.-03.03.)	St. Christoph/Arlberg	AT
2019	(10.03.-16.03.)	Baqueira Beret	ES
2020	(01.03.-07.03.)	St. Christoph/Arlberg	AT

Peter Varga 3S-Poster Prize

In memory of one of the founding fathers of the 3S workshop series, Peter Varga (1946 – 2018), the Peter Varga 3S-Poster Prize is awarded every year starting with 3S*19.

List of prize winners

3S*19 Ales Cahlik (Praha, Czech Republic)

SYMPOSIUM ON SURFACE SCIENCE 2018

St. Christoph am Arlberg, Austria
March 1 – March 6, 2020

Time Schedule

Sunday, 1 March 2020

16:00 – 18:30	**Registration**
20:00 – 20:20	**Opening**
	Chair: F. Aumayr
20:25 – 20:45	**G. Rupprechter** *Structure dependence of the initial oxidation of Rh and its effect on catalytic H_2 oxidation*
20:45 – 21:05	**A. J. Heinrich** *Electron Spin Resonance of single atoms on a surface observed with STM*
21:05 – 21:25	**P. Jelínek** *Tailoring topological order and π-conjugation to engineer quasi-metallic polymers*

Monday, 2 March 2020

Chair: H. Ibach

08:00 – 08:20 **C. Wöll**
Surface-Ligand IR Spectroscopy: From Single Crystals to Oxide Powders to In-Operando Studies

08:20 – 08:40 **C. Rameshan**
Nanoparticle Exsolution: Tailoring Surface Reactivity for Chemical Energy Conversion

Chair: U. Diebold

16:40 – 17:00 **K. Morgenstern**
A local view on the poisoning of a surface during laser induced CO_2 dissociation

17:00 – 17:20 **E. Lundgren**
Surface composition of $Pt_3Sn(111)$ during CO oxidation

17:20 – 17:40 **M. Shipilin**
Syngas reactions over Rh-Fe catalysts. First steps on the way to XPS experiments at realistic pressure

17:40 – 18:00 **H. Edström**
Reaction driven ordering of the surface of a PtRh alloy model catalyst

18:00 – 18:20 **J. Suchorski**
New spatially-temporal phenomena studied using nanosized surface structure libraries

Chair: P. Kocan

19:30 – 19:50 **L. Hammer**
Unexpected bimetallic overlayers formed by Tellurium on Ag(111) and Cu(111) surfaces

19:50 – 20:10 **C. Linsmeier**
Characterization of beryllium-titanium intermetallic compounds with X-ray photoelectron spectroscopy

20:10 – 20:30 **J. E. Ortega**
Atomically precise step grids for engineering helical states

20:30 – 20:50 **H. Dil**
Single helical spin-polarised Fermi surface in $SrTiO_3$ thin film homostructures

Tuesday, 3 March 2020

Chair: P. M. Echenique

08:00 – 08:20 **M. Setvin**
Polarons frozen in a crystal lattice observed by nc-AFM

08:20 – 08:40 **H. Oberhofer**
Stability and Dynamics of Polarons near Oxide Surfaces

Chair: M. E. Messing

16:40 – 17:00 **A. Arnau**
Varying the chirality of spin textures in ultrathin Pt/Co/Graphene heterostructures by Dzyaloshinskii-Moriya Interactions

17:00 – 17:20 **N. A. Vinogradov**
Formation and structure of two-dimensional boron on Ir(111)

17:20 – 17:40 **P. Brandimarte**
Emerging magnetism in boron-doped graphene nanoribbons

17:40 – 18:00 **D. Sánchez-Portal**
Probing the magnetism of topological end-states in 5-armchair graphene nanoribbons

18:00 – 18:20 **G. Renaud**
Growing perfect graphene on a liquid metal: from self-assembled flakes to the single layer

Chair: S. Förster

19:30 – 19:50 **A. Gölzhäuser**
Ultra-High Ionic Exclusion Through Carbon Nanomembranes

19:50 – 20:10 **J. Schwestka**
Perforation of 2D heterostructures

20:10 – 20:30 **C. Lemell**
Neutralization of moderately charged ions transmitted through graphene sheets – what is it good for?

20:30 – 20:50 **T. Šikola**
Graphene single layer grown on the FeRh (001) thin film

Wednesday, 4 March 2020

Chair: F. P. Netzer

08:00 – 08:20 **F. J. Giessibl**
Atomic Force Microscopy Studies of a Quantum Corral

08:20 – 08:40 **J. V. Barth**
Structural and Electronic Properties of FeSi(110)

Chair: T. Berghaus

16:40 – 17:00 **M. Maier**
Recent advancements in surface science instrumentation

17:00 – 17:20 **T. Stempel**
Low Energy Electron Microscopy at Near Ambient Pressures

Chair: E. Lundgren

17:25 – 18:20 **Poster Introduction**

J. Appenroth
A mussel inspired hydrogel

B. Baretzky
Interfaces-controlled properties of solid polycrystals: Ferromagnetic ZnO and hard-magnetic Nd-Fe-B alloys

H. Brune
Single Ion Molecular Magnets Adsorbed at Surfaces

A. Cahlík
Tuning electronic properties of 1D coordination polymers by the choice of the transition metal: Fe, Co and Ni

M. Deimel
Active site representation in first-principles microkinetic models: Data-enhanced computational screening for improved methanation catalysts

U. Diebold
Assessing the proton affinity of individual surface OH groups with nc-AFM

S. Filimonov
Accurate surface energies by van der Waals inclusive DFT calculations

S. Förster
Occupied and unoccupied electronic structure of the $BaTiO_3$-derived oxide quasicrystal

G. Franceschi
Movable holder for a quartz crystal microbalance for exact doses in pulsed laser deposition

N. G. Hörmann
Understanding pH and potential effects from ab-initio simulations of electrochemical interfaces using implicit solvation models

H. Ibach
The quest for magnons in ultra-thin nickel films

P. Kocán
Revision of role of hydrogen bonding in self-ordering of partialy fluorinated phthalocyanines

F. Kraushofer
The TensErLEED Management Package: A new environment for analysis and calculation of LEED I(V)

J. Kunze-Liebhäuser
Electroreduction of water on Mo_2C film electrodes affected by the presence of CO_2

F. Ligmajer
Epitaxial vanadium dioxide – material for anisotropic switchable thin films

A. Niggas
How to clean a sample when sputtering is not possible because the sample has only one atomic layer?

J. Oelmann
Laser-induced analysis of the deuterium retention in Ta and W

J. Pavelec
Methods for exposing single-crystal metal-oxide samples to liquid/high pressure with preparation and characterization in UHV

D. Rath
Design of an IRAS Setup to Investigate Adsorbates on Metal-Oxide Single Crystals

M. Riva
Detecting Tiny Cation Nonstoichiometry in Complex Oxide Films

P. Szabo
Solar Wind Sputtering Investigations on Planetary Mineral Analogues

19:30 – 21:30 **Postersession**

Thursday, 5 March 2020

Chair: J. Kunze-Liebhäuser

08:00 – 08:20 **R. Widmer**
Molecular motor at the frontier of classical motion and quantum tunneling

08:20 – 08:40 **O. M. Magnussen**
The dynamic nature of CO adlayers on Pt(111) electrodes

Chair: M. Riva

16:40 – 17:00 **A. Stierle**
Adsorption of Carboxylic Acids on Magnetite Surfaces

17:00 – 17:20 **Z. Jakub**
Local environment defines reactivity of model single-atom catalysts: Ir and Rh on Fe_3O_4(001)

17:20 – 17:40 **V. Vonk**
Near-surface iron diffusion in magnetite

17:40 – 18:00 **M. Sterrer**
Control of charge transfer into organic molecules on ultrathin MgO(001) films

18:00 – 18:20 **M. Rocca**
Interface oxygen induced internal structures of ultrathin MgO islands grown on Ag(100) observed with STM

Chair: H. Seitsonen

19:30 – 19:50 **F. Mittendorfer**
Accuracy in the theory of oxides – the many phases of ZrO_2

19:50 – 20:10 **V. M. Silkin**
Acoustic surface plasmon on Ni(111)

20:10 – 20:30 **W. Eberhardt**
fs timescale Charge Carrier Dynamics in organic Photovoltaics

20:30 – 20:50 **F. P. Netzer**
Thermodynamic Stability of 2-D WO_3 Nanosheets: Growth on a Ag Foil

Friday, 6 March 2020

Chair: U. Starke

08:00 – 08:20 **K. Reuter**
Insight into the Structural Evolution of Working IrO_2 Catalysts in Proton-Exchange Membrane Electrolyzers

08:20 – 08:40 **J. Libuda**
Supported catalytically active liquid metal solutions: A new concept in single-site catalysis explored by surface science and operando methods

Chair: M. Valtiner

16:30 – 16:50 **W. Linpé**
The brightest Au(111) surface.

16:50 – 17:10 **A. Auer**
In-situ electrochemical STM imaging of Cu(111) under reaction conditions

17:10 – 17:30 **J. Dziadkowiec**
Interactions between reactive mineral surfaces studied with the surface forces apparatus

17:30 – 17:50 **P. Cyganik**
All in One: N-Heterocyclic Carbenes for the Self-Assembly of Monolayers of Superior Quality and Stability

17:50 – 18:10 **M. Buck**
Coordination controlled electrodeposition of metal nanostructures on top of self-assembled monolayers

Chair: M. Rocca

18:30 – 18:50 **M. Ammon**
Epitaxial Cobalt Oxide Films with Wurtzite Structure Grown on Au(111)

18:50 – 19:10 **W.-D. Schneider**
Growth and atomic-scale characterization of ultrathin silica and germania films: The crucial role of the metal support

19:10 – 19:40 **Giant Slalom Race Award Ceremony**

20:00 **Conference Dinner**

CONTRIBUTIONS

Content

Sunday

Structure dependence of the initial oxidation of Rh and its effect on catalytic H_2 oxidation

P. Winkler[1], J. Zeininger[1], M. Stöger-Pollach[2], J. Bernardi[2], P. Zeller[3], M. Amati[3], L. Gregoratti[3], Y. Suchorski[1], G. Rupprechter[1]

[1]*Institut für Materialchemie, Technische Universität Wien, A-1060 Wien, Austria*
[2]*USTEM, Technische Universität Wien, A-1040 Wien, Austria*
[3]*Elettra – Sincrotrone, IT-34149 Basovizza, Trieste, Italy*
(corresponding author: G. Rupprechter, e-mail: guenther.rupprechter@tuwien.ac.at)

It is well accepted that as-prepared catalyst may undergo chemical modifications, which depend on the specific reaction conditions. For oxidation reactions on rhodium, different stoichiometric or transient oxide states have been suggested as possible active phases [1], mainly based on single crystal studies. However, the exact role of the crystallographic surface structure of Rh catalysts has been hardly considered under oxidative conditions. This is mainly due to the fact that the initial stages of surface oxidation, namely the formation of (dissolved, interstitial) subsurface oxygen and of surface oxides are difficult to access with conventional surface analysis techniques, particularly under reaction conditions (operando). Synchrotron-based photoelectron microscopes, which enable to perform chemical imaging and micro-spectroscopic analysis with lateral resolution around 0.1 μm, are powerful devices to overcome this analytical challenge. A scanning photoelectron microscope (SPEM), using an X-ray microprobe and scanning the specimen with respect to the microprobe, performs e.g. XPS chemical imaging with submicrometer lateral resolution [2]. Particularly, in combination with tuneable X-ray beams provided by 3rd generation low emittance synchrotron radiation sources, SPEM represents an effective surface sensitive tool [3].

In the present contribution, the advantages of the SPEM technique are combined with those of the recently introduced concept of *surface structure libraries*, the latter based on model systems consisting of many crystallographically different regions within one sample [4]. Using polycrystalline platinum group foils consisting of many μm-sized grains of different orientations, this concept allows to study catalytic reactions on different surface structures *simultaneously* [4-6]. Herein, polycrystalline Rh foil was crystallographically fully characterized by EBSD and applied to study the surface oxidation of Rh in an oxygen pressure range of 10^{-5} mbar and temperature of 673 K by *in situ* SPEM. The results are summarized as an "oxidation map", in which a specific oxidation state was assigned to each Rh domain (20 to 100 μm in size). The results revealed a clear anisotropy in the initial oxidation of Rh, i.e. the surface oxidation rate depends on the crystallographic orientation.

Subsequently, the same polycrystalline Rh sample was used for studying catalytic H_2 oxidation via another novel approach, namely *kinetics by imaging* [7]. In this approach, a catalytic reaction on a heterogeneous sample (e.g. polycrystalline [5, 6] or consisting of many supported particles [8]) is imaged *in situ* by PEEM and the local reaction kinetics for

individual µm-sized domains is then extracted from the *in situ* recorded video-files. Based on the SPEM data, the Rh surface prepared in a particular oxidation state and subsequently the H_2 oxidation were *in situ* monitored by PEEM. The results were summarized in a kinetic phase diagram, displaying the steady states of high and low catalytic activity and the region of bistability [9]. A comparison of these diagrams for metallic and partially oxidized Rh surfaces revealed a pronounced surface oxide effect: the external parameters (pressure of reactants, temperature) required for kinetic transitions to occur (from catalytically active state to inactive and *vice versa*) significantly differed for metallic and partially oxidized Rh. For catalytic H_2 oxidation, this effect had not yet been directly observed for any metal active in this reaction.

This work was supported by the Austrian Science Fund (FWF) [SFB F45 FOXSI]

[1] J. Gustafson, O. Balmes, C. Zhang, M. Shipilin, A. Schaefer, B. Hagman, L. R. Merte, N. M. Martin, P-A. Carlsson, M. Jankowski, E. J. Crumlin, E. Lundgren, ACS Catal. 8, 4438 (2018)
[2] M. Amati, B. Aleman, B. Bozzini, L. Gregoratti, H. Sezen, M. Kiskinova, Surf. Sci. 652, 20 (2016)
[3] M. Marsi, L. Casalis, L. Gregoratti, S. Günther, A. Kolmakov, J. Kovac, D. Lonza, M. Kiskinova, J. Electron Spectrosc. Relat. Phenom. 84, 73 (1997)
[4] Y. Suchorski, G. Rupprechter, Cat. Lett. 148, 2947 (2018)
[5] Y. Suchorski, M. Datler, I. Bespalov, J. Zeininger, M. Stöger-Pollach, J. Bernardi, H. Grönbeck, G. Rupprechter, Nature Comm. 9, 600 (2018)
[6] Y. Suchorski, M. Datler, I. Bespalov, J. Zeininger, M. Stöger-Pollach, J. Bernardi, H. Grönbeck, G. Rupprechter: J. Phys. Chem. C 123, 4217 (2019)
[7] Y. Suchorski, G. Rupprechter, Surf. Sci. 643, 52 (2016)
[8] Y. Suchorski, S. Kozlov, I. Bespalov, M. Datler, D. Vogel, Z. Budinska, K. Neyman, G. Rupprechter, Nature Mat. 17, 519 (2018)
[9] Y. Suchorski, I. Bespalov, J. Zeininger, M. Raab, M. Datler, P. Winkler, G. Rupprechter, Cat. Lett. 2020, in print, DOI: 10.1007/s10562-019-02950-0

Electron Spin Resonance of single atoms on a surface observed with STM

A.J. Heinrich[1,2]

[1]*Center for Quantum Nanoscience, Institute for Basic Science (IBS), Seoul 03760, Republic of Korea.*

[2]*Department of Physics, Ewha Womans University, Seoul 03760, Republic of Korea.*

(corresponding author: A.J. Heinrich, e-mail: Heinrich.andreas@qns.science)

The scanning tunneling microscope is an amazing tool because of its atomic-scale spatial resolution. This can be combined with the use of low temperatures, culminating in precise atom manipulation and spectroscopy with microvolt energy resolution. In this work we will apply these techniques to the investigation of the quantum spin properties of magnetic atoms sitting on thin insulating films.

Magnetic atoms sitting directly on metal surfaces typically interact quite strongly with the conduction electrons of the underlying metal surface. This has two consequences: first, it may quench the magnetic moment of the atom and render it non-magnetic. Second, if the atom retains its magnetic properties, the strong interaction gives rise to the so-called Kondo effect. In this work, we will therefore place the magnetic atoms on a thin insulating film that is grown on a metal substrate. This film has two main purposes: first, it acts like a decoupling layer from the substrate electrons that now have to tunnel through the thin insulator in order to reach the magnetic atom. Second, if the insulator is polar, the local charges of the insulator act as ligand field for the magnetic atom. Combined with the ever-present spin-orbit interaction, we find interesting magnetic (low-energy) states in such systems [1]. To measure these states in scanning tunneling microscopy, we rely on energy-loss spectroscopy (inelastic electron tunneling) of the tunneling electrons, which gives rise to spin excitation energy thresholds [2]. The STM spectroscopy findings can be beautifully corroborated with x-ray absorption spectroscopy where we found amazing agreement of those vastly different techniques [3].

The majority of our work will deal with a recent advance in STM, namely the combination of STM with electron spin resonance [4]. Electron spin resonance utilizes a static magnetic field to create a controllable energy splitting between two levels and then induces coherent interaction between these levels through a transverse, oscillating magnetic field. When the frequency of this oscillating magnetic field is in resonance with the energy splitting of the two levels, transitions between these levels occur. The major advantage of any spin resonance technique is the simple fact that the energy resolution is independent of the temperature and thus can be much higher than a Fermi-function limited spectroscopy technique such as STM tunneling. In ESR STM we apply a microwave-frequency electric field to the STM tunnel junction and convert this AC electric field into a driving field for the ESR [5]. This technique combines the power of STM of atomic-scale spectroscopy with the unprecedented energy

resolution of spin resonance techniques, which is about 10,000 times better than low-temperature STM spectroscopy.

ESR STM has by now been demonstrated for several 3d transition metal atoms sitting on a double layer of MgO on Ag(100). Here we will focus on two examples: Fe and Ti atoms. Fe on MgO has a spin of S=2 with a very strong out-of-plane easy-axis magnetic anisotropy. This leads in essence to two levels that are degenerate at B=0 and that only split when applying a magnetic field along the z-axis [4, 6]. These ESR active Fe atoms can be used to measure the local magnetic field very precisely and with atomic-scale spatial resolution. For example, when placing a stable single-atom magnet nearby, namely Ho on MgO [7], we observe two different ESR frequencies depending on the state of the Ho magnet. The splitting between those ESR frequencies depends on the distance of the two atoms via the dipolar coupling and allows the measurement of the magnetic moment of Ho [8]. We note that Ho does not show any spin excitations in STM. We recently found another single-atom magnet in STM which appears to be even more stable than Ho [unplublished].

Ti atoms on MgO are an S=1/2 system – at least when a single H atom is attached to them, which is practically always the case in UHV systems. This simpler spin has an interesting nuclear spin system, consisting of several isotopes, including nuclear spin I=0, I=5/2 and I=7/2. ESR STM is sensitive enough to directly measure the hyperfine interaction of the electron spin with the nuclear spin of the Ti atom [9]. The hyperfine interaction is a sensitive measure of the local bonding geometry and we show that it changes dramatically for different binding sites on MgO. ESR STM is just in its begging phase and we expect many strong results from many research groups in the coming years.

Support from Institute for Basic Science (IBS-R027-D1) is gratefully acknowledged.

[1] C.F. Hirjibehedin, C.-Y. Lin, A.F. Otte, M. Ternes, C.P. Lutz, B.A. Jones, A.J. Heinrich, *Science* **317**, 1199 (2007)

[2] A.J. Heinrich, J.A. Gupta, C.P. Lutz, and D.M. Eigler, *Science* **306**, 466 (2004)

[3] S. Baumann, F. Donati, S. Stepanow, S. Rusponi, W. Paul, S. Gangopadhyay, I. G. Rau, G. E. Pacchioni, L. Gragnaniello, M. Pivetta, J. Dreiser, C. Piamonteze, C. P. Lutz, R. M. Macfarlane, Barbara Jones, Pietro Gambardella, Andreas J. Heinrich, and Harald Brune, *PRL* **115**, 237202 (2015)

[4] Susanne Baumann, William Paul, Taeyoung Choi, Christopher P. Lutz, Arzhang Ardavan, Andreas J. Heinrich, "Electron Paramagnetic Resonance of Individual Atoms on a Surface", *Science* **350**, 417 (2015)

[5] Reina Gálvez, C. Wolf, F. Delgado, and N. Lorente, *Physical Review B* **100**, 035411 (2019)

[6] Philip Willke, Aparajita Singha, Xue Zhang, Taner Esat, Andreas Heinrich, Taeyoung Choi, *Nano Letters* **19**, 8201 (2019)

[7] Fabio Donati, S Rusponi, Sebastian Stepanow, C Wäckerlin, Aparajita Singha, Luca Persichetti, R Baltic, K Diller, Francois Patthey, E Fernandes, Jan Dreiser, Željko Šljivančanin, K Kummer, Corneliu Nistor, Pietro Gambardella, Harald Brune, *Science* **352**, 318 (2016)

[8] Fabian D. Natterer, Kai Yang, William Paul, Philip Willke, Taeyoung Choi, Thomas Greber, Andreas J. Heinrich and Christopher P. Lutz, "Reading and Writing Single Atom Magnets", *Nature* **543**, 226 (2017)

[9] Philip Willke, Yujeong Bae, Kai Yang, Jose L. Lado, Alejandro Ferrón, Taeyoung Choi, Arzhang Ardavan, Joaquín Fernández-Rossier, Andreas J. Heinrich and Christopher P. Lutz, "Hyperfine interaction of individual atoms on a surface", *Science* **362**, 336 (2018)

Tailoring topological order and π-conjugation to engineer quasi-metallic polymers

B. de la Torre,[1,2] B. Cirera,[3] A. Sánchez-Grande,[3] A. Matěj,[1,2] J. Santos,[3] S. Edalatmanesh,[2] E. Rodríguez-Sánchez,[3] K. Lauwaet,[3] B. Mallada-Faes,[1,2] A. Cahlík,[1,2] R. Miranda,[3] O. Gröning,[4] P. Jelínek,[1,2] N. Martín,[3] P. Jelínek,[1,2] D. Écija[3]

Institute of Physics, Czech Academy of Sciences, Prague, CZ-162 00, Czechia
(corresponding author: P. Jelínek, e-mail: pavel.jelinek@fzu.cz)

[1] *Institute of Physics, Czech Academy of Sciences, Prague, CZ-162 00, Czechia*

[2] *RCPTM, Palacký University, CZ-78371 Olomouc, Czechia*

[3] *IMDEA Nanociencia. ES-28049 Madrid, Spain*

[4] *EMPA, CH-8600 Dübendorf, Switzerland*

We introduce a novel strategy to synthesize a new class of intrinsically quasi-metallic one-dimensional (1D) π-conjugated polymers featuring topologically non-trivial quantum states using the concept of on-surface chemistry [1]. Furthermore, we unveiled the fundamental relation between quantum topology, π-conjugation and metallicity of polymers. Thus, our work bridges the two distinct worlds of topological band theory (condensed matter physics) and π-conjugation polymer science (chemistry), which may stimulate new routes towards a design of organic polymers with unprecedented material properties.

The rational design of increasingly complex electronic materials for molecular electronics and quantum technologies has been an active field of research in organic electronics. Particularly appealing are π-conjugated polymers [2] due to their relevant optical and electronic properties stemming from the delocalization of the π-electrons, which are the key for the incoming revolution of transparent and plastic electronics. However, despite great advances in the field from the synthetic point of view, we still lack of 1D π-conjugated polymers that feature intrinsic ultra-narrow or even zero bandgaps, accomplishing the dream of engineering intrinsic metallic organic polymers [3].

On the other hand, topological band theory [4] proves that the quantum phase transition between two insulators of distinct topological class must proceed via closing of the electronic

gap. Therefore, such theory offers a conceptual solution to the instability of metallic phases in π-conjugated 1D polymers.

In this work, we demonstrate that a clever design and on-surface synthesis of polymers consisting of linearly bridged polyacene moieties [5] can position the resulting polymer near the topological transition, moving from a trivial to a non-trivial quantum phase featuring a very low, quasi-metallic bandgap [6]. At the same time, we observe that the presence of the topological non-trivial phase perturbs significantly the π-conjugation by increasing the quinoid contribution of central ring of the acene units simultaneously accompanied by the promotion of a cumulene-like character in the linear bridge. We demonstrate that this change of the π-conjugation driven by the level crossing of frontier orbitals is intimately related to the topological phase transition. This finding reveals the fundamental connection between topological phase and electronic forms of π-conjugated polymers, thus establishing the link between two worlds of condensed matter and chemistry. What is more, using the novel design strategy proposed here, we can design new class of stable biradical π-conjugated polymers featuring intrinsic magnetic properties.

[1] Q. Shen, H.-Y. Gao, H.Fuchs, *Nano Today* **13**, 77-96 (2017)
[2] A.J. Heeger, Angew. Chem. Int. Ed. **40**, 2591-2611 (2001)
[3] J. Roncali, J. *Chem. Rev.* **97**, 173-206 (1997)
[4] J.K. Asbóth, L. Oroszlány, A. Pályi, in *A short course on topological insulators: band structure and edge states in one and two dimensions.* Springer International Publishing, (2016)
[5] A. Sánchez-Grande, et al, Angew. Chem. Int. Ed. 58, 6559 – 6563 (2019)
[6] B. Cirera, et al, arXiv:1911.05514 (2019)

Innovative SPM and XPS solutions for Surface Science

SIGMA Surface Science

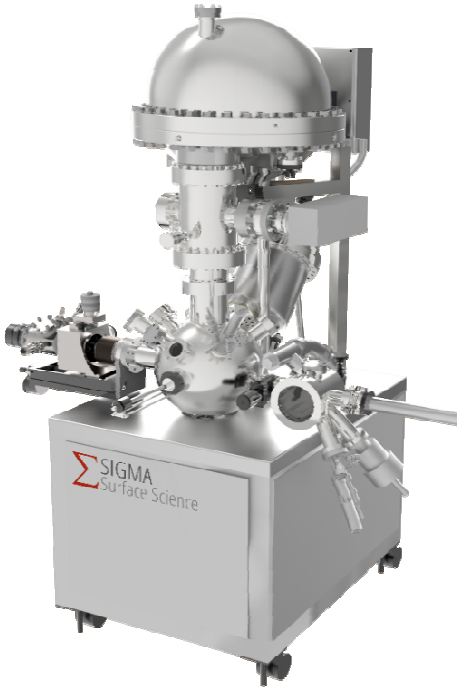

PULSE for Dynamic XPS

- Real-time observation of surface transformations
- Fast data acquisition
- High transmission Aspect analyser and sophisticated Neo control suite
- High power monochromated and dual-anode X-ray source
- Flexible and fully accessible system layout

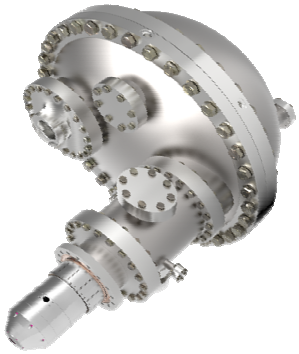

ASPECT analyzer

- Highest transmission
- Snapshot capability with multichannel detector
- Energy range up to 3.5 keV
- Dynamic XPS with Multi Peak Monitoring
- Fast XPS with survey spectrum acquisition in 2 seconds
- Neo control suite for advanced data acquisition

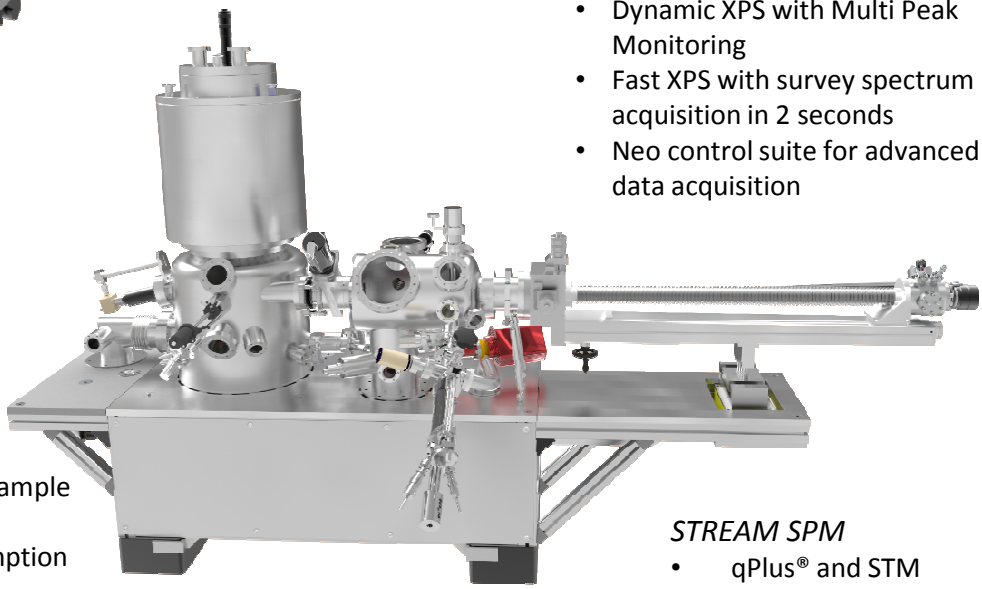

POLAR SPM

- qPlus® and STM
- *Bath cryostat*
- 3D coarse motor
- 5K-420K
- Optical access to tip & sample
- Hold time: > 200h
- Peerless Helium consumption
- B_Z = ±5T (option)

STREAM SPM

- qPlus® and STM
- *Flow cryostat for LN_2 and LHe*
- 3D coarse motor
- 9K-420K

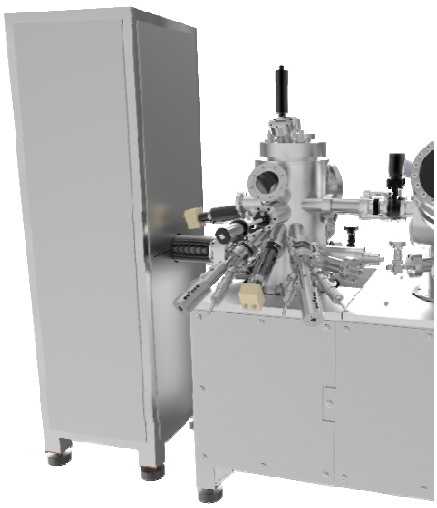

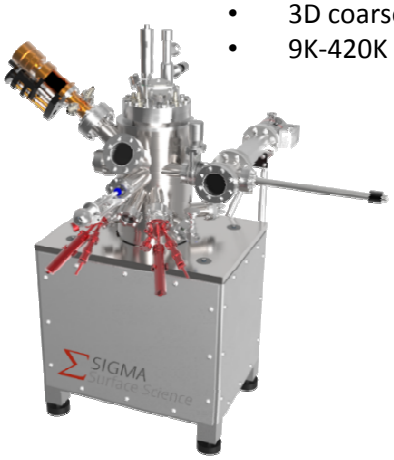

INFINITY SPM

- qPlus® and STM
- *Pulse Tube cryostat*
- 3D coarse motor
- 10K - 420K
- No Helium consumption
- Interruption free operation
- Acoustic noise cancellation

www.sigma-surface-science.com

Monday

Surface-Ligand IR Spectroscopy: From Single Crystals to Oxide Powders to In-Operando Studies

Christof Wöll
Institute of Functional Interfaces (IFG), Karlsruhe Institute of Technology (KIT), FRG
christof.woell@kit.edu, www.ifg.kit.edu

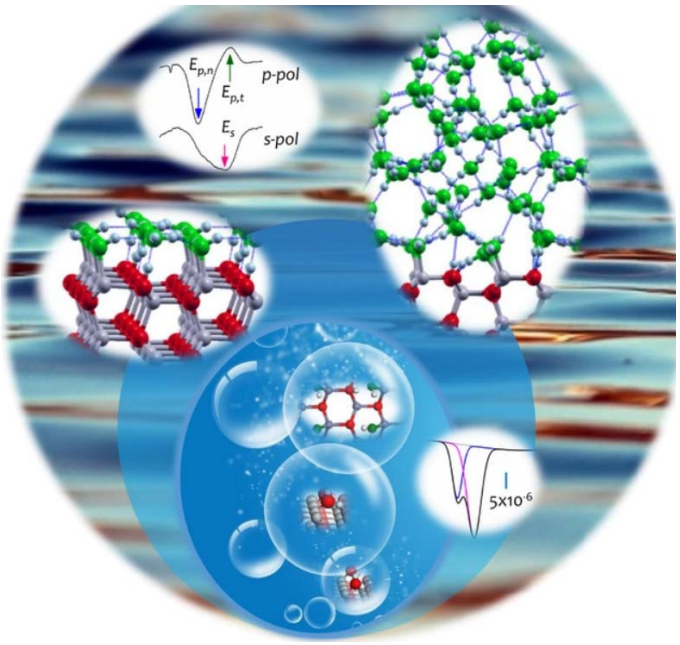

Fig. 1 IRRAS allows for a detailed investigation of water interaction with ZnO(10-10) surfaces, extending from the submonolayer to the multilayer regime. (Ref. 3).

While infrared reflection absorption spectroscopy, IRRAS, has over the last decades developed into one of the most important pillars of Surface Science, the application of this technique to well-defined single crystals has been mainly restricted to metal surfaces. In case of transition metal oxides, the fairly low reflectivity of dielectrics for infrared light have made the application very difficult. In a few instances, it was possible to apply IR spectroscopy in transmission, but such work has been rather restricted and MgO appears to be the only transition metal oxide which has been studied with this method.[1] As a result, information on the vibrational spectrum of small molecules (e.g. CO, O_2, N_2O,…) adsorbed on oxides has been restricted to powder materials and to thin films of oxides grown on metal substrates. In both cases, recording of IR-spectra is rather straightforward, for powders either in transmission or by using the so-called DRIFTS approach (diffuse reflectance infrared spectroscopy). For oxide thin films the underlying metal substrate acts as a mirror, thus yielding high intensities. Due to the often not well-defined shape and the coexistence of different surface terminations of the powder nanoparticles an unambiguous interpretation of the IR vibrational bands has not been possible – and in fact there are a few examples in the literature where these assignments were not correct. (See [4] for a discussion).

Recent progress in instrumentation [2] has provided the basis for characterizing the surfaces of catalytically active oxide materials by using surface-ligand IR (SLIR) spectroscopy using reflection geometries (for a list of materials, including CeO_2, TiO_2, ZnO, Fe_2O_3, Fe_3O_4,… see Ref. 4). This reference data for macroscopic, well-defined single crystal surfaces, in particular for the prototype ligand CO, now allows characterizing the facets exposed by nanoparticles also for powder materials. These advantages can also be applied in the context of in-situ and operando studies, thus allowing observing dynamical changes of the shapes of oxide nanoparticles as well as the number, type, and charge state of exposed metal ions. In particular, the SLIR method can also be used to characterize single-atom active sites in heterogeneous catalysis. [5]

In addition, IRRAS data recorded for surfaces of dielectric monocrystals offers the possibility to record data also for s-polarization, which is not possible for metal substrates (so-called surface selection rule). Also for thin films of metal oxides grown on metals this restriction applies – s-polarization cannot be used. The fact for dielectrics spectra can also be recorded using the component of the incident light polarized perpendicular to the plane of incidence opens up the possibility to also measure vibrations with dynamic dipoles orientated parallel to the substrate, e.g. in the case of isolated water molecules and water monolayers adsorbed on ZnO(10-10) [3].
A particular important point for DRIFTS operando studies are studies on adsorbed dioxygen. While the excitation of the O_2-stretch vibration is symmetry-forbidden in the gas phase, the breaking of the symmetry as a consequence of adsorbate-substrate interactions (in some cases including charge transfer leading to the formation of superoxo- and peroxo-species) makes the observation of the dioxygen stretch vibrations possible, e.g. in case of monocrystal ceria substrates.[6] This fact is of particular importance for operando studies, since – in contrast to CO – free O_2 molecules are IR inactive. As a result, the adsorbate lines are not obscured by gas-phase signals.

References:

[1] Heidberg, J.; Kandel, M.; Meine, D.; Wildt, U., The monolayer CO adsorbed on MgO(100) detected by polarization infrared-spectroscopy. Surface Science 1995, 331, 1467-1472.
[2] Y. Wang, Ch. Wöll, IR spectroscopic investigations of chemical and photochemical reactions on metal oxides: bridging the materials gap, Chem. Soc. Rev., 46, 1875-1932, (2017)
[3] X. Yu, P. Schwarz, A. Nefedov, B. Meyer, Y. Wang, and C. Wöll, Structural evolution of water on zinc oxides: From isolated monomers via anisotropic H-bonded 2D and 3D structures to isotropic multilayers. Angew. Chemie Int. Ed., 2019, 131, 17915-17921
[4] Ch. Wöll, Structure and Chemical Properties of Oxide Nanoparticles Determined by Surface-Ligand IR Spectroscopy, ACS Catal. 10, 168 (2020)
[5] Chen, A. L.; Yu, X. J.; Zhou, Y.; Miao, S.; Li, Y.; Kuld, S.; Sehested, J.; Liu, J. Y.; Aoki, T.; Hong, S.; Camellone, M. F.; Fabris, S.; Ning, J.; Jin, C. C.; Yang, C. W.; Nefedov, A.; Wöll, C.; Wang, Y. M.; Shen, W. J., Structure of the catalytically active copper-ceria interfacial perimeter. Nat. Catal. 2019, 2, 334-341
[6] Yang, C. W.; Yu, X.; Heißler, S.; Weidler, P. G.; Nefedov, A.; Wang, Y.; Wöll, C.; Kropp, T.; Paier, J.; Sauer, J., O2 Activation on Ceria Catalysts - The Importance of Substrate Crystallographic Orientation. Angew. Chem. Int. Ed. 2017, 56, 16399-16404

Nanoparticle Exsolution: Tailoring Surface Reactivity for Chemical Energy Conversion

L. Lindenthal[1], R. Rameshan[1], T. Ruh[1], H. Summerer[1,2], J. Raschhofer[1], A. Nenning[2], S. Löffler[3], A.K. Opitz[2], C. Rameshan[1]

[1] *Technische Universität Wien, Institute of Materials Chemistry, Vienna, Austria*
(corresponding author: C. Rameshan, e-mail: Christoph.rameshan@tuwien.ac.at)

[2] *Technische Universität Wien, Institute of Chemical Technologies and Analytics, Vienna, Austria*

[3] *Technische Universität Wien, USTEM, Vienna 1040 (Austria)*

Perovskite-type oxides are a large class of materials with many interesting properties, including mixed ionic-electronic conductivity and high catalytic activity. Their general chemical formula is ABO_3, where both cation sites A and B can be occupied by one or more elements. The high versatility of the material class is due to the possibility of adjusting the properties by choosing different elements for the cations and by doping either of the cation sites, thus opening up a large matrix for materials design.
In terms of catalysis, a recently shown outstanding property of perovskites is the exsolution of metal nanoparticles under reducing conditions [1]. This surface modification (by migration of cations to the surface) can change the catalytic activity and selectivity of the perovskite surface completely and is the core topic of our ERC project. Advantages over other preparation techniques for nanoparticle decorated surfaces (e.g. deposition or impregnation) include a very homogeneous distribution [1], an improved sintering stability during catalytic reaction [2] and the possibility of easy catalyst regeneration by oxidation-reduction-cycles [3].

Perovskite-type oxides (e.g. $La_xCa_{1-x}FeO_3$ or $Nd_xCa_{1-x}FeO_3$), that are promising catalyst materials, were synthesised and subsequently characterised. In addition, for some of the samples the B-site was doped with the catalytically active elements Co and Ni. Characterisation included X-ray diffraction (XRD), X-ray photoelectron spectroscopy (XPS), scanning electron microscopy (SEM), transmission electron microscopy (TEM) and energy-dispersive X-ray spectroscopy (EDX). Using different reducing conditions, the stability and reducibility of the synthesized perovskites were investigated. Also, catalytic testing was performed for several energy related reactions, such as the (reverse) water gas shift reaction (rWGS) or methane dry reforming. To correlate the material properties with the catalytic performance, in situ and operando XRD and XPS experiments were conducted.

Tailored and reversible exsolution of metal nanoparticles from a stable perovskite backbone was achieved upon reduction of the materials. This was visible in the diffraction patterns, XPS spectra and SEM images after reduction. The exsolution behavior (e.g. size and composition of the resulting particles) could be controlled by the design of the materials and

the exsolution conditions. Doping with Co or Ni facilitated the exsolution process. In this case, the resulting nanoparticles had diameters of 30-40 nm and were homogeneously distributed on the material surface (SEM, figure 1b). They consisted predominantly of the catalytically active elements Co (TEM-EDX, figure 1c) or Ni, respectively.

The catalytic testing showed that exsolution strongly enhanced the catalytic activity of the materials (e.g. for rWGS, figure 1a). The nanoparticles can be either exsoluted during a pretreatment step or even in situ during the reaction (followed with operando techniques).

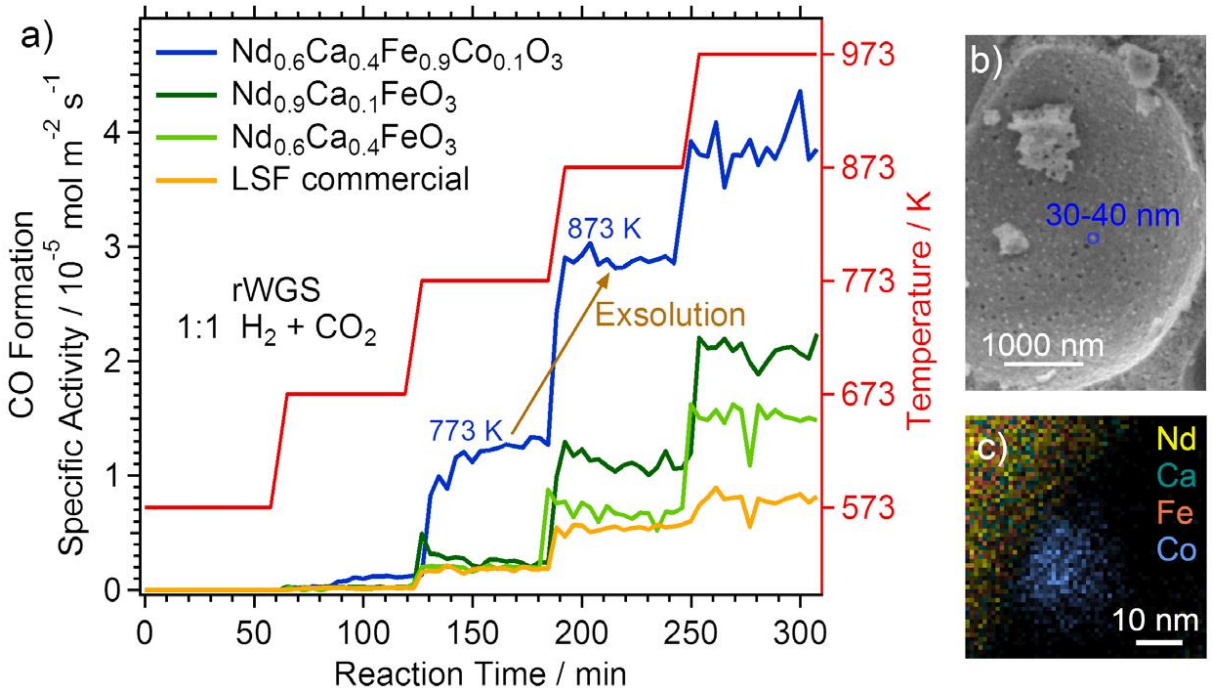

Figure 1: a) Catalytic performance of various materials during rWGS. b) SEM image of Nd0.6Ca0.4Fe0.9Co0.1O3-δ with exsoluted nanoparticles. c) EDX mapping of a Co particle.

The growth of nanoparticles via exsolution offers a novel, easy and cost-efficient route for preparation of catalysts decorated with nanoparticles, as an alternative to conventional techniques. This is interesting for both industrial applications and fundamental research.

This project has received funding from the European Research Council (ERC) under the European Union's Horizon 2020 research and innovation programme (grant agreement n° 755744 / ERC - Starting Grant TUCAS)

[1] D. Neagu, G. Tsekouras, D. N. Miller, H. Menard and J. T. S. Irvine, Nat. Chem. 5, 916-923 (2013).

[2] D. Neagu, T. S. Oh, D. N. Miller, H. Menard, S. M. Bukhari, S. R. Gamble, R. J. Gorte, J. M. Vohs and J. T. S. Irvine, Nat. Commun. 6 (2015).

[3.] D. Burnat, R. Kontic, L. Holzer, P. Steiger, D. Ferri and A. Heel, J. Mater. Chem. A 4, 11939-11948 (2016).

A local view on the poisoning of a surface during laser induced CO2 dissociation

Michael Vyshnepolsky, Patrik Tesarik, and Karina Morgenstern

Lehrstuhl für physikalische Chemie I, Ruhr-Universität Bochum,
Universitätsstraße 150, D-44801 Bochum, Germany
(corresponding author: K. Morgenstern, e-mail: morgenstern@rub.de)

Several mechanisms are known to influence the effciency of a catalyst. One of these, called poisoning, may deactivate it. A poisoning occurs for instance, if species block catalytically active sites from further catalytic reactions . A detailed understanding of poisoning would facilitate to develop strategies to decrease or even suppress this undesired process.

In other cases, femtochemistry was used to understand the underlying physical principles of surface reactions [1]. We use in this study femtochemistry on the local scale, employing low-temperature scanning tunneling microscopy (STM), to obtain real space information about the reactivity of individual molecules in a specific environment [2], here to observe and understand the poisoning process during a reaction.

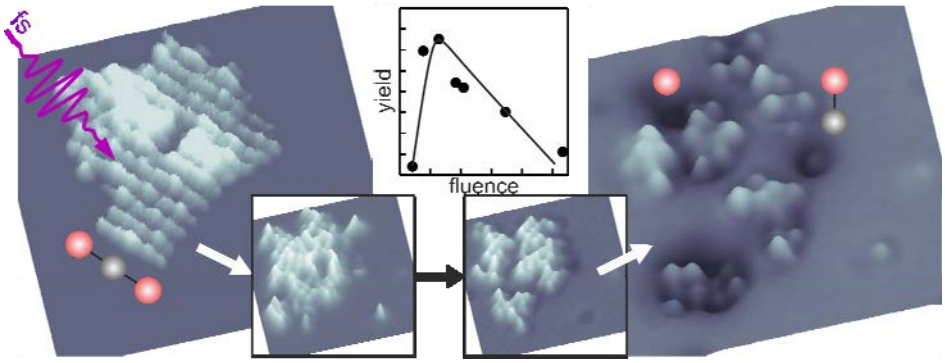

Femtosecond laser illumination dissociates CO_2 molecules from crystalline clusters adsorbed on both, Ag(100) and Cu(111). We use low-temperature scanning tunneling microscopy to follow this dissociation in real space with single-molecule resolution. We reveal how the local surrounding of the CO_2 clusters, and with it the propensity for dissociation, evolves with progressing dissociation. Dissociation is preceded by a loss of crystallinity of the CO_2 clusters. After a boost in dissociation yield, the dissociation products in vicinity of the CO_2 molecules poison the surface and thus reduce the dissociation yield substantially. Our study thus constitutes an unprecedented local view on poisoning during a femtochemical reaction. The thus gained local view on surface poisoning enlarges the scope of femtochemistry.

[1] C. Frischkorn and M. Wolf, Chem. Rev. 106, 4207 (2006)

[2] L. Bartels, F. Wang, D. Möller, E. Knoesel and T. F. Heinz, Science, 305, 648 (2004); H. Gawronski, M. Mehlhorn and K. Morgenstern, Angew. Chem. Int. Ed. 49, 122, 6049 (2010); M. Mehlhorn, H. Gawronski and K. Morgenstern, Phys. Rev. Lett. 104, 076101 (2010); C. Zaum, K. M. Meyer-auf-der-Heide, M. Mehlhorn, S. McDonough, W. F. Schneider and K. Morgenstern, Phys. Rev. Lett. 114, 146104 (2015).

Surface composition of $Pt_3Sn(111)$ during CO oxidation

H. Wallander[1], F. Oropeza[2], B. Hagman[3], J. Knudsen[3,4], E. Lundgren[3], and L. R. Merte[1]
[1]*Malmö University, Malmö, Sweden,*
[2]*Eindhoven University of Technology, Eindhoven, Netherlands,*
[3]*Lund University, Lund, Sweden, 4MAX IV Laboratory, Lund, Sweden*
Edvin.Lundgren@sljus.lu.se

Compared to pure platinum, Pt-Sn alloys show enhanced performance as catalysts in several reactions, including CO oxidation. Although a weakening of CO bonding due to alloying is generally viewed as a major contributor to the catalytic properties, a number of studies have shown that the metal is oxidized during reaction conditions, and it has been suggested that the tin oxides which form can promote catalytic activity [1-4]. We performed an AP-XPS study of a $Pt_3Sn(111)$ single crystal surface during CO oxidation at the HIPPIE beamline at MAX IV, with the goal of characterizing the surface state, with particular focus on the formation of oxides and their effects on catalytic activity. Our measurements show that tin is oxidized during the reaction, and that a higher $CO:O_2$ ratio actually promotes tin oxidation: substantial Sn(IV) was formed during CO oxidation in a 1:1 gas mixture, while only Sn(II) was detected in a 1:10 (oxygen-rich) feed. CO conversion was found to be significantly higher in the oxygen-rich feed. For initially-metallic surfaces, the turnover rate was found to decrease with time, while for a pre-oxidized surface the turnover rate was lower and constant. The results generally point toward an inhibitory effect of oxide formation, rather than a promotional effect, under these conditions.

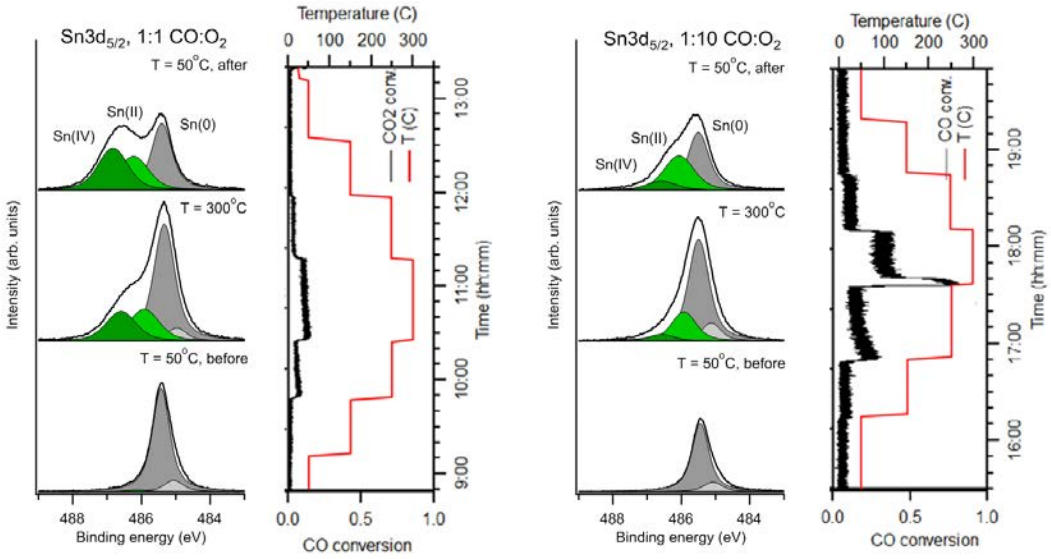

Figure 1: AP-XPS and reactivity measurements during CO oxidation at 1 mbar in 1:1 and 1:10 mixtures of $CO:O_2$.

[1] W. D. Michalak et al., J. Catal. 2014, **312**, 17 - 25.
[3] Y. Jugnet et al., J. Phys. Chem. Lett. 2012, **3**, 3707-3714.
[3] S. Axnanda et al., J. Phys. Chem. C 2014, **118**, 1935-1943.
[4] M. Vandichel et al., ACS Catalysis, 2017, **7**, 7431.

Syngas reactions over Rh-Fe catalysts. First steps on the way to XPS experiments at realistic pressure.

M. Shipilin[1], P. Amann[1], D. Degerman[1], P. Lömker[2], C. Goodwin[1], U. Hejral[3], S. Albertin[3], M. Soldemo[1], J. Gladh[1,4], H.-Y. Wang[1], M. Wagstaffe[2], H. Noei[2], G. L. S. Rodrigues[1], C. Schlueter[2], E. Lundgren[3], A. Stierle[2,5], and A. Nilsson[1]

[1]*Division of Chemical Physics, Physics Department, Stockholm University, 11421 Stockholm, Sweden (corresponding author: M. Shipilin, e-mail: mikhail.shipilin@fysik.su.se)*

[2] *Deutsches Elektronen-Synchrotron DESY, 22607 Hamburg, Germany*

[3] *Division of Synchrotron Radiation Research, Lund University, 22100 Lund, Sweden*

[4] *PULSE Institute, SLAC National Accelerator Laboratory, CA 94025, USA*

[5] *Department of Physics, University of Hamburg, 20148, Hamburg, Germany*

The current contribution aspires to deliver an insight into the direct thermochemical heterogeneous catalytic conversion of syngas ($CO + CO_2 + H_2$) into value-added hydrocarbon products over the model catalysts of Rh-Fe system. In particular, Fe(110), Rh(111) and $Rh_{80}Fe_{20}$(111) single crystal surfaces are investigated and compared for various reaction mixtures and temperatures in the 100-200 mbar regime. The main method utilized in the work is high-pressure hard X-ray photoelectron spectroscopy. The data has been collected using the POLARIS instrument developed in the group of Prof. Nilsson at Stockholm University [1] which allows for measuring photoelectron spectra of a surface in a locally created gas environment at pressures of up to several bar using, in this study, 4.6 keV synchrotron radiation at the P22 beamline of Petra III at DESY.

The catalytic performance of the Rh-Fe system for syngas spans over a wide range of reaction pathways and products from one-carbon-atom molecules, like methane or methanol, to long carbon chains synthesized by the Fisher-Tropsch (FT) process. The latter is characteristic for Fe catalysts and widely accepted to follow a carbide-based reaction scheme, i.e. when the dissociative adsorption of CO generates C species that are hydrogenated to alkyl monomers, which undergo C-C coupling forming higher carbon species [2,3]. In line with this picture, our *in situ* photoelectron spectra of CO hydrogenation reaction on Fe(110) clearly show the presence of iron carbide species on the surface with the fraction of the more-carbon-rich compound increasing with time at the moderate temperature. At higher temperatures, the hydrocarbon chains start appearing on the surface and quickly cover it in a thick layer while the spectra seem to still indicate the presence of the carbon-rich iron carbide phase. This

observation goes in perfect accord with the literature on *ex situ* studies of real iron-based catalysts in the FT process, e.g. [4,5], where the formation of χ-Fe_5C_2 and ε-$Fe_{2.2}C$ is observed with the ratio of first to second phases decreasing throughout the catalytic cycle.

At the same time, the CO_2 hydrogenation reaction on the same surface and under the similar conditions does not produce nearly as much hydrocarbon products, at least not long living enough on the surface for being detected by XPS. Furthermore, the reaction covers the surface with a significant amount of iron oxide phase accompanied by traces of $Fe(CO_3)$ in the lower temperature regime and restores the metallic state at higher temperatures. The constant presence of carbidic carbon in moderate amounts and a weak but clear signal in the CH_x and C_xH_y binding energy region can also be pointed out. The latter reaches its maximum surface coverage at the temperatures slightly above 500K.

Rh and RhFe catalysts have promising properties for synthesis of ethanol [6-9] – a highly desirable liquid fuel and an essential feedstock for the chemical industry – which has low toxicity and high volumetric density of energy stored in chemical bonds. The process of higher alcohol synthesis, including ethanol, is widely considered to be a mixture of FT and methanol synthesis [10]. Our photoelectron spectra collected for these systems under various reaction conditions demonstrate a rich pallet of hydrocarbon products with the distribution highly dependent on the temperature. The data acquired for the RhFe alloy sample is especially interesting and provides an insight into the changes in catalytic activity due to the presence of two types of atoms on the surface.

Support by the Swedish Research Council (project 2017-00559), the Knut and Alice Wallenberg Foundation, the project CALIPSOplus under the Grant Agreement 730872 from the EU Framework Programme for Research and Innovation HORIZON 2020 is gratefully acknowledged. Parts of this research were carried out at P22 and P07 beamlines at DESY, a member of the Helmholtz Association (HGF).

[1] P. Amann et al., Review of Scientific Instruments 90, 103102 (2019)
[2] C. K. Rofer-DePoorter, Chem. Rev. 81, 447–474 (1981)
[3] R. A. van Santen et al., Phys. Chem. Chem. Phys. 15, 17038–17063 (2013)
[4] C. S. Kuivila et al., Appl. Surf. Sci. 32, 99-121 (1988)
[5] V. R. R. Pendyala et al., Chem. Cat. Chem. 6, 1952-1960 (2014)
[6] J. Wang et al., Catal. Today 171, 257 (2011)
[7] M. A. Haider et al., J. Catal. 261, 9 (2009)
[8] Liu Y., et al., ACS Catal. 7, 4550−4563 (2017)
[9] R. M. Palomino et al., J. Catal. 329, 87 (2015)
[10] H. T. Luk, et al., Chem. Soc. Rev. 46, 1358 (2017)

Reaction driven ordering of the surface of a PtRh alloy model catalyst

H. Edström,[1] U. Hejral,[1] S. Albertin,[1] K. von Allmen,[1] B. Hagman,[1] E. Lundgren,[1] A. Stierle,[2] C. Seitz,[2] V. Vonk,[2] A. Schaefer,[3] and J. Gustafson[1]

[1]*Synchrotron Radiation Research, Lund University, Box 118, SE-221 00 Lund, Sweden*
(corresponding author: H. Edström, email: helen.edstrom@sljus.lu.se)
[2]*Deutsches Elektronen-Synchrotron (DESY), D-226 03 Hamburg, Germany*
[3]*Department of Physics and Competence Centre for Catalysis, Chalmers University of Technology, SE-412 96 Gothenburg, Sweden*

Transition metals have proved to be efficient in oxidation catalysis [1, 2]. If two transition metals are combined in a supported bimetallic catalyst, this alloy catalyst may exhibit improved activity, selectivity, stability etc compared to the pure metals [3]. One bimetallic catalyst that is often used as a three-way catalyst in automobile engines for oxidation of CO and reduction of NO_x contains Pt and Rh [2–6]. There is a synergism between Pt and Rh in the bimetallic catalyst; for CO oxidation, Pt is more active than Rh during strongly oxidizing conditions, while the opposite is valid for reducing conditions [3]. The PtRh alloy system is well-studied, but not completely understood.

To better understand the catalytic reactions on the atomic level for this bimetallic catalyst, we investigated a $Pt_{25}Rh_{75}(100)$ single-crystal using high-energy surface X-ray diffraction (HESXRD) at beamline P21.2 at PETRA III, DESY, in Hamburg, Germany. Under oxidizing conditions, we found two Rh-O structures that have been observed previously, namely a p(3×1) reconstruction with chemisorbed O [1, 4, 5] and a c(8×2) surface oxide [1, 5, 7]. Under reducing conditions, we found an unexpected c(2×2) structure, see Figure 1a. On Rh(100), CO adsorbs in this structure [1, 8], but the scattering from the adsorbate molecules is usually too weak to be observed in HESXRD. This indicates that we have an ordered surface of the substrate rather than only an adsorbate structure.

We drew the conclusions that the Pt and Rh atoms segregated during catalysis and formed an ordered surface alloy. Our suggested model was that CO molecules adsorb in a c(2×2) structure. The more reactive Rh atoms are pulled towards the adsorbed CO molecules while the Pt atoms are pulled towards positions without adsorbates. If this hypothesis was correct, it would be possible to create this ordered alloy by exposing the crystal to a suitable pressure of pure CO. Despite covering a CO pressure range of 10^{-7} mbar to 10^{-1} mbar, we were not able to recreate the structure in this way. However, after this experiment, we annealed the sample in ultra-high vacuum (UHV), after which the c(2×2) was found. The updated hypothesis is that the gas exposure resulted in a first layer of Rh and a second layer of Pt. When annealing in UHV, the Pt atoms approached the surface, causing a mixed surface layer of 50 at% Pt and 50 at% Rh in a well-ordered c(2×2) structure, as shown in Figure 1b-c.

We see this as a new route to create systems similar to so-called single atom alloy catalysts, avoiding evaporation that is often very time consuming, especially during beamtimes. Further experiments including other alloys, such as $Pd_3Au(100)$, are planned and will be carried out in the near future.

Support by the Swedish Reasearch Council and the Knut and Alice Wallenberg Foundation is gratefully acknowledged.

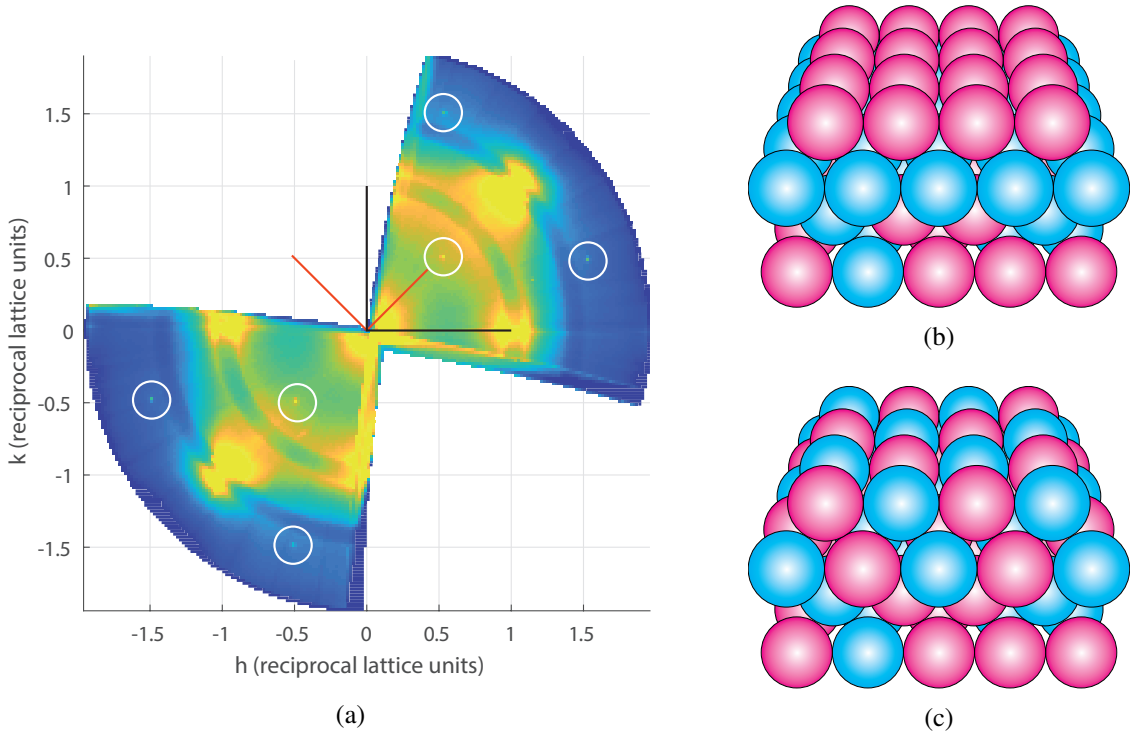

FIG. 1: a) An HESXRD plot of $Pt_{25}Rh_{75}(100)$ during reducing conditions and high temperature reveals the additional spots from the c(2×2) structure, marked by white rings. The black and red lines in the center of the plot mark the unit cells of p(2×2) and c(2×2), respectively. b) Gas exposure pulls out Rh atoms (magenta) to the surface, causing a second layer of Pt atoms (cyan). c) During annealing, Pt atoms segregate towards the surface and a mixed layer is formed, resulting in a well-ordered c(2×2) structure.

[1] J. Gustafson et al., Structure of a thin oxide film on Rh(100), *Phys. Rev. B*, **71**, 1 (2005)
[2] J. Gustafson et al., Sensitivity of catalysis to surface structure: The example of CO oxidation on Rh under realistic conditions, *Phys. Rev. B*, **78**, 1 (2008)
[3] S. H. Oh and J. E. Carpenter, Platinum-rhodium synergism in three-way automotive catalysts, *J. Cat.*, **98**, 178 (1986)
[4] M. Sporn et al., A quantitative LEED analysis of the oxygen-induced p(3 x 1) reconstruction of Pt25Rh75(100), *Surf. Sci.*, **416**, 384 (1998)
[5] R. Westerström et al., Structure and reactivity of a model catalyst alloy under realistic conditions, *J. Phys. Cond. Mat.*, **20**, 6 (2008)
[6] J. Zheng et al., Roadmap for Modeling RhPt/Pt(111) Catalytic Surfaces, *J. Phys. Chem. C*, **122**, 26430 (2018)
[7] J. Gustafson et al., Structure and catalytic reactivity of Rh oxides, *Cat. Tod.*, **145**, 227 (2009)
[8] A. Baraldi et al., CO adsorption and CO oxidation on Rh(100), *Appl. Surf. Sci.*, **99**, 1 (1996)

New spatially-temporal phenomena studied using nano-sized surface structure libraries

Y.Suchorski, J. Zeininger, M. Raab, and G. Rupprechter

Institut für Materialchemie, Technische Universität Wien, A-1060 Wien, Austria
(corresponding author: Y. Suchorski, e-mail: yuri.suchorski@tuwien.ac.at)

Recently, a concept of *surface structure libraries* was introduced based on systems consisting of many crystallographically different regions combined in one sample [1]. Such concept allows studying different surface structures simultaneously, without the necessity to repeat experiments using each time a sample with another structure. Particularly in catalysis, such concept appeared to be promising, since it allows studying reactions on differently structured surfaces at exactly the same external parameters, a condition, which is difficult to fulfil in "sequential" experiments. This concept can be combined with the *kinetics by imaging* approach, where analysis of video-files obtained *in situ* by parallel imaging of differently oriented regions, e,g, by PEEM, provides the kinetic data [2]. This combination allowed detection of new phenomena, such as multifrequential oscillations in H_2 oxidation reaction [4], which cannot be observed on homogeneous, e.g., single crystal surfaces, or revealing the size and shape effects in CO oxidation on Pd [5].

Until now, the polycrystalline metal foils consisting of many μm-sized domains were mainly used as *surface structure libraries* with PEEM as a parallel imaging tool [3,4]. It is challenging to extend such concept to the nm-scale, i.e. to combine differently oriented nm-sized regions in one sample. Curved crystals exposing a continuous variation of surface structure can offer such possibility, provided they can be fabricated in the corresponding size range. Using the etching technology known from the field electron (FEM) and field ion (FIM) microscopies and field evaporation procedure, curved crystal surfaces of platinum group metals can be prepared with smooth, defect free facets ranging from 5 to 100 nm. The hemispherical or ellipsoidal apexes of such specimens (Fig. 1) resemble in shape and size the nanoparticles commercially used in catalysis. However, in contrary to such nanoparticles, they can be characterized with atomic resolution by FIM, and realistic atomic models can be constructed (Fig.1). Subsequently, various catalytic reactions ongoing on such specimens can be imaged in real time by FEM and local reaction kinetics for individual nm-sized facets can be extracted from the *in situ* recorded video-files [6].

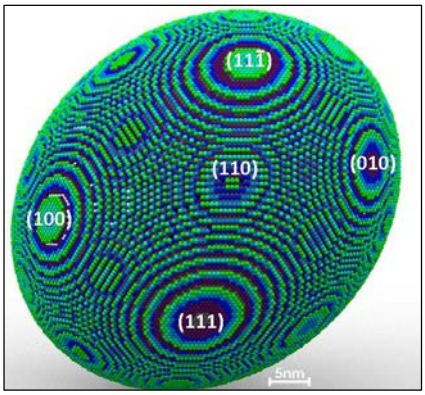

Fig. 1. Realistic 3D ball model of the ellipsoidal nm-sized apex of a Rh specimen, as constructed on the basis of FIM images. The main low Miller index facets are labelled.

In the present contribution, a row of new spatial-temporal phenomena observed in catalytic H_2 oxidation in the 10^{-6} mbar pressure range on differently sized Rh nanofacets is discussed: a nanoclock behaviour, where the reaction exhibit a synchronized oscillating behaviour on differently oriented facets of 5 to 10 nm size, lost of synchronization, when the facet size increases and even multifrequential oscillations, where the reaction oscillates with different frequencies on differently oriented facets, despite of the strong diffusional coupling (the length of diffusion for hydrogen exceeds the specimen size at present temperatures of 400 to 500 K). A particularly interesting effect, a transition from regular self-sustaining periodic oscillations to irregular oscillations was observed for the ellipsoidal specimen. A specific parameter range could be assigned to each type of oscillating process apart of the steady states of high and low activity and bistability. The time-series recorded for the irregular oscillations were studied for the presence of a deterministic chaotic character. The correlation dimension was calculated as a measure of spatial complexity while the approximate entropy was determined to quantify the temporal irregularity and predictability (Fig. 2). Both these parameters display an approximately linear increase along the transition from regular to irregular oscillations, indicating that the spatial and temporal complexity of the observed oscillations increases when reaching the irregular parameter region. Such behaviour of catalytic H_2 oxidation was observed for the first time, moreover, on the nm-scale chaotic behaviour was not yet observed for any catalytic reaction.

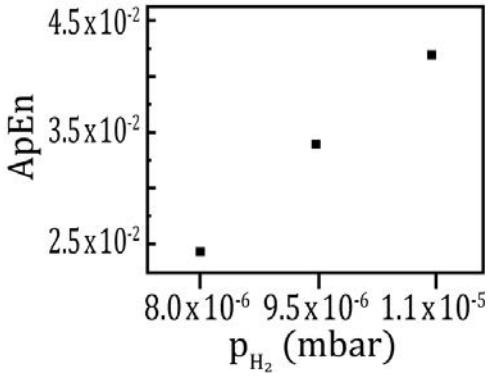

Fig. 2. Approximate entropy ApEn calculated using the method by Pincus [7] in dependence of the partial H_2 pressure at constant O_2 pressure of $4.4 \cdot 10^{-6}$ mbar and temperature of 453 K.

This work was supported by the Austrian Science Fund (FWF) [SFB F45 FOXSI]

[1] Y. Suchorski, G. Rupprechter, Cat. Lett. 148, 2947 (2018)
[2] Y. Suchorski, G. Rupprechter, Surf. Sci. 643, 52 (2016)
[3] Y. Suchorski, M. Datler, I. Bespalov, J. Zeininger, M. Stöger-Pollach, J. Bernardi, H. Grönbeck, G. Rupprechter: J. Phys. Chem. C 123, 4217 (2019)
[4] Y. Suchorski, M. Datler, I. Bespalov, J. Zeininger, M. Stöger-Pollach, J. Bernardi, H. Grönbeck, G. Rupprechter, Nature Comm. 9, 600 (2018)
[5] Y. Suchorski, S. Kozlov, I. Bespalov, M. Datler, D. Vogel, Z. Budinska, K. Neyman, G. Rupprechter, Nature Mat. 17, 519 (2018)
[6] Y. Suchorski, I. Bespalov, J. Zeininger, M. Raab, M. Datler, P. Winkler, G. Rupprechter, Cat. Lett. 2020, in print, DOI: 10.1007/s10562-019-02950-0
[7] S. M. Pincus, Proc. Nat. Acad. Sci. 88, 2297 (1991).

Unexpected bimetallic overlayers formed by Tellurium on Ag(111) and Cu(111) surfaces

T. Kißlinger, A. Raabgrund, M. Ammon, M. A. Schneider, and L. Hammer
Lehrstuhl für Festkörperphysik, Universität Erlangen-Nürnberg, Germany
(corresponding author: L. Hammer, e-mail: lutz.hammer@fau.de)

Tellurium (Te) based alloys play an important role in metallurgy, thermoelectricity and photovoltaics [1] as well as spintronics due to their Rashba-split bands [2]. Dichalcogenides in the 2D limit have also received great attention [3] serving as motivation to look for similar systems grown epitaxially on single crystal surfaces. Such systems would allow for an accurate surface structure determination, which is mandatory for a correct understanding of their diverse physical properties. We studied the formation of Te containing monolayer structures on Ag(111) and Cu(111) with quantitative low-energy-electron diffraction (LEED), scanning tunneling microscopy (STM) and density-functional theory (DFT).

Deposition of Te on a clean Ag(111) surface and subsequent annealing to 100-600°C or direct evaporation within this temperature interval leads to the formation of a (√3×√3)R30° superstructure, which starts at about 0.15 ML of Te and is developed best at 0.33 ML (Fig.1a). STM reveals an almost defect-free film (Fig.1b) with, however, a couple of protruding lines indicating registry shifts with respect to the substrate. This is a clear sign that the film is under enormous tensile stress and indeed, with slight Te overexposure the film starts to shrink unilaterally in $[1\bar{1}0]$ direction by up to about 10%, eventually leading to a wave-like moiré structure.

Atomically resolved images (Fig.1b, inset) suggest a TeAg honeycomb lattice as already reported recently [4]. A quantitative LEED intensity analysis (LEED-IV) for the optimally developed (√3×√3)R30° phase clearly corroborates this model (Pendry R-factor R = 0.15) and finds the Ag and Te atoms of the honeycomb-like overlayer at hcp sites of the substrate, cf. Fig.1c. All other potential surface structures and alternative stackings can be excluded on the basis of their R-factors (R > 0.4) [5]. In contrast to the findings of Liu, et al. [4], the Te atoms are found to be relaxed outwards slight (0.07 Å) in quantitative agreement (as all other structural parameters) with the corresponding DFT model. Our DFT calculations further reveal that the energetic preference of hcp over fcc sites is not more than 6 meV per unit cell, so that registry shifts for strain relief are readily conceivable. Indeed, considering small fractions of a fcc (14%) and bridge site (7%) stacked honeycomb structure, the latter to simulate the transition areas, further improves the LEED fit significantly (R = 0.10).

On the Cu(111) surface we do not find such a (√3×√3)R30° honeycomb phase upon Te deposition (T=100-600°C) but instead a (2√3×√3)*R*30° structure, which starts to evolve at about 0.1 ML and is completed for a coverage of 1/3 ML of Te (Fig.1d). This finding is at variance to earlier reports [6] and has been reproduced in two separate UHV systems. STM

shows an almost perfectly ordered stripe-like phase with a quasi-hexagonal arrangement of protrusions (Fig.1e). The crystallographic structure of this phase is again solved by a LEED-IV analysis (R = 0.10) and consists of Te_2Cu_2 chains with a glide-symmetry plane in the centre (see Fig.1f). All surface atoms are situated at hcp-sites of the substrate with Te atoms protruding by about 0.2 Å. DFT finds within error margins the same geometrical, the structure being 32 meV in total energy per $(2\sqrt{3}\times\sqrt{3})R30°$ cell more favourable than the CuTe-honeycomb phase at hcp sites.

The reason to form one-dimensional chain structures rather than a highly symmetric honeycomb phase as found on Ag(111) may be due to the 12% smaller lattice parameter of Cu. Here, a commensurate honeycomb structure would be under severe compressive strain, with Te atoms pushed further out and by that weakening the bonds towards the substrate. Since the energetic cost of a site switch towards fcc for strain relief is also much higher here (27 meV), the system prefers to realize realize the double chain structure with lower symmetry which allows to relieve strain via a local lateral relaxation of Te atoms (0.14 Å) while preserving the number of nearest neighbour Cu atoms (6).

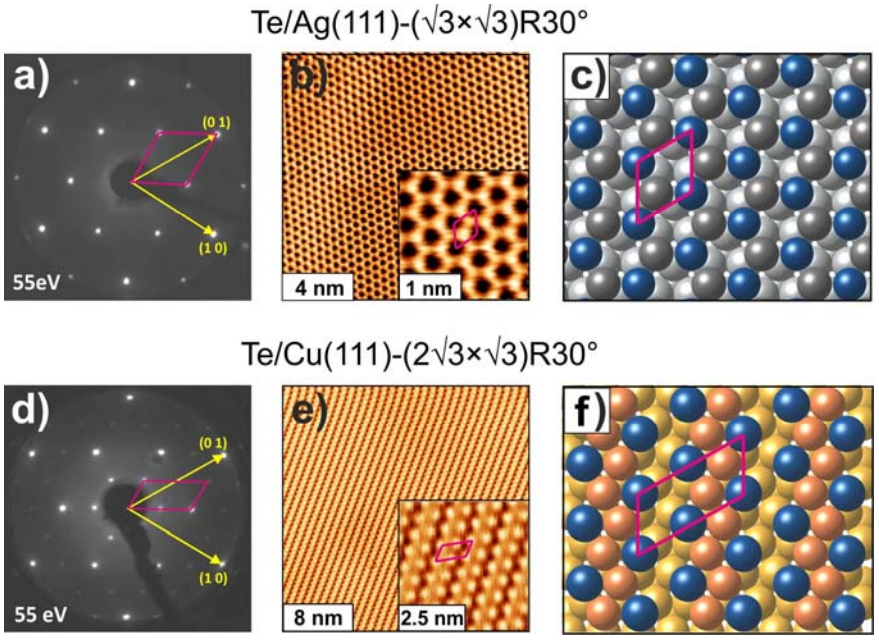

Fig.1:

Results for the 0.33 ML Te phases grown on Ag(111) (top) and Cu(111) (bottom).

a) and d): LEED image with substrate unit vectors (yellow) and superstructure cell (purple).

b) and e): Large scale STM images of the closed films and close-ups with atomic resolution.

c) and f): Ball models of the respective structures in top view.

[1] J. Ibers., Nat. Chem. **1**, 508 (2009).

[2] K. Nakayama, et al., Phys. Rev**. B 95**, 125204 (2017).

[3] K.S. Novoselov et al., PNAS **102**, 10451 (2005).

[4] L. Dong et al., Chin. Phys. Lett. **36**, 028102 (2019); B. Liu et al., J. Phys. Chem. Lett. **10**, 1866 (2019).

[5] M. Ünzelmann, et al., Phys. Rev. Lett. submitted.

[6] S. Andersson, et al., Surf. Sci**. 12**, 269 (1968); M.O. King et al., Surf. Sci. **606**, 1353 (2012); M. Lahti et al., Surf. Sci. **622**, 35 (2014).

Characterization of beryllium-titanium intermetallic compounds with X-ray photoelectron spectroscopy

N. Helfer[1], J. Bröder[2], H. R. Koslowski[1], N. Aghdassi[1], D. Wortmann[2], S. Blügel[2] and Ch. Linsmeier[1]

Corresponding author: ch.linsmeier@fz-juelich.de

[1] *Forschungszentrum Jülich GmbH, Institut für Energie- und Klimaforschung – Plasmaphysik, 52428 Jülich, Germany*

[2] *Forschungszentrum Jülich GmbH, Peter Grünberg Institut and Institute for Advanced Simulation, 52425 Jülich, Germany*

Beryllium is an excellent neutron multiplier and of high interest for the pebble bed blanket design, but cannot be used in metallic form due to its high swelling under neutron irradiation [1][2]. Beryllium intermetallic compounds (beryllides) with high Be content as $Be_{12}V$ and $Be_{12}Ti$ have promising properties of still high breeding rates but reduced hydrogen retention [3][4]. Thermal stability and possible phase transitions of these materials are two important criteria in view of a possible application in a future fusion power plant.

Bulk $Be_{12}Ti$ samples (Materion, formely Brush Wellman, 1950s) show a phase transition within the surface region after annealing over 1000 K [5]. Due to the age of the investigated material and its unknown history several uncertainties arise and a clearly defined system is needed to get a better understanding of the ongoing processes.

Thin titanium films on beryllium are used as such a model system to characterize temperature dependent phase changes with X-ray photoelectron spectroscopy (XPS). Since XPS literature data of the Be-Ti system is not available, the development of a new analysis method is necessary [6]. Chemical shifts of the individual phase contributions are calculated with a full-potential linearized augmented plane wave method (FLAPW), implemented within the FLEUR code [7]. For each chemical environment of individual Be atoms within the unit cell of each phase of the Be-Ti system, a chemical shift (relative to metallic Be) is calculated. Applying Voigt functions according to the experimental conditions and weighted with the number of electrons per chemical environment, artificial pure phase photoelectron spectra are obtained. Figure 1 shows such an artificial pure phase spectrum for $Be_{12}Ti$. The identical number of Be atoms per chemical environment within the unit cell leads to the same intensity for all three contributions. For the analysis of the experimental data, the measured spectra are fitted with a linear combination of the pure phase spectra and allow therefore the determination of the phase composition.

Thin Ti films between 0.5 nm and 4 nm are deposited by electron beam evaporation on polycrystalline beryllium samples. The formation of intermetallic compounds at the interface is enforced by annealing and can already be observed at an intermediate temperature of 600 K, as shown in Figure 2. Under these conditions, in particular Ti-rich phases are formed. The surface phase composition shifts to Be-rich phases with increasing temperature. The metallic Be content is simultaneously decreasing within the information depth.

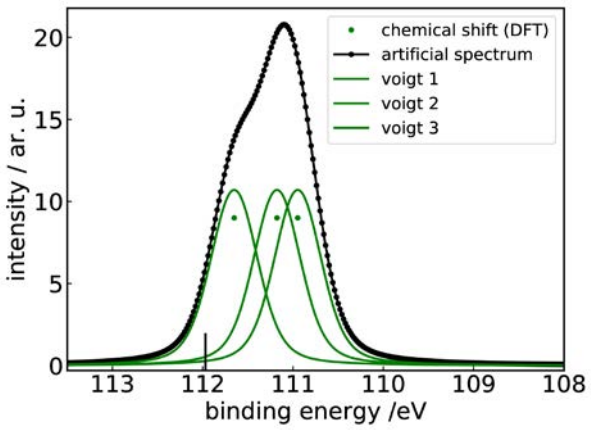

Figure 1: The chemical shift of the three chemical environments compared to metallic beryllium is clearly visible. A Voigt function is centered at each of this distinct energies. Since all of the three possible chemical environments for beryllium host eight atoms, the intensity of these Voigt functions is the same. The sum of all contributions (black) is an artificially generated pure phase $Be_{12}Ti$ spectrum.

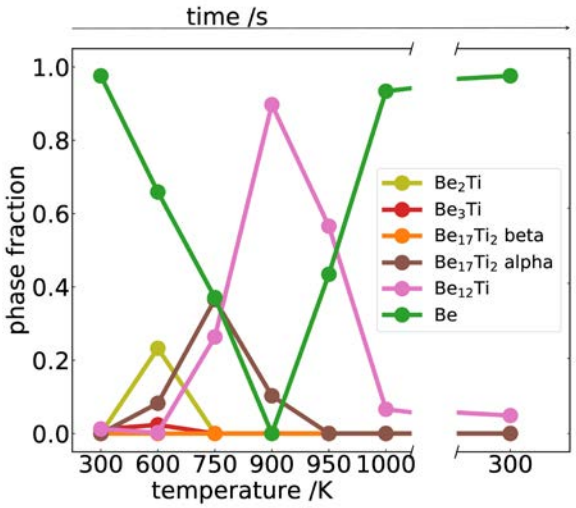

Figure 2: Phase composition within the surface of a beryllium sample covered with a 0.5 nm titanium film. XPS measurement performed under normal emission with samples at the respective elevated temperatures and after final cool down (last data point).

At 900 K $Be_{12}Ti$ is with about 90% the dominating phase. Further increasing the temperature leads to a Be enrichment at the surface, at 1000 K already over 90% of the phase mix consists of metallic Be. Angle-resolved XPS measurements confirm that behavior with increasing temperature with increased surface sensitivity. In these measurements, the contribution of metallic beryllium dominates already at 950 K,. The difference of the phase composition between normal emission and shallow emission angle measurements is largest at 50°. At 1000 K this difference vanishes, since the Be enrichment propagates and covers now the entire information depth.

A decomposition of $Be_{12}Ti$ into $Be_{17}Ti_2$ and metallic Be is one possible process for this enrichment, but segregation and diffusion phenomena need to be considered, too. Further experiments have to elucidate the origin of the beryllium enrichment. Phase formation will be investigated in dependence of available titanium amount and temperature, especially the stability of $Be_{12}Ti$ between 900 and 1000 K.

[1] R. A. Anderl et al., J. Nucl. Mater. 258-263, 750-756 (1998)

[2] M. Nakamichi et al., Nucl. Mater. Energy. 15, 71-75 (2018)

[3] M. Uchida et al., J. Nucl. Mater. 307-311, 653-656 (2002)

[4] H. Yamada et al., Fusion Eng. Des. 69, 269-273 (2003)

[5] N. Helfer, Komparative Untersuchung von Berylliden mit Photoelektronen-Spektroskopie, MA Thesis, TU Dortmund, 2017

[6] J. Bröder, High-Throughput All-Electron Density Functional Theory Simulations for a Data-Driven Chemical Interpretation of X-Ray Photoelectron Spectra, PhD thesis, to be published

[7] Forschungszentrum Jülich. FLEUR: The Jülich FLAPW code family URL: http://www.flapw.de (visited on 15/11/2019

Atomically precise step grids for engineering helical states

J. E. Ortega[1,2,3,*], G. Vasseur[3], I. Piquero-Zulaica[2], F. Schiller[2], J. Raoult[4], M. A. Valbuena[5], S. Schirone[5], S. Matencio[5], Y. Koroteev[3], E. Chulkov[3], A. Mugarza[5,6], and J. Lobo-Checa[7,8]

[1]*Departamento Física Aplicada I, Universidad del País Vasco, San Sebastian, Spain*

[2]*Centro de Física de Materiales CSIC/UPV-EHU, San Sebastian, Spain*

[3]*Donostia International Physics Centre, San Sebastian, Spain*

4 Synchrotron SOLEIL, Gif-sur-Yvette Cedex, France

[5]*Catalan Institute of Nanoscience and Nanotechnology (ICN2), CSIC, Barcelona, Spain.*

[6]*ICREA Institució Catalana de Recerca i Estudis Avançats, Barcelona, Spain*

[7]*Instituto de Ciencia de Materiales de Aragón, CSIC-Universidad de Zaragoza, Spain*

[8]*Departamento Física de la Materia Condensada, Universidad de Zaragoza, Spain*

Conventional spin-degenerated surface electrons have been effectively manipulated by using organic[1,2] and inorganic[3] self-assembled nano-arrays as resonators. Step superlattices naturally assembled in vicinal surfaces are a particularly interesting case since they represent simple one-dimensional (1D) models for fundamental studies, and can imprint strong anisotropies in surface electron transport in real devices. Here we present the first realization of periodic resonator arrays on the $BiAg_2$ atom-thick surface alloy with unprecedented atomic precision, and demonstrate their potential ability for tuning helical Rashba states. We employ a Ag cylindrical crystal curved around the Ag(645) vicinal surface [c-Ag(645) sample] to be able of selecting local vicinal planes with kinked steps[4]. After sublimation and post-annealing of a 0.3 ML Bi layer, we achieve a homogenous $BiAg_2$ surface alloy, featuring sharp arrays of extraordinarily straight Bi-terminated, monoatomic steps, with variable (tunable) density across the curved surface (Figure 1, left). Scanning the ultraviolet light beam on such Bi/c-Ag(645) interface in angle-resolved photoemission (ARPES) experiments allowed us to observe the characteristic signatures of strong and coherent step-lattice scattering in the spin-textured bands of the $BiAg_2$ alloy (Figure 1, right), that is, step-umklapps, and a large, step-density-dependent Rashba band shift. First-principle DFT calculations reveal a complex terrace/step spin/orbital composition, which in turn explains the large spectral broadening and strong photon-energy dependence observed in ARPES. DFT also predicts the split-off of 1D electron-like step and terrace bands dispersing parallel to surface steps[5].

We acknowledge the CERCA programme (Generalitat de Catalunya), the Spanish Ministry of Science, Innovation and Universities (Grants MAT2016-78293-C6 (2-R, 4-R and 6-R), MAT-2017-88374-P and Severo Ochoa No. SEV-2017-0706), the Basque Government (Grant IT-1255-19), the Government of Aragón (RASMIA project) and

the European Regional Development Fund (ERDF) under the program Interreg V-A España-Francia-Andorra (Contract No. EFA 194/16 TNSI).

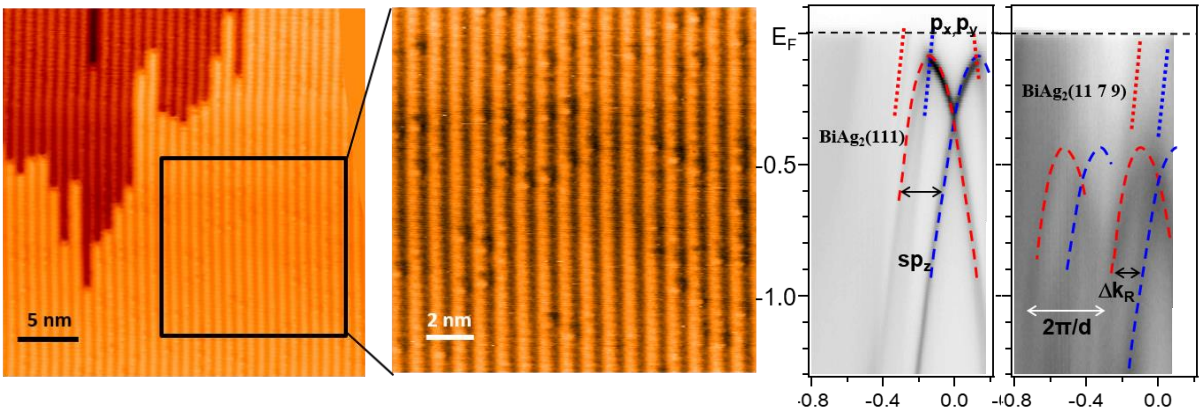

Left, *STM topographic images from $BiAg_2$ surface alloy at the local Ag(11 7 9) plane on a c-$Ag(111)_{fk}$ sample. Sharp, almost defect-free monatomic step arrays are observed.* ***Right, a*** *Rashba helical states (red and blue mark different helicities) measured at two characteristic points on the $BiAg_2$/c-$Ag(111)_{fk}$ system, namely the (111) and the (11 7 9) substrate planes. In the latter, band-shift and step-lattice umklaps are signatures of scattering at the step superlattice.*

1. Lobo-Checa, J. et al. Science 325, 300–303 (2009).
2. Pennec, Y. et al. Nat. Nanotechnol. 2, 99 (2007).
3. Mugarza, A. et al. Phys. Rev. Lett. 87, 107601 (2001).
4. Ortega, J. E. et al., New J. of Phys. 20, 073010 (2018).
5. Ortega, J. E. et al., arXiv:1902.05777 (2019), and submitted.

Single helical spin-polarised Fermi surface in $SrTiO_3$ thin film homostructures

Eduardo Guedes, Stefan Muff, Milan Radovic, and Hugo Dil

Institute of Physics, Ecole Polytechnique Fédérale de Lausanne, Switzerland
Photon Science Division, Paul Scherrer Institut, Villigen, Switzerland
(corresponding author: H. Dil, e-mail: hugo.dil@epfl.ch)

The prospect of a single helical spin-polarised Fermi surface has been one of the driving forces in the research of topological insulators. The main reason is that such a spin texture allows for the formation of quasiparticle responses which are usually forbidden. Prominent examples of this are the magnetic monopole in the presence of a point charge in front of the surface and the Majorana fermion in combination with superconductivity. However, one of the main problems with topological insulators is that most behave like narrow band gap semiconductors, thus making it very difficult to avoid spurious bulk conductivity. This has stimulated the search for systems with a similar surface response but more predictable, or technology ready, bulk characteristics.

One proposal to achieve a single spin-polarised Fermi surface is to combine a Rashba-type spin splitting with magnetic interactions, or an external magnetic field, to open up a Zeeman gap around the zone centre. As illustrated in Figure 1 this leads to a single spin-polarised Fermi surface if the chemical potential is tuned in the gap. This has been the approach used to form the prerequisite for Majorana-type excitations in InSb nanowires in contact to an Al superconductor and in an external magnetic field [1]. However, if the coupling between magnetic dopants and the polar order responsible for the Rashba effect is strong enough a large Zeeman gap can be opened up without the need of an external field [2].

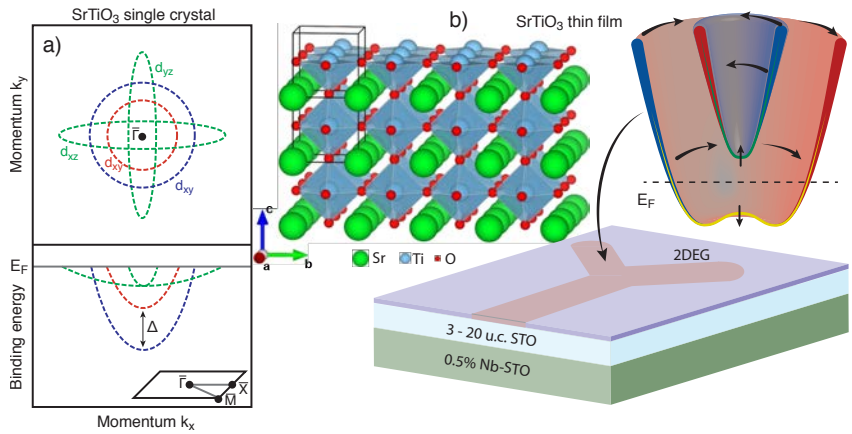

Figure 1 *Electronic structure for the 2DEG on the surface of STO crystals (a) and thin films (b).*

Here it will be shown that exactly this situation can be achieved for the 2DEG on the surface of $SrTiO_3$ (STO) thin films grown on a doped $SrTiO_3$(001) substrate [3]. The band filling of

the 2DEG does not depend on the thickness of the STO film in the measured range from 3-20 unit cells (u.c.) as shown in Figure 2, which indicates that quantum size effects related to the

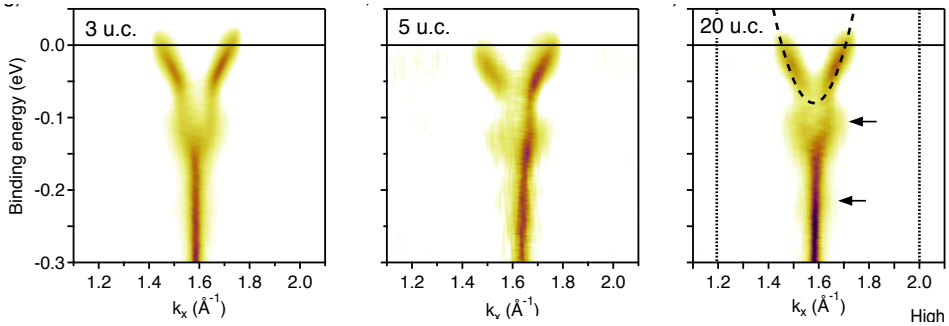

Figure 2 *ARPES data for STO films of various thickness.*

film thickness have no influence. This excludes the common interpretation that the origin of the 2DEG can be found in band bending effects. Instead, it will be shown that the origin can be found in the dielectric response of the system to additional free charges. This interpretation is supported by temperature and surface vicinality (miscut) dependent studies [4].

The data in Figure 2 show only one state crossing the Fermi level, but the verification of the spin texture can only be obtained from spin- and angle-resolved photoemission (SARPES) measurements. The results of these experiments are shown in Figure 3(a) and it is clear that only one spin state is present. Furthermore, as shown in Figure 3(b), the band filling can be altered by changing the doping level of the substrate. Whereby higher electron doping of the substrate results in a lower band filling, which again goes against a simple band bending model.

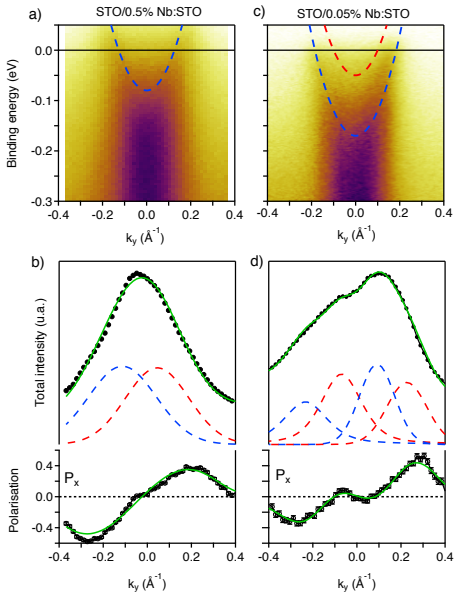

Figure 3 *(S)ARPES data for STO films on substrates with different doping level*

Together with the superconducting properties of STO, this combines all the ingredients to form a 2D Majorana platform on which the required structures can be written by a photon beam, conducting tip, or by local gating of the STO substrate.

[1] V. Mourik et al. Science 336, 1003 (2012)
[2] J. Krempasky et al. Nature Communications 7, 13071 (2016)
[3] Eduardo B. Guedes et al. arXiv:1908.07379 (PRL under review)
[4] Eduardo B. Guedes et al. (in preparation)

HIDEN ANALYTICAL

Mass Spectrometers for Surface Science

Residual Gas Analysis

- Vacuum diagnostics, leak detection and trend analysis
- Ultra-fast data acquisition
- Mass range options: 50, 100, 200, 300 510 amu
- Pulse ion counting detector option for fast event studies including UHV TPD

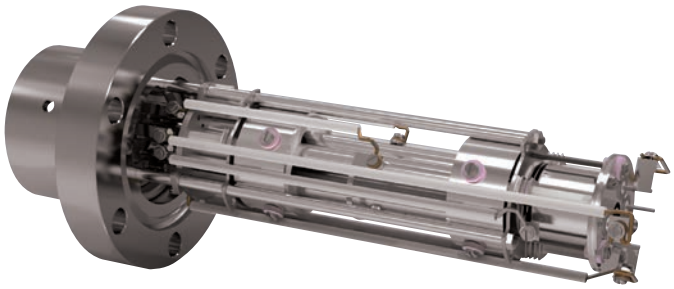

SIMS Systems

- Detect elements, molecules and isotopes
- Static SIMS & dynamic SIMS
- Depth profiling
- Nanometre depth resolution
- Chemical imaging
- Measurement depth from top monolayer to over 30 microns

Mass Spectrometers for Gas Analysis & Catalysis

- Atmospheric pressure gas and vapour analysis
- Fast data acquisition
- 150 ms response time
- Detection from PPB to 100%
- TPD/TPR/TPO and reaction studies

Tuesday

Polarons frozen in a crystal lattice observed by nc-AFM

J. R. L. Redondo,[1,2,3], L. Patera,[4] F. Kraushofer,[1] M. Riva,[1] G. Franceschi,[1] Z. Jakub,[1] I. Sokolovic,[1] M. Schmid,[1] G. S. Parkinson,[1] J. Repp,[4] U. Diebold,[1] M. Setvin[1,2]

[1] *Institute of Applied Physics, TU Wien, Vienna, Austria*
[2] *Faculty of Mathematics and Physics, Charles University in Prague, Prague, Czech Republic*
[3] *Institute of Physics of the Czech Academy of Sciences, Cukrovarnicka 10, Prague, Czech Republic*
[4] *Institute of Experimental and Applied Physics, University of Regensburg, Regensburg, Germany*

(corresponding author: M. Setvin, e-mail: setvin@iap.tuwien.ac.at)

The behaviour of excess electrons and holes in a semiconductor determines the material's physical and chemical properties. In ionic lattices, charge carriers typically do not keep their delocalized character, but adopt a certain degree of localization due to strong electron-phonon coupling. The resulting quasiparticle consisting of the charge carrier and the accompanying phonons is called a polaron [1]. The degree of localization is linked to the polaron mobility: Large polarons, delocalized over several lattice parameters, typically move freely through the lattice and provide metal-like electronic properties. In contrast, small polarons localize within a single unit cell and typically require an activation energy for moving through the lattice.

Polarons influence many intriguing materials properties such as charge transport, superconductivity, colossal magnetoresistance, magnetism, or thermoelectricity, to name just a few. The understanding of polaron physics is limited, and novel experimental approaches are needed to address this problem. Here we show that combined atomic force microscopy/scanning tunnelling microscopy (AFM/STM) holds potential for understanding polaron dynamics. We report results on the hematite (1-102) surface (see Fig. 1a), where electrons and holes form small polarons with high activation energies for hopping to adjacent sites.

The STM functionality allows injection of electrons into the surface; these electrons remain localized near the injection site for days. The electrostatic potential induced by such electrons is shown in Fig. 1b; the image was obtained with Kelvin probe force microscopy (KPFM). The polarons can become mobile under the influence of electric fields, under illumination by visible light, or upon raising the sample temperature above the base temperature of the system (4.8 K).

We have investigated the influence of temperature on polaron mobility in detail, see Fig. 1c. Annealing to increasing temperatures results in a gradual spreading of the polaronic cloud. Our data indicate that the hopping is induced by a combination of the electric field induced by electrostatic polaron-polaron repulsions and thermal activation. The relevant electrostatic fields acting in the system are in order of millivolts per nanometre, and the temperatures relevant for hopping of polarons lie in the range from 4 to 30 K. Experiments were performed

on stoichiometric and Ti-doped hematite samples; on the doped samples we observe a significantly easier mobility of polarons.

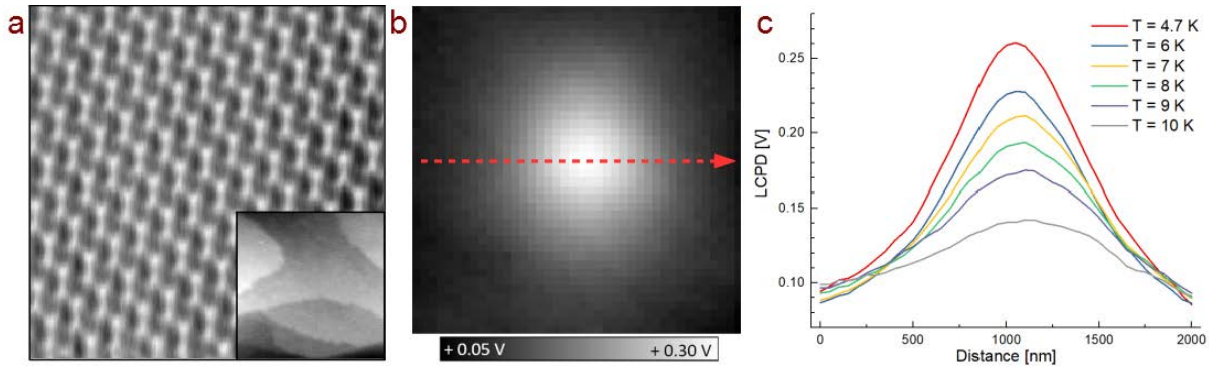

Figure 1. a) Atomically-resolved AFM image of the hematite (1-102) surface. The inset shows a 100 × 100 nm^2 topographic image. b) 2×2 µm^2 map of the electrostatic potential, measured by KPFM, induced by local injection of electrons into the surface. c) Evolution of the electrostatic potential after annealing the sample to various temperatures, measured along the line marked in b). Data obtained for hematite doped with 3% Ti.

Support by the Fonds zur Förderung der Wissenschaftlichen Forschung (FWF), projects SUPER (P32148-N36) and Wittgenstein Preis (Z-250), is gratefully acknowledged.

[1] I. G. Austin and N. F. Mott, Adv. Phys. **50**, 757 (2001)

Stability and Dynamics of Polarons near Oxide Surfaces

Matthias Kick and Harald Oberhofer

Chair for Theoretical Chemistry, Technical University Munich

The importance of oxide materials—and specifically their surfaces—for energy applications is continuously increasing, with applications ranging from photo-electrocatalysts[1,2] to batteries.[3,4] Yet, while this class of materials is highly diverse and versatile, many representatives share common properties, such as the formation of polarons.[4,5] In our contribution we will focus on the formation of polarons in the battery anode material lithium titanium oxide $Li_4Ti_5O_{12}$ (LTO) and especially on the influence polarons have on the material's intended function.

LTO, on the other hand, shows the potential of being an excellent alternative to current state-of-the-art graphite anodes in modern lithium ion batteries. Its volume stays stable during charge cycles and its high intercalation potential hampers Li dendrite formation. Unfortunately, the low conductivity of LTO still limits its use. To improve on this drawback, an elegant way is to introduce oxygen vacancies resulting in formation of Ti^{3+} centers. As a result, this blue colored LTO shows a lowering in its electronic resistance with improved electronic conductivity. By performing *Hubbard corrected density functional theory* (DFT+U) calculations we are able to show that in fact polaron formation and a possible polaron hopping mechanism can play a significant role in the experimental observed improved conductivities.[5] Moreover we are able to gauge polaronic conductivity by explicitly calculating polaron hopping barriers in excellent agreement with experiments.

With a view on its application in batteries we cover both, LTO bulk and surface polarons, considering that the latter are theorized to mediate the formation of dendrites that can potentially destroy the battery.

[1] H. Oberhofer, K. Reuter, J. Chem. Phys. **139**, 44710 (2013)

[2] A. Valdes, ZW. Qu, GJ. Kroes, J. Rossmeisl, JK. Nørskov, J. Phys. Chem. C **112**, 9872 (2008)

[3] B. Zhao, R. Ran, M. Liu, Z. Shao, Mater. Sci. Eng. R Rep. **98**, 1 (2015)

[4] M. Kick, K. Reuter, H. Oberhofer, J. Chem. Theor. Comput. **15**, 1705 (2019)

[5] M. Kick, C. Grosu, M. Schuderer, C. Scheurer, H. Oberhofer, *submitted* (2019)

Varying the chirality of spin textures in ultrathin Pt/Co/Graphene heterostructures by Dzyaloshinskii-Moriya Interactions

M. Blanco Rey[1,2], C. García Fernández[2,3] , M. M. Otrokov[4,2,3], J. I. Cerdá[5] and A. Arnau[1,2,3]

(corresponding author: Andrés Arnau, e-mail: andres.arnau@ehu.eus)

[1] *Departamento de Física de Materiales, UPV/EHU, 20018 Donostia, Spain*

[2] *Donostia International Physics Center (DIPC), 20018, Donostia, Spain*

[3] *Centro de Física de Materiales (CFM-MPC) CSIC/UPV-EHU, 20018, Donostia, Spain*

[4] *Ikerbasque, Basque Foundation for Science, 48011, Bilbao, Spain*

[5] *Instituto de Ciencia de Materiales de Madrid, ICMM-CSIC, Cantoblanco, 28049 Madrid, Spain*

The Dzyaloshinskii-Moriya interaction (DMI) has its origin in the spin-orbit correction of the Heisenberg exchange interactions. It is also called antisymmetric exchange interaction, described by a rank-one first-order effect that favours canting of neighbouring spins and it is, thus, one of the interactions that governs long-range non-collinear spin textures.

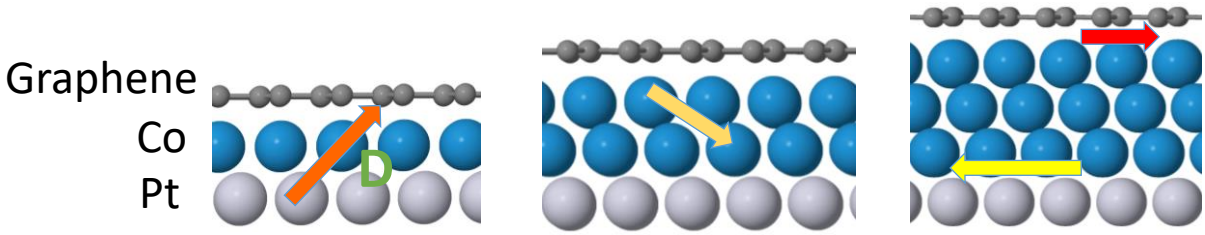

Figure: Schematic representation of the DMI vector (D) directions for three different Co thicknesses of the Pt/Co/Graphene heterostructures.

The DMI is behind the chirality of spin spirals that leads to magnetic domain wall movement [1] or the formation of skyrmions [2]. Since the DMI is forbidden by inversion symmetry, it often appears localized at surfaces and interfaces. Moreover, in multilayer heterostructures the interactions present at each interface can be combined additively [3]. This property opens the door to controlling the chirality of domain wall displacement at selected buried interfaces by epitaxial growth. For example, recent experiments reveal that the strong DMI at a Pt/Co interface may be reduced if the Co film is (pseudomorphically) grown by intercalation between Pt and graphene [4], therefore, suggesting opposite directions of the DM vectors at the Pt/Co and Co/Gr interfaces (see the red and yellow arrows in the Figure for the heterostructure with 3 Co monolayers).

In this work, taking the Pt/Co/Graphene heterostructure as case study, we show how the principle of additivity of interfacial DMI breaks down in the limit of ultrathin films of 1 or 2 Co monolayers, while it is satisfied for Co thicknesses larger than 3 MLs. Our results are based on DFT calculations of spin spirals [5] that permit to obtain the interatomic DMI vectors, D, by fitting total energy differences of long wave length spin spirals with opposite chirality to a model hamiltonian. We find that the magnitude of the in-plane component of D vector, which is likely to modulate the Néel-type domain wall velocity, has a non-trivial oscillatory behaviour as function of Co thickness up to 3ML of Co. Interestingly, we also find a significant out-of-plane component of D, compatible with a more complex chiral spin structure.

[1] Z. Luo, et al., Science 363, 1435-1439 (2019).

[2] A. Fert, V. Cros, J. Sampaio, Nat. Nanotech. 8, 152 (2013).

[3] C. Moreau-Luchaire, et al, Nat. Nanotech. 11, 444 (2016).

[4] F. Ajejas, et al., Nano Lett. 18, 5364-5372 (2018).

[5] M. Heide, G. Bihlmayer, and S. Bluegel, Physica B, 404. 2678-2683 (2009).

Formation and structure of two-dimensional boron on Ir(111)

N. A. Vinogradov, A. Lyalin[1,2], T. Taketsugu[1,3], A. S. Vinogradov[4], and A. B. Preobrajenski

MAX IV Laboratory, Lund University, 22100, Lund, Sweden
(corresponding author: N. A. Vinogradov, e-mail: nikolay.vinogradov@maxiv.lu.se)

[1] *Institute for Chemical Reaction Design and Discovery (WPI-ICReDD), Hokkaido University, Kita 21 Nishi 10, Sapporo 001-0021, Japan*

[2] *Center for Green Research on Energy and Environmental Materials (GREEN), National Institute for Materials Science, Namiki 1-1, Tsukuba 305-0044, Japan*

[3] *Department of Chemistry, Faculty of Science, Hokkaido University, Kita 10 Nishi 8, Sapporo 060-0810, Japan*
[4] *St. Petersburg State University, St. Petersburg, 198504, Russia*

Unique synthetic 2D materials, which host electronic or spatial structure and properties not typical for their bulk allotropes, can be grown epitaxially on atomically-flat surfaces; the design and investigation of these novel materials are thus at the forefront of current research.

Borophene – a synthetic 2D material composed of elemental boron arranged in a planar structure – is a relatively new member of the 2D material family. Borophene is particularly interesting for its polymorphism, which allows for the atomic-scale design of its structure and properties. The reason for this remarkable structural flexibility is the electron deficiency in boron, resulting in the competition between two- and three-centre bonding in borophenes [1]. As the balance between directional and multicentre bonding can be achieved in a variety of structural motifs, polymorphism is common in both bulk boron [2] and in borophenes [3,4]. Borophenes exhibit many exciting physical properties, such as metallicity in the majority of phases [1,4,5], high mechanical flexibility and strength [6,7], optical transparency [8] and ability to host Dirac cones [9] with tremendous potential for electronic applications.

These properties of borophene stipulated an extensive research in the field of synthetic 2D boron-based materials. Since a formation of true two-dimensional boron has been reported on Ag(111) substrates [10,11], silver seemed to provide the best metallic substrates for borophene growth. However, in the last year the research of borophenes was almost explosive, with different borophenes reported growing on Al(111) [12], Cu(111) [13], and Au(111) [14]. A similarity between all these substrates is that these are not prone to boride formation, yet active enough to stabilize a two-dimensional boron blanket on top. In this

respect, it was very curious and instructive whether a true 2D boron blanket could also be formed on Ir(111) substrate.

Indeed, we found that it is possible to grow borophene on surface of Ir(111) by exposing it, while annealing, to the flux of elemental boron. By means of scanning tunnelling microscopy and density functional theory calculations we reveal a complex structure of this borophene, different from all planar boron allotropes reported earlier. This structure forms as a unique single phase on iridium substrate in a wide range of experimental conditions and may be then decoupled from the substrate via intercalation [15]. These findings allow for production of large, defect-free borophene sheets and advance theoretical understanding of polymorphism in boron and its two dimensional allotrope – borophene.

[1] Tang, H. and Ismail-Beigi, S. Phys. Rev. Lett. 99, 115501 (2007).
[2] An, Q.; Reddy, K. M.; Xie, K. Y.; Hemker, K. J.; Goddard III, W. A. Phys. Rev. Lett. 117, 085501 (2016).
[3] Wu, X.; Dai J.; Zhao Y.; Zhou Z.; Yang J.; Zeng X. C. ACS Nano 6, 7443 (2012).
[4] Penev, E. S.; Bhowmick, S.; Sadrzadeh, A.; and Yakobson, B. I. Nano Lett. 12, 2441 (2012).
[5] Feng, B.; Zhang J.; Liu R.-Y.; Takushi I.; Lian C.; *et al*. Phys. Rev. B 94, 041408(R) (2016).
[6] Zhang, Z.; Mannix A. J.; Hu Z.; Kiraly B.; Guisinger N. P.; *et al*. Nano Lett. 16, 6622 (2016).
[7] Zhang, Z.; Yang, Y.; Penev, E. S.; Yakobson, B. I. Adv. Funct. Mater. 27, 1605059 (2017).
[8] Adamska, L.; Sadasivam, S.; Foley IV, J. J.; Darancet, P.; Sharifzadeh, S. J. Phys. Chem. C 122, 4037 (2018).
[9] Zhou, X.-F.; Dong, X.; Oganov, A. R.; Zhu, Q.; Tian, Y.; Wang, H.-T. Phys. Rev. Lett. 112, 085502 (2014).
[10] Mannix A. J.; Zhou X.-F.; Kiraly B.; Wood J. D.; Alducin D.; *et al*. Science 350, 1513 (2015).
[11] Feng, B.; Zhang J.; Zhong Q.; Li W.; Li S.; *et al*. Nat. Chem. 8, 563 (2016).
[12] Li, W.; Kong, L.; Chen, C.; Gou, J.; Sheng, S.; *et al*. Sci. Bull. 63, 282 (2018).
[13] Wu, R.; Drozdov I. K.; Eltinge S.; Zahl P.; Ismail-Beigi S.; *et al*. Nature Nanotech. 14, 44 (2019).
[14] Kiraly, B.; Liu, K.; Wang, L.; Zhang, Z.; Mannix, A. J.; *et al*. ACS Nano 13, 3816 (2019).
[15] N. A. Vinogradov, A. Lyalin, T. Taketsugu, A. S. Vinogradov, and A. B. Preobrajenski, ACS Nano, *in print*

Emerging magnetism in boron-doped graphene nanoribbons

Pedro Brandimarte,[1*] Niklas Friedrich,[2*] Jingcheng Li,[2] Shohei Saito,[3] Shigehiro Yamaguchi,[4] Iago Pozo,[5] Diego Peña,[5] Thomas Frederiksen,[1,6] Aran Garcia-Lekue,[1,6] Daniel Sánchez-Portal,[1,7] and Jose Ignacio Pascual[2,6]

[1]*Donostia International Physics Center (DIPC), 20018 Donostia-San Sebastián, Spain (corresponding author: Pedro Brandimarte, e-mail: brandimarte@pm.me)*

[2]*CIC nanoGUNE, 20018 Donostia-San Sebastián, Spain*

[3]*Graduate School of Science, Kyoto University, Kyoto 606-8502, Japan*

[4]*Graduate School of Science, Nagoya University, Nagoya 464-8602, Japan*

[5]*CIQUS, Centro Singular de Investigación en Química Biolóxica e Materiais Moleculares, 15705 Santiago de Compostela, Spain*

[6]*Ikerbasque, Basque Foundation for Science, 48013 Bilbao, Spain*

[7]*Centro de Física de Materiales CSIC-UPV/EHU, 20018 Donostia-San Sebastián, Spain*

Graphene nanoribbons (GNRs) are strong candidates as a platform for future nanoelectronics. On the one hand, they present a highly tunable electronic structure, that depends on the structure width and edge topology,[1] as well as on chemical functionalization[2] and doping[3]. On the other hand, they can be fabricated with atomic precision via bottom-up approaches, such as metal-catalysed on-surface synthesis,[4] and their electronic properties engineered through controlled growth.

Spin polarized states were long ago theoretically predicted on GNRs with zigzag edges[5] and more recently on the boundary of ribbons junctions and on the terminations of finite ribbons.[6] Nevertheless, unambiguous experimental observation of the magnetism in defect-free GNRs is still scarce, e.g., via spin-polarized scanning tunneling microscope (STM) or electron spin resonance (ESR) STM or Kondo fingerprints.

Here we present a joint theoretical and experimental determination of spin polarized states on 7-armchair GNRs induced by pairs of boron-substituted atoms in the ribbon backbone (2B-GNR). The presence of those states were revealed by a zero-bias Kondo resonance at electronic transport measurements, performed on a lift off configuration where the boron-doped GNR bridged the STM tip and the metallic substrate. First principles calculations via density functional theory (DFT) demonstrated that the Kondo signature can be associated to a spin 1/2 state localized in the suspended GNR when the first boron atom detaches from the metal (**Figure a**). After detaching the full boron pair segment, the magnetic state is predicted to evolve into a spin 1 state localized around the boron-group (**Figure b**). When two boron pair segments are put together, spin 1/2 states appear at the boundary between pristine and borylated segments. Therefore, depending on the concentration of the boron pair segments, different kinds of spin chains can be formed, making the 2B-GNRs attractive for spintronic devices.

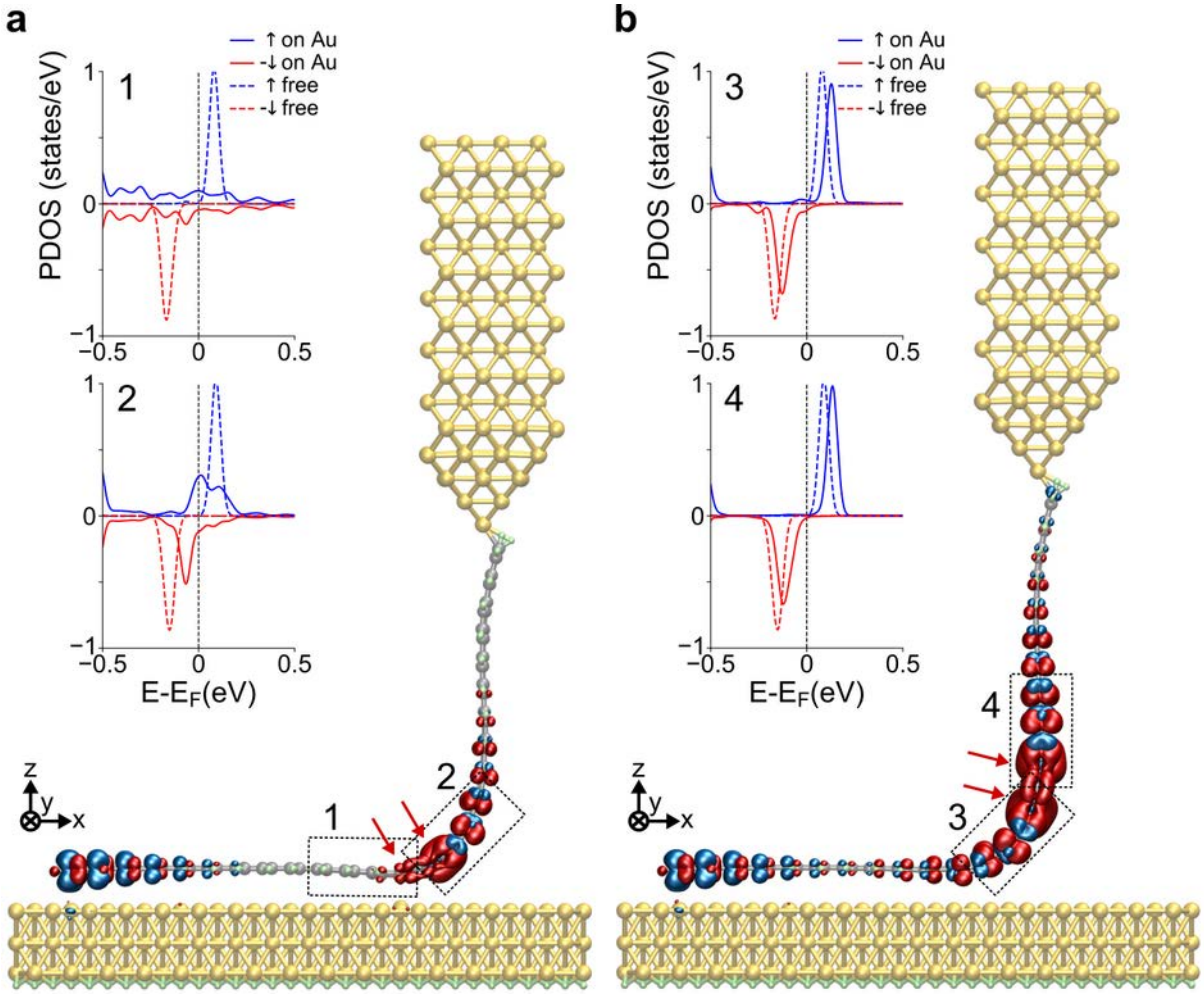

Figure: DFT optimized structures of two different configurations of a 2B-GNR contacted and lifted by a model STM tip. Red arrows indicate the position of the boron pair. Magnetization isosurfaces are shown over the atomic structure (1.7×10^{-3} e/Å^3, spin up in blue and down in red). The insets show the spin polarized density of states of a free standing ribbon (dashed lines) and of the contacted ribbons on the surface (solid lines) projected on the C and B atoms belonging to the regions marked with dashed rectangles in the atomic structures. The GNR zigzag termination holds a radical state with spin-polarization, which is quenched in the side contacted by the gold tip.

Support by the European Union FET Open project SPRING (grant 863098) and by the Spanish Ministry of Economy and Competitiveness, MINECO (grants FIS2017-83780-P and MAT2016-78293-C6).

[1] Y.-W. Son *et al*. *Phys. Rev. Lett.* **97**, 216803 (2006).
[2] E. Carbonell-Sanromà *et al*. *ACS Nano* **11**, 7355 (2017).
[3] E. Carbonell-Sanromà *et al*. *Nano Letters* **17**, 50 (2017);
E. Carbonell-Sanromà *et al*. *J. Phys. Chem. C* **122**, 16092 (2018).
[4] J. Cai *et al*. *Nature* **466**, 470 (2010).
[5] M. Fujita *et al*. *J. Phys. Soc. Jpn.* **65**, 1920 (1996).
[6] T. Cao *et al*. *Phys. Rev. Lett.* **119**, 076401 (2017).

Probing the magnetism of topological end-states in 5-armchair graphene nanoribbons

J. Lawrence,[1, 2,†] P. Brandimarte,[1,†] A. Berdonces,[1,2] M. S. G. Mohammed,[1,2] A. Grewal,[3] Ch. C. Leon,[3] D. Sanchez-Portal,[1,2,*] D. G. de Oteyza[1,2,4,*]

1 Donostia International Physics Center, 20018 San Sebastián, Spain
2 Centro de Fisica de Materiales, CSIC-UPV/EHU, 20018 San Sebastián, Spain
3 Max-Planck-Institut für Festkörperforschung, 70569 Stuttgart, Germany
4 Ikerbasque, Basque Foundation for Science, 48011 Bilbao, Spain
† These authors contributed equally
** (corresponding authors: daniel.sanchez@ehu.eus, d_g_oteyza@ehu.eus)*

We extensively characterize the electronic structure of ultra-narrow graphene nanoribbons (GNRs) with armchair edges and zig-zag termini that have 5 carbon atoms across their width (5-AGNRs), as synthesised on Au(111), by means of Scanning Tunnelling Microscopy and Spectroscopy (STM/STS) experiments and Density Functional Theory (DFT) and tight-binding calculations. STM/STS measurements on the ribbons, recorded on both the metallic substrate and a decoupling NaCl layer, show well-defined dispersive bands and in-gap states. In combination with theoretical calculations, we show how these in-gap states are topological in nature and localised at the zig-zag termini of the nanoribbons. Besides rationalising the driving force behind the topological class selection of 5-AGNRs, we also uncover the length-dependent behaviour of these end states which transition from singly occupied spin-split states to a closed-shell form as the ribbons become shorter. Finally, we demonstrate the magnetic character of the end states via transport experiments in a model two-terminal device structure in which the ribbons are suspended between the scanning probe and the substrate that both act as leads.

We acknowledge funding from the European Union's Horizon 2020 programme (Grant Agreement Nos. 635919 and 863098 from ERC and FET Open projects, respectively), from the Spanish MINECO (Grant Nos. FIS2017-83780-P and MAT2016-78293-C6) and from the University of the Basque Country (Grant IT1246-19). D. G. O. thanks the Alexander von Humboldt Foundation for supporting his research stay at the MPI, and Klaus Kern for hosting him. We thank Peter Liljeroth for his generous donation of the molecular precursors used in this study.

Growing perfect graphene on a liquid metal: from self-assembled flakes to the single layer

M. Jankowski, A. Saedi[1], F. La Porta[2], A. Manikas[3], C. Galiotis[3], J.M. de Voogd[4], G.J.C. van Baarle[4], I. Groot[1], O. Konovalov[2], and G. Renaud

Univ. Grenoble Alpes, CEA, IRIG/MEM/NRS 38000 Grenoble, France (corresponding author: G. Renaud, e-mail: gilles.renaud@cea.fr)

[1]Leiden University, P.O. Box 9502, 2300 RA Leiden, The Netherlands

[2]ESRF−The European Synchrotron, 71 Avenue des Martyrs, 38000 Grenoble, France

[3] Dept. of Chem. Eng., University of Patras, Patras 26504, Greece

[4] Leiden Probe Microscopy (LPM), Leiden, The Netherlands

The current approach to graphene (Gr) synthesis generally relies on CVD growth on solid substrates, mainly copper. Despite recent progresses and fine-tuning of the growth procedures there are significant obstacles in transferring the current knowledge towards mass production of good quality sheets over large scales. The main showstoppers are slow procedures of 2DMs separation from solids, their environmental unfriendliness, and low quality of produced layers. All these factors significantly affect process costs, speed, and waste production. In this talk, we present the first experimental results of graphene growth on liquid copper. Contradictory to solid, this later is an atomically smooth, isotropic and mobile medium, which allows producing graphene crystals of extremely high quality and large sizes limited only by the liquid bath surface.

The aim of the LMCat (liquid metal catalysis) EU Horizon 2020 project has been first to develop a new CVD reactor, dedicated to the study of chemical reactions on LMCats, and second to investigate *in situ* and *operando* the growth of 2D materials (2DMs) on liquid metal surfaces by combining *in situ* synchrotron X-ray diffraction and optical microscopy, supported by *ex situ* Raman spectroscopy. These allowed us to resolve in *real-time* the growth dynamics and atomic structure of graphene during its growth on liquid copper.

Optical microscopy, used *operando* during the growth, happened to be an excellent tool not only to describe and possibly understand the growth processes, but even more importantly, to monitor the growth in real time, by tuning the growth parameters (pressures, temperatures, flows) to direct the growth into particular directions. It is known that the shape of the nucleated graphene flakes is a strong function of the CVD conditions, and the flakes tend to

self-assemble into a hexagonal mosaic pattern on molten copper. Analysis of the real-time movies taken by *in situ* optical microscopy has provided us with unpreceded details about the dynamics of the flake growth and self-assembly. Combined with theoretical simulations, a theoretical model has been developed to explain the observed long-range interactions between the flakes, based on the capillary and electrostatic forces between them. Different growth scenario were tested, leading either to organized flakes of largely varying sizes, up to several tenth of mm, or even to the growth a one single perfectly single-crystalline large flake, up to several millimeters in size. The shape of the flakes is also found to evolve from hexagons with rounded corners to perfect hexagons to concave equilateral dodecagon as a function of growth time (and thus of size).

Grazing Incidence X-Ray Diffraction, performed at different European Synchrotron Radiation facilities, showed that all flakes are perfect single crystal, without the height undulation usually present in graphene, and with the lattice parameter expected for graphene. Moreover, X-Ray Reflectivity confirmed that the grown graphene is one single layer high, and sits above the liquid copper, with a gap shorter than expected for a simple van der Waals interaction.

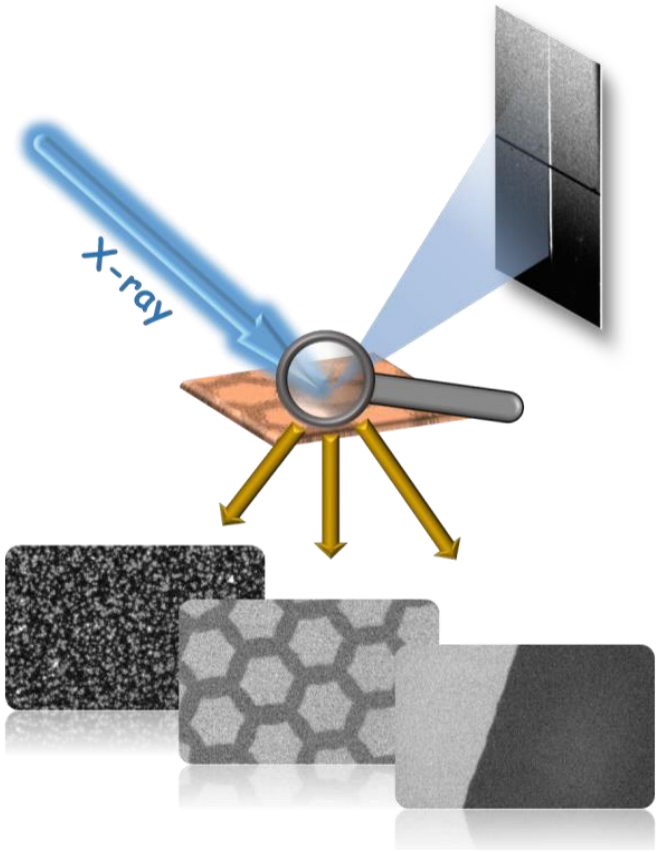

A myriad of interesting growth scenarios was observed which allowed to fine-tune the fabrication procedures and to identify key factors influencing the growth of individual flakes, their self-assembly and further association into a single layer with a coherent atomic structure.

The obtained results are mandatory to establish the methodology for the continuous production of graphene sheets on LMCats and pave a new way for the future cost-effective and large-scale fabrication of 2DMs.

Support by the EU Horizon 2020 FET-Open Fond , project LMCat, is gratefully acknowledged.

[1] Taccardi, N. et al. Nat. Chem. 9, 862– 867 (2017).
[2] Kula, P. et al. App. Mech. Mat. 510, 8–12 (2014).
[3] Geng, D. et al. PNAS 109, 7992-7996 (2012).

Ultra-High Ionic Exclusion Through Carbon Nanomembranes

Yang Yang*, Roland Hillmann, Yubo Qi, Riko Korzetz, Niklas Biere, Daniel Emmrich, Michael Westphal, André Beyer, Dario Anselmetti and Armin Gölzhäuser

Faculty of Physics, Bielefeld University, 33615 Bielefeld, Germany
(corresponding author: A. Gölzhäuser, e-mail: ag@uni-bielefeld.de)
**also with Barrer Center, Imperial College London, London SW7 2AZ, United Kingdom*

Osmotic water transport is a fundamental process enabling life. To achieve it, nature utilizes membrane proteins (aquaporin) with only 0.3 nm wide channels that efficiently transport water molecules in a "single-file" motion across cell membranes but block all ionic species [1]. In recent years, this collective movement of water in natural nanoconduits inspired the creation of artificial membranes with similar "sub-nanometer" channels for water treatment [2]. However, a thin membrane material that contains a large number of sub-nm pores combining rapid water flow with superior ion rejection is still highly desirable.

It has been shown that 1.2 nm thick carbon nanomembranes (CNMs) [3] made from cross-linking of terphenylthiol (TPT) self-assembled monolayers possess an extremely high pore density of $\sim 10^{18}$ m^{-2}*, i.e. one sub-nm channel per square nanometer* [4]. In this presentation, it will be demonstrated by conductivity measurements in aqueous salt solutions that TPT CNMs efficiently hinder the translocation of ions, including protons, while they let water molecules rapidly pass through [5]. Their membrane resistance reaches $\sim 10^4$ $\Omega \cdot cm^2$ in 1 M Cl^- solutions, comparable to lipid bilayers of a cell membrane. Consequently, a single CNM channel yields a $\sim 10^8$ higher resistance than pores in lipid membrane channels and carbon nanotubes. The ultra-high ionic exclusion by CNMs is likely dominated by a steric hindrance mechanism, coupled with electrostatic repulsion, surface functional groups and entrance effects. We demonstrate the operation of TPT CNMs as semipermeable membranes in forward osmosis [5], and discuss possible applications in cold concentration and membrane distillation. These observations highlight the potential of utilizing CNMs for water treatment and open up simple avenues to create 2D membranes through molecular self-assembly for highly selective and fast separations.

[1] P. Agre, *Angew. Chem. Int. Ed.* **2004**, 43, 4278.
[2] K. Gopinadhan, S. Hu, A. Esfandiar, M. Lozada-Hidalgo, F. C. Wang, Q. Yang, A. V. Tyurnina, A. Keerthi, B. Radha, A. K. Geim, *Science* **2019**, *363*, 145.
[3] A. Turchanin and A. Gölzhäuser: Carbon Nanomembranes (review), *Adv. Mater.* **2016**, 28, 6075.
[4] Y. Yang, P. Dementyev, N. Biere, D. Emmrich, P. Stohmann, R. Korzetz, X. Zhang, A. Beyer, S. Koch, D. Anselmetti, A. Gölzhäuser, *ACS Nano* **2018**, *12*, 4695.
[5] Y. Yang, R. Hillmann, Y. Qi, R. Korzetz, N. Biere, D. Emmrich, M. Westphal, B. Büker, A. Hütten, A. Beyer, D. Anselmetti, A. Gölzhäuser, *Adv. Mater.*, *DOI:10.1002/adma.201907850, in press.*

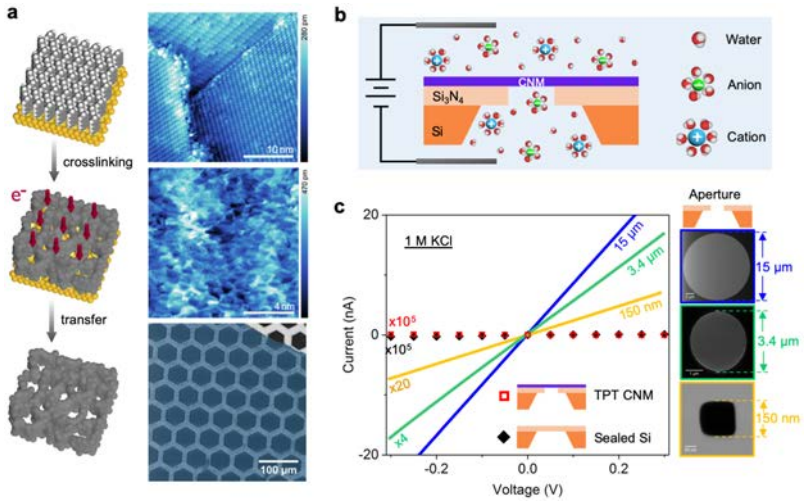

Fig. 1 a) Scheme and AFM images of CNM fabrication by crosslinking of TPT monolayers (top and middle), Helium Ion Microscope (HIM) image of a CNM suspended over a hexagonal copper grid (bottom). **b)** Diagram of ion transport experiments with freestanding TPT CNMs. **c)** I–V curves in 1 M KCl solution using open apertures (size determined by HIM), TPT CNMs suspended over a 15-μm-sized aperture, and a sealed Si_3N_4/Si chip (from ref. [5]).

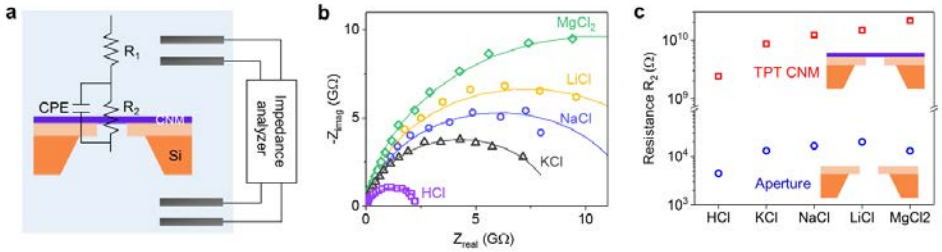

Fig. 2. a) Equivalent circuit for impedance spectra. **b)** Nyquist plots of impedance spectra for a TPT CNM in 1 M solutions of HCl, LiCl, KCl, NaCl and $MgCl_2$. **c)** Comparison of transport resistance through the aperture and TPT CNM in 1 M chloride solutions (from ref. [5]).

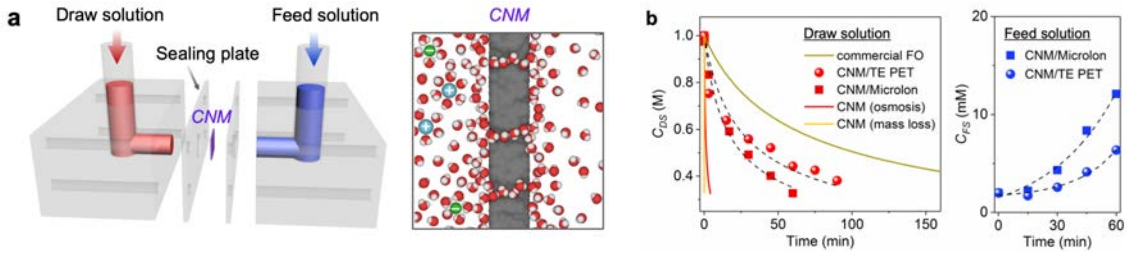

Fig. 3. Forward osmosis with CNMs. **a)** diagram of the permeation cell and schematic illustration of an effective osmotic process with CNMs: single-file water motion and high ionic exclusion in CNM sub-nm channels. **b)** Concentration of the draw solution side C_{DS} (1 M NaCl at $t = 0$) and the feed solution side C_{FS} (2 mM NaCl at $t = 0$) as a function of time (from ref. [5]).

Perforation of 2D heterostructures

J. Schwestka[1], A. Niggas[1], H. Inani[2], S. Creutzburg[3], J. Kotakoski[2],
R.A. Wilhelm[1,3] and F. Aumayr[1]

[1]*TU Wien, Institute of Applied Physics, 1040 Vienna, Austria*
[2]*University of Vienna, Faculty of Physics, Boltzmanngasse 5, 1190 Wien, Austria*
[3]*Helmholtz-Zentrum Dresden-Rossendorf, Institute of Ion Beam Physics and Materials Research, 01328 Dresden, Germany*

Two-dimensional materials such as graphene and transition metal dichalcogenide monolayers open a wide range of potential applications including biological sensors, electronic devices, DNA sequencing, water desalination and purification. Especially for the latter, it is essential to consider that the efficiency for separation is limited by the transmission speed of the particles and by the selectivity. Therefore, 2D materials as sieving membranes and sophisticated ways to perforate them are highly requested [1]. Using high-energy electrons, ion beam lithography or focussed ion beams for hole drilling results either in creation of single or double vacancies only or high fluencies are necessary for the required results, which is not suitable for mass production [2]. Slow highly charged ions (HCIs) on the other hand, carry high potential energy initially stored in their production process. They are favoured for surface-only modifications, i.e. 2D membranes, as they enable deposition of large fractions of their ionization energy within a very shallow area. Once the potential energy exceeds a certain threshold perforation with pores of tunable sizes becomes feasible, depending on the applied ion charge state [3].
Figure 1 shows the successful perforation of a 1nm thick carbon nanomembrane (CNM) after irradiation with 176 keV Xe^{40+} ions.

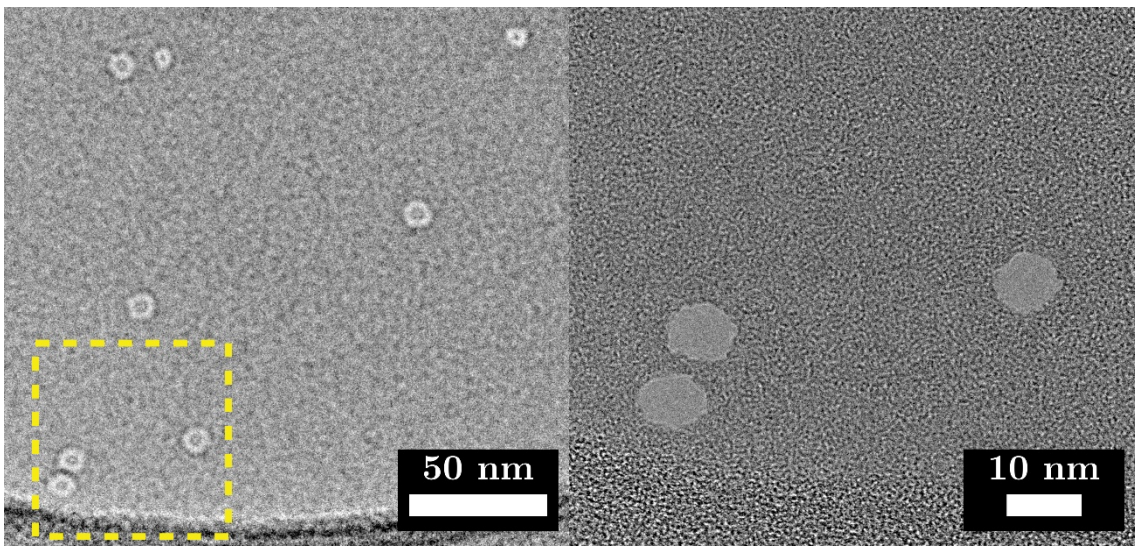

Figure 1 - TEM images of observed pore formation in 1nm thick carbon nanomembrane after irradiation with 176 keV Xe^{40+} ions. The right image shows zoom of yellow marked area in left image. Taken from [3].

Further, it was recently shown that such holes with an adjustable radius of 0.3-3 nm can also be drilled not only in supported molybdenum disulfide (MoS_2) but also in the free-standing monolayer [2] via slow HCI impact. The nature for damage creation is very likely the same for both materials, the release of energy due to the neutralization and deexcitation of the HCI.
However, bombarding a single layer of graphene (SLG) under the same experimental conditions, has not shown any evidence for efficiently drilling of pores into the membrane so far. We therefore assume the high electron mobility within the semimetal graphene sheet as the reason for prevention of perforation. The missing charge, created through the fast charge exchange with the ion, is promptly resupplied leading therefore to suppression of Coulomb explosion [4].

In current experiments, we irradiate heterostructured 2D samples consisting of a monolayer MoS_2 on top of SLG and vice versa with slow HCIs. Large areas of the sample consist of regimes covered by the MoS_2-SLG structure while small areas with either SLG or MoS_2 only remain. In earlier studies, stacks of CNMs were irradiated with HCIs and pore formation was observed in all stacks even tough with decreasing efficiency for higher stack number [3]. However, our results on the irradiation of the heterostructures again indicate no pore formation when SLG faces the ion beam and covers the MoS_2. Further, when reversing the order of layers, i.e. the MoS_2 faces the ion beam, nano-sized damages in the monolayer are observed. Possible mechanism for SLG protecting the MoS_2 from pore formation will be discussed.

Support by the TU-D doctoral collage of the TU Wien is gratefully acknowledged.

[1] K. Celebi, J. Buchheim, R.M. Wyss, A. Droudian, P. Gasser, I. Shorubalko, J.-I. Kye, C. Lee, H.G. Park, Science 344, 289–292 (2014)

[2] R. Kozubek, M. Tripathi, M. Ghorbani-Asl, S. Kretschmer, L. Madauß, E. Pollmann, M. O'Brien, N. McEvoy, U. Ludacka, T. Susi, G.S. Duesberg, R.A. Wilhelm, A. V Krasheninnikov, J. Kotakoski, M.Y. Schleberger, J. Phys. Chem. Lett. 10, 904–910 (2019)

[3] R.A. Wilhelm, E. Gruber, R. Ritter, R. Heller, A. Beyer, A. Turchanin, N. Klingner, R. Hübner, M. Stöger-Pollach, H. Vieker, G. Hlawacek, A. Gölzhäuser, S. Facsko, F. Aumayr, 2D Mater. 2, 35009 (2015)

[4] E. Gruber, R.A. Wilhelm, R. Petuya, V. Smejkal, R. Kozubek, A. Hierzenberger, B.C. Bayer, I. Aldazabal, A.K. Kazansky, F. Libisch, A. V Krasheninnikov, M. Schleberger, S. Facsko, A.G. Borisov, A. Arnau, F. Aumayr, Nat. Commun. 7, 13948 (2016)

Neutralization of moderately charged ions transmitted through graphene sheets – what is it good for?

B. Seiferle[1], L. von der Wense[1], P. V. Bilous[2], I Amersdorffer[1], C Lemell[3], F Libisch[3], S. Stellmer[4], T. Schumm[5], C. E. Düllmann[6,7,8], A. Pálffy[2], and P. G. Thirolf[1]

[1]*Ludwig-Maximilians-University Munich, Garching, Germany*
[2]*Max-Planck-Institut für Kernphysik, Heidelberg, Germany*
[3]*Institute for Theoretical Physics, TU Wien, Vienna, Austria*
[4]*University of Bonn, Bonn, Germany*
[5]*Atominstitut, TU Wien, Vienna, Austria*
[6]*GSI Helmholtzzentrum für Schwerionenforschung, Darmstadt, Germany*
[7]*Helmholtz Institute Mainz, Mainz, Germany*
[8]*Johannes Gutenberg University, Mainz, Germany*

Interest in neutralization of ions in front of surfaces has been renewed over the past years due to the advent of exotic target materials such as, e.g., free standing ultrathin target layers, in particular (multi-layer) graphene sheets. Apart from academic interest, this process extensively investigated over decades has recently been used in an unexpected research field: it can help to indirectly measure the excitation energy of the first excited isomeric state of ^{229m}Th known to have the lowest excitation energy of all nuclear states.

Typically, nuclear excitation energies are in the keV range. For ^{229m}Th, however, previous measurements have shown an excitation energy in the range of 7.6 ± 0.5 eV [1]. This small excitation energy will possibly allow for an optical control of the transition opening the pathway to the creation of a nuclear optical clock expected to outperform current electronic-shell-based atomic clocks. Its development has so far been impeded by the imprecise knowledge of the energy of ^{229m}Th. Using our experimental setup (Fig. 1, [2]) we could reduce the error bar

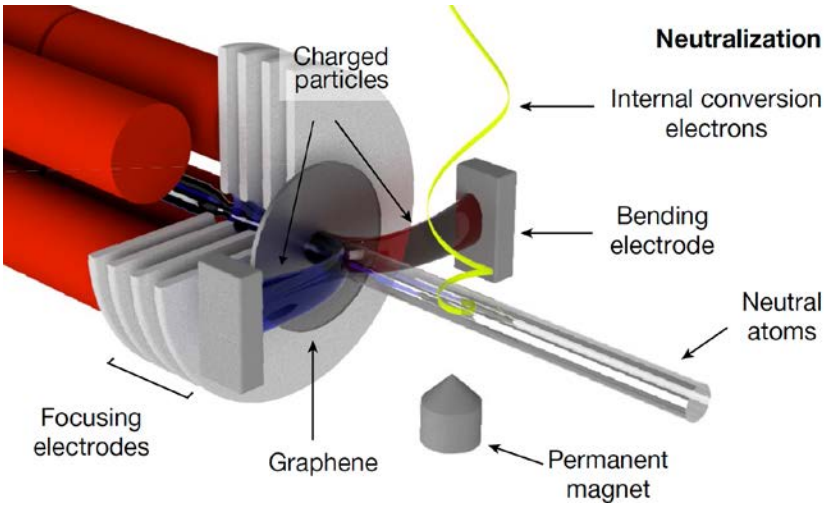

Fig. 1: Experimental setup to measure the excitation energy of the first isomeric state of ^{229m}Th. A beam of Th^{3+} ions is transmitted through a bilayer graphene sheet where the dominant fraction of projectiles is neutralized. Atoms with excited cores may relax downstream to the nuclear ground state imparting the transition energy to an electron whose kinetic energy is measured.

to 0.17 eV or, equivalently, a wavelength uncertainty of only 3.1 nm expected to facilitate the application of high-resolution laser spectroscopy on thorium nuclei.

Our group's task in this collaboration was to model the neutralization process of the ion in vicinity to the graphene sheet providing an estimate for the abundance of electronically excited neutrals in the beam after traversal of the target. When multiply charged ions approach a surface, energy levels are shifted due to the interaction with the image charge of the ion and the additional shielding of the ionic core by the target electrons. During the approach, the dominant neutralization process is resonant transfer of electrons from the valence band to (excited) resonant states of the projectile. Upon impact on the surface, loosely bound electrons are stripped from the projectile and quasi-molecular states form in the target system [3]. In the case of very thin target layers, enough electrons will remain with the projectile after separation to form a neutral, yet moderately excited, atom. As graphene is an efficient electron donor for multiply charged ions passing through it [4], it was expected (and also observed) that most of the moderately charged Th^{3+} ions would leave the bilayer graphene sheet as neutral atoms.

To understand which orbitals become resonant with the valence band of graphene we performed density-functional theory (DFT) calculations of the combined thorium–graphene system for different distances of the atom from the topmost layer (Fig. 2).

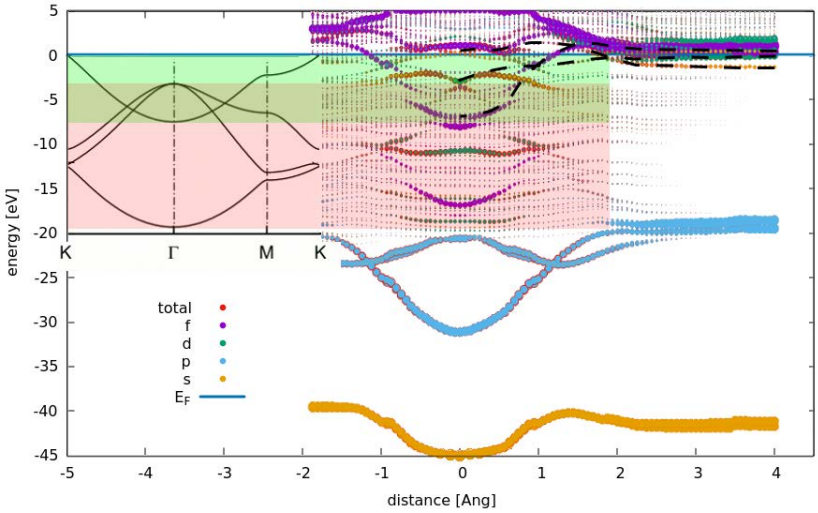

Fig. 2: Level shift of electronic thorium states in front and inside a bilayer graphene sheet as calculated with DFT. The ground state ($6d^27s^2$, orange dotted line) is shifted upwards while f states (purple dots) get into resonance with the graphene valence and conduction bands. Upon separation of projectile and target it is estimated that a considerable fraction of neutralized Th atoms remain in an electronically excited state. Electrons from such atoms will carry higher kinetic energies.

We acknowledge support by DFG (Th956/3-2), by the LMU Chair of Medical Physics via the Maier-Leibnitz Laboratory Garching and by the European Union's Horizon 2020 research and innovation programme under grant agreement number 664732 (nuClock).

[1] B. R. Beck, J. A. Becker, P. Beiersdorfer, G.V. Brown, K. J. Moody, J. B. Wilhelmy, F. S. Porter, C. A. Kilbourne, and R. L. Kelley, Phys. Rev. Lett. **98**, 142501 (2007).

[2] B. Seiferle, L. von der Wense, P. V. Bilous, I. Amersdorffer, C. Lemell, F. Libisch, S. Stellmer, T. Schumm, C. E. Düllmann, A. Pálffy, and P. G. Thirolf, Nature **573**, 243 (2019).

[3] A. Arnau, et al., Surf. Sci. Rep. **27**, 113 (1997).

[4] E. Gruber, et al., Nat. Commun. **7**, 13948 (2016).

Graphene single layer grown on the FeRh (001) thin film

V. Uhlíř[1,2], F. Pressacco[3], J. A. Arregi[1], P. Procházka[1,2], S. Průša[1,2], M. Potoček[1,2], T. Šikola[1,2], J. Čechal[1,2], A. Bendounan[4] and F. Sirotti[4,5]

[1] *Central European Institute of Technology, Brno University of Technology, Purkynova 123. 612 00 Brno, Czech Republic*
(corresponding author: T. Šikola, e-mail: sikola@fme.vutbr.cz)

[2] *Institute of Physical Engineering, Faculty of Mechanical Engineering, Brno University of Technology, Technicka 2. 616 69 Brno, Czech Republic*

[3]*Center for Free Electron Laser Science, University of Hamburg, Luruper Chaussee 149, 22761 Hamburg, Germany*

[4]*Synchrotron SOLEIL, Saint-Aubin, BP 48, F-91192 Gif-sur-Yvette Cedex, France*

[5]*Physique de la Matière Condensée, CNRS and École Polytechnique, Université Paris Saclay, F-91128 Palaiseau, France*

Graphene is a 2D material that displays excellent electronic transport properties with prospective applications in many fields. Introducing and controlling magnetism in the graphene layer, for instance by proximity of magnetic materials, may enable its utilization in spintronic devices.

Epitaxial FeRh thin films are magnetic materials which feature a first-order antiferromagnetic (AF) to ferromagnetic (FM) phase transition present around 360 K. FeRh is a highly tunable material [1] where the phase transition can be controlled by different stimuli: temperature, magnetic field, strain, electrical current and optical pulses. To ensure stability of such a material under air conditions, capping layers like metallic (Pt, Au) or insulating (Al2O3) ones have been generally used. We report on an alternative way of such a protection using a graphene layer formed in situ by the simple thermal annealing of a magnetically active epitaxial FeRh thin film prepared by magnetron sputtering. The quality of the graphene layer was characterized using X-ray Photoemission and X-ray Absorption Spectroscopy (Synchrotron Soleil), and Low Energy Ion Scattering, Scanning Tunneling Microscopy, and Low-Energy Electron Microscopy (complex UHV system at CEITEC). It has proved that graphene is polycrystalline and covers at least 97% of the FeRh (001) surface. Two preferential orientations of graphene domains mutually rotated by 30° has been identified. We will propose the mechanism of formation of graphene on the FeRh (001) surface and show that the graphene layer is capable of protecting the film from oxidation when exposed to air for several

weeks, which enables production of functional devices based on stacking of 2D materials on tunable magnetic surfaces.

We thank P. Varga for discussion on the graphene domain contrast in STM. VU and JAA acknowledge the Grant Agency of the Czech Republic (grant no. 16-23940Y). SP, MP and TS acknowledge the support from the H2020 Twinning programme (project SINNCE, 810626) and Technology Agency of the Czech Republic (grant No. TE01020233) . Access to the CEITEC core facilities was supported by the Ministry of Education, Youth and Sports (MEYS) of the Czech Republic under the projects CEITEC 2020 (LQ1601) and CEITEC Nano (LM2015041). PP and JC acknowledge the project TC17021 of the Inter-Excellence program of MEYS. VU was supported by funding from the European Union's Horizon 2020 research and innovation program under the Marie Skłodowska-Curie that is co-financed by the South Moravian Region under grant agreement No. 665860. This project has received funding from the EU-H2020 research and innovation program under grant agreement No 654360 having benefitted from the access provided by CNRS to the SOLEIL Synchrotron, within the framework of the "NFFA-Europe Transnational Access Activity".

[1] S. Maat, J.-U. Thiele, and E. E. Fullerton, Temperature and field hysteresis of the antiferromagnetic-to-ferromagnetic phase transition in epitaxial FeRh films, Phys. Rev. B 72,214432 (2005).

Wednesday

Atomic Force Microscopy Studies of a Quantum Corral

Fabian Stilp,[1] Julian Berwanger,[1] Nadine Mundigl,[1] Andreas Bereczuk,[2] Klaus Richter,[2] Franz J. Giessibl[1]

[1]*Institute of Experimental and Applied Physics, University of Regensburg, D-93053 Regensburg, Germany*

[2]*Institute of Theoretical Physics, University of Regensburg, D-93053 Regensburg, Germany*

e-mail: Franz.Giessibl@ur.de

The surface state on Cu(111) can be described by a quasi-free 2D electron gas with an energy dispersion with respect to the Fermi level of $E(\mathbf{k}) = -0.44\pm0.01$ eV + $\hbar^2\mathbf{k}^2/(2m^*)$ with an effective mass of $m^*=0.38\pm0.02\ m_e$ where $\mathbf{k}$ is a wave vector parallel to the surface, leading to a Fermi wave vector of $k_F = 2\pi/\lambda_F$ with $\lambda_F \approx 3$ nm [1]. Scattering of these surfaces state by step edges leads to interference patterns that have been observed at low temperature on Cu [1] and at even at room temperature on Au(111) [2]. It has been shown that Fe adatoms act as repulsive scatterers to the surface state, and arranging Fe adatoms to a circular "quantum corral" forces the modified surface states to a cylindrical geometry [3]. We have revisited the quantum corral with a combined atomic force-/scanning tunneling microscope.

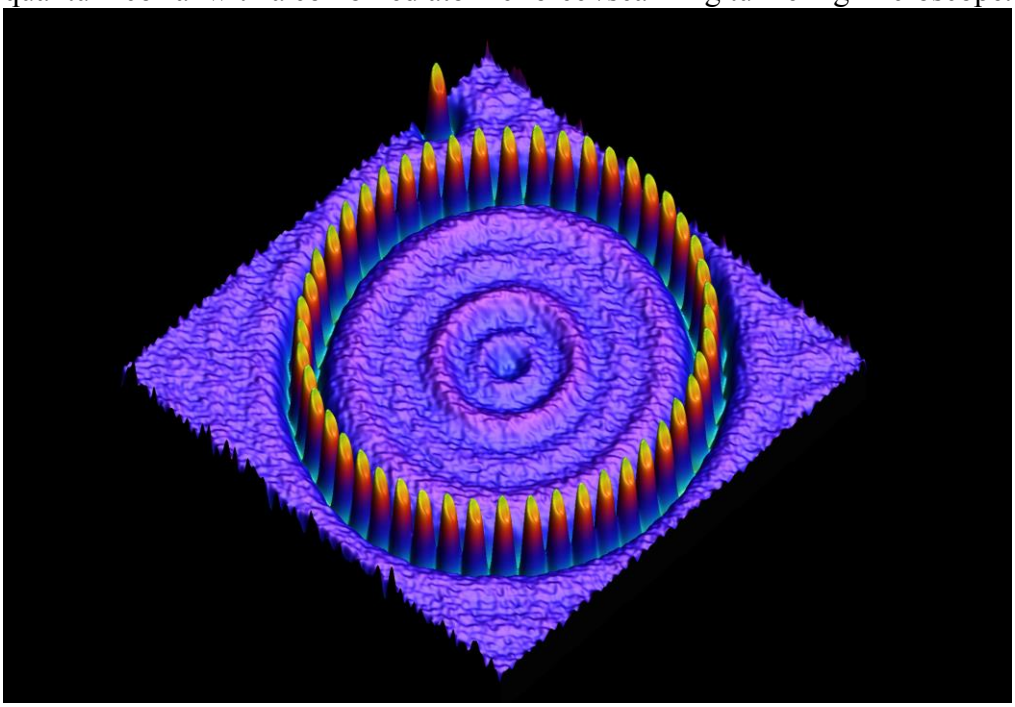

Fig. 1: AFM data of Quantum corral consisting of 48 Fe atoms on Cu (111) using a CO terminated tip. Data shows frequency shift at constant average current (-1mV, 20pA).

The figure above shows the AFM signal (frequency shift) while the corral was recorded in topographic STM mode with a vibrating tip (amplitude 50 pm). As expected from previous studies for Fe clusters on Cu(111) [4], and single Fe adatoms on Cu(111) [5], the Fe adatoms appear as ring-like features when imaged by AFM with a CO tip.

The electronic states within the corral separate into Bessel type eigenfunctions for the radial functions [3] and azimuthal dependencies given by $e^{il\phi}$ with angular momentum l. The original corral data by Crommie et al. did not show an azimuthal dependence of the topographic data. Here, we impose barriers that lift the degeneracy of the wave functions with respect to ϕ, leading to azimuthal undulations.

The STM channel is sensitive to the electrons at the Fermi energy, while AFM is sensitive to all occupied states. Therefore, we expect and observe differences between STM and AFM channels. We expected to see an electrostatic force due to the occupied Bessel states and observed interesting deviations that point to 2D-atom like properties of the quantum corral.

We thank Christopher P. Lutz for help with creating the original type of a 48 Fe atom corral on Cu(111). Support by the Deutsche Forschungsgemeinschaft under grant SFB 1277 project A02 is gratefully acknowledged.

[1] M. F. Crommie, C. P. Lutz and D. M. Eigler, Imaging standing waves in a two-dimensional electron gas, *Nature* **363**, 524 (1993)

[2] Y. Hasegawa and Ph. Avouris, Direct observation of standing wave formation at surface steps using scanning tunneling spectroscopy, *Phys. Rev. Lett*. **71**, 1071 (1993)

[3] M. F. Crommie, C. P. Lutz and D. M. Eigler, Confinement of Electrons to Quantum Corrals on a Metal Surface, *Science* **262**, 218 (1993)

[4] M. Emmrich et al., Subatomic resolution force microscopy reveals internal structure and adsorption sites of small iron clusters, *Science* **348**, 308 (2015)

[5] F. Huber et al., Chemical bond formation showing a transition from physisorption to chemisorption, *Science* **366**, 235 (2019)

Structural and Electronic Properties of FeSi(110)

Martin Uphoff, Biao Yang, Yi-Qi Zhang, Joachim Reichert, Ari P. Seitsonen,† Andreas Bauer, Christian Pfleiderer, Johannes V. Barth*

Physics Department, Technical University of Munich, D-85748 Garching, Germany
† Département de Chimie, École Normale Supréieure, 24 rue Lhomond, F-75005 Paris, France

Iron silicide (FeSi) is a fascinating material which has attracted numerous research efforts for decades.[1] Its B20 crystal structure has a cubic unit cell without an inversion center, similar to, e.g., MnSi, CoSi, and CrSi, which family of compounds displays a rich variety of physical phenomena of great interest for both explorative science and potential applications. Notably, the *d*-electron compound FeSi belongs to the class of small-band-gap semiconductors and features correlated electron characteristics, closely resembling to those of *f*-electron Kondo insulators, which have been recently predicted to host topological protected surface states.[2] Moreover, careful transport studies of high-quality FeSi single crystals indicate a high-mobility surface conduction channel.[3] To gain direct insight into the properties of this system, we developed a preparation protocol to obtain an atomistically well-defined FeSi(110) surface by Ar-ion sputtering and annealing. The atomically flat FeSi(110) surface shows a distinct step-terrace topology and atomic arrangement as determined by scanning tunneling microscopy (STM). The surface termination was analysed by combined STM data analysis and density functional theory (DFT) modeling. High-resolution scanning tunneling sprectroscopy (STS) under cryogenic conditions (ca. 1.2 – 4K) clearly reveals a small asymmetric energy gap at the Fermi level. Intriguingly, there is evidence for electronic in-gap states and surface magnetism.

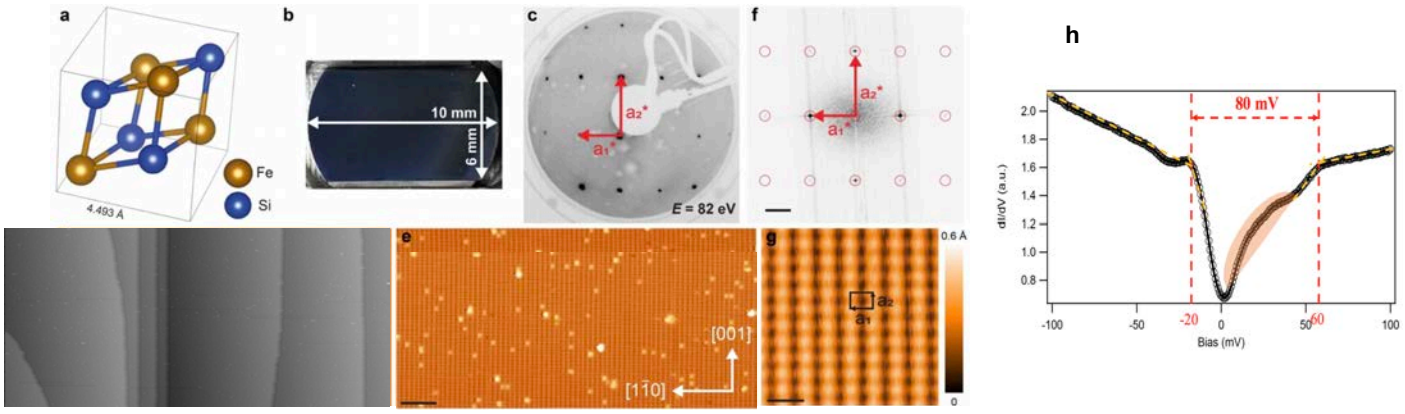

a, b FeSi in B20 crystal form and photo of employed specimen. **c** LEED pattern of clean FeSi(110) (*E* = 82 eV; reciprocal lattice vectors indicated by red arrows). **d** Overview STM image and **e** flat terrace with atomic corrugation (scale bar 45 Å) with the corresponding 2D FFT reproduced in **f**: the rectangular lattice is consistent with LEED. **g** High-resolution STM data reflecting the regular surface atomic arrangement. **h** STS signature of the energy gap.

1. L. Pauling, A. M. Soldate. *The nature of the bonds in the iron silicide, FeSi, and related crystals*, Acta Cryst. **1** (1948), 212; V. Jaccarino, G. K. Wertheim, J. H. Wernick, L. R. Walker, S. Arajs. *Paramagnetic excited state of FeSi*, *Phys. Rev.* **160** (1967) 476.
2. M. Dzero, J. Xia, V. Galitski, P. Coleman. *Topological Kondo Insulators*, *Annu. Rev. Cond. Matt. Phys.* **7** (2016) 249.
3. M. Wagner, R. Korntner, A. Bauer and C. Pfleiderer, to be published; Y. Fang, S. Ran, W. Xie, S. Wang, Y.S. Meng, M. Brian Maple. *Evidence for a conducting surface ground state in high-quality single crystalline FeSi*, *PNAS* **115** (2018) 8558

*jvb@tum.de

Recent advancements in surface science instrumentation

Markus Maier

Scienta Omicron GmbH
65232 Taunusstein, Germany
(Corresponding author: M.Maier, e-mail: markus.maier@scientaomicron.com)

We will report on most recent developments at Scienta Omicron regarding Scanning Probe Microscopy at low temperatures and high magnetic fields as well as current state-of-the art of closed-cycle cooling approaches. We will also present the newest developments in the field of photo electron spectroscopy with a focus on XPS and HAXPES.

Low Energy Electron Microscopy at Near Ambient Pressures

T. Stempel[1], M. Breitschaft[1], S. Hagen[1], Q. Fu[2], A. Thissen[1], O. Schaff[1]

[1]SPECS Surface Nano Analysis GmbH, Voltastr. 5, 13355 Berlin, Germany
[2]State Key Lab of Catalysis, Dalian Institute of Chemical Physics, CAS, Dalian 116023, China
(corresponding author: T. Stempel, e-mail: thomas.stempel@specs.com)

Low-energy electron microscopy (LEEM) is a spectromicroscopy technique, which allows the study of dynamic processes at surfaces and interfaces, such as thin-film growth, surface reactions, and phase transitions. With the FE-LEEM P90 from SPECS, which is based on the instrument design by Rudolf Tromp from IBM [1], lateral and energy resolution of below 5 nm and 250 meV, respectively, can be achieved. Depending on the excitation source and the settings on the instrument a variety of different imaging modes are possible: mirror electron microscopy, low energy electron diffraction (LEED), phase contrast imaging, reflectivity contrast, dark field imaging and bright field imaging, as well as photoelectron emission microscopy and spectroscopy.

We have enhanced the technical capabilities of the FE-LEEM P90 towards studies under near ambient conditions by developing a special sample geometry. This enables the analysis of materials and devices under near ambient conditions and even in situ during operation. Lateral resolved studies of chemical processes are required to reveal the changes in the chemical nature of molecules and reactions which happen in nanospaces due the nanoconfinement effects [2-4]. The new FE-LEEM/PEEM P90 NAP offers the possibility to study such processes at pressures up to 1mbar and lateral resolution down to 30nm.

In this talk we will present the design of this machine, which includes differentially pumped high energy electron optics and a unique in-situ gas-cell operating at high voltages, and measurement results obtained on 2D model electrodes.

[1] R. M. Tromp, M. Mankos, M.C. Reuter, A.W. Ellis and M. Copel, Surface Review and Letters, Vol. 5, No. 6 (1998), 1189-1198

[2] Q. Fu and X.H. Bao, Nat. Catal., 2019, 2, 834

[3] Q. Fu and X.H. Bao, Chem. Soc. Rev., 2017, 46, 1842

[4] H.B. Li, J.P. Xiao, Q. Fu, X.H. Bao, PNAS, 2017, 23, 5930

Postersession

A mussel inspired hydrogel

J. Appenroth[1,2], A. Imre[1], L. Moreno Ostertag[1], L.Mears [1,2] and M. Valtiner[1]

[1] *Institute of Applied Physics, Vienna University of Technology, 1040 Vienna, Austria*
(corresponding author: J. Appenroth, e-mail: appenroth@iap.tuwien.ac.at)

[2] *CEST competence center*

The adhesion properties of mussels have long been the focus of scientific studies. Their ability to stick to almost any surface and in highly corrosive environments is still not fully understood. Of great interest are practical applications such as wound dressing or anticorrosive coatings [1].
Mussel foot proteins have a high DOPA content and are thought to be pH sensitive. This sensitivity was tested in our experiments for different catechols and catecholamines in aqueous solutions by performing tests at different pH levels. the amine group of the catecholamines is thought to be responsible for the polymerizationof the molecule after oxidation. As shown before [2] the catecholamines polymerized irreversibly. Additionally cyclic voltammetry was used to study the reversibility of the catecholamines reactions. For DOPA an irreversible chemical reaction could be shown in addition to the redox reaction, as seen when increasing the pH value. To show that the amine group is responsible for polymerization, molecules that are similar but have no amine group where studied. A different catechol was found that allowed for near reversible redox reactions. It was later crosslinked to a polyamine in acidic solution using EDC/NHS. By increasing the pH a hydrogel was formed at the liquid-air interface that showed good adhesive properties. It therefore constitutes a promising biocompatible adhesive hydrogel that is currently being investigated further.

[1] Eric W. Danner et al., Biochemistry 51.33, pp. 65116518 (Aug. 2012)
[2] Sabrina Schindler and Thomas Bechtold, Journal of Electroanalytical Chemistry 836, pp. 94101 (Mar. 2019)

Interfaces-controlled properties of solid polycrystals: Ferromagnetic ZnO and hard-magnetic Nd-Fe-B alloys

B. Baretzky[1], B.B. Straumal[1-3], S.G. Protasova[2,3], A.A. Mazilkin[1,2], P.B. Straumal[4], E. Goering[3], and G. Schütz[3]

[1] *Karlsruher Institut für Technologie, Institut für Nanotechnologie, 76344 Eggenstein-Leopoldshafen, Germany*

(corresponding author: B. Baretzky, e-mail: Brigitte.baretzky@kit.edu)

[2] *Institute of Solid State Physics, Russian Academy of Sciences, 142432 Chernogolovka, Russia*

[3] *Max-Planck-Institut für Intelligente Systeme, 70569 Stuttgart, Germany*

[4] *Institute of Metallurgy and Materials Science, Russian Academy of Sciences, 117991 Moscow, Russia*

Frequently, interfaces (like grain boundaries, GBs) determine the important properties of solid polycrystals. For example, diamagnetic oxides can, under certain conditions, become ferromagnetic at room temperature and therefore are promising candidates for future material in spintronic devices. We observed that the ferromagnetism of transparent semiconductor oxides like ZnO is not an intrinsic property of ZnO crystalline lattice but is that of ZnO/ZnO grain boundaries. If ZnO polycrystal contains enough GBs, it can transform into ferromagnetic (FM) state even without doping by "magnetic atoms" like Mn, Co, Fe or Ni. Using low energy muon spin relaxation in combination with SQUID and TEM techniques, we demonstrated that the magnetic volume fraction is strongly related to the sample volume fraction occupied by grain boundaries (Figs. 1 and 2) [1]. With molecular dynamics and density functional theory we found ferromagnetic coupled electron states in ZnO GBs [1]. However, doping by "magnetic atoms" eases the appearance of FM in ZnO. It increases the saturation magnetisation and decreases the critical amount of grain boundaries needed for FM [2]. The drastic increase of the total solubility of dopants in ZnO with decreasing grain size has been also observed. It is explained by the multilayer grain boundary segregation.

The NdFeB-based alloys remain the best ones among other permanent magnets since their discovery in 1980-ies. High-performance NdFeB sinter magnets are also crucial for electric vehicle power train. Their properties and performance are controlled by the boundaries between the grains of $Nd_2Fe_{14}B$ ferromagnetic phase and can be optimized by post-sinter processes. The layers in the $Nd_2Fe_{14}B/Nd_2Fe_{14}B$ GBs should magnetically isolate the ferromagnetic $Nd_2Fe_{14}B$ grains from each other. This is the condition for the high coercivity of permanent magnets. It has been long time believed that such isolating GB layers are only formed by layers of a metallic Nd-rich phase. Recently, we demonstrated that also thin layers of Nd_2O_3 oxide are present at $Nd_2Fe_{14}B/Nd_2Fe_{14}B$ GBs (Fig. 3), by systematically investigating commercial high-performance NdFeB sinter magnets by using high resolution TEM, FFT patterns, EELS analysis and Lorentz micro-magnetic contrast TEM images. Moreover, the GB layers of Nd_2O_3 can also effectively decouple the $Nd_2Fe_{14}B$ grains from each other. Thus, grain boundary oxide layers also ensure improved hard-magnetic properties of NdFeB alloys.

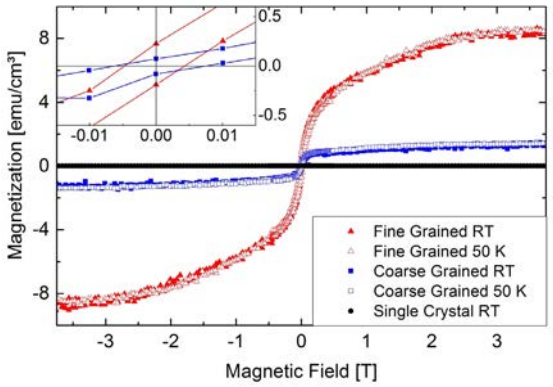

Figure 1: Temperature dependent SQUID magnetization curves for the fine grained (red triangles), and the coarse grained ZnO samples (blue squares). Even at RT, ferromagnetic magnetization curves with small but sizeable remanence and coercivitiy have been measured (see inset). For both sample types, SQUID loops measured at RT and 50 K show no significant difference which is an important feature identifying ferromagnetism in magnetic oxides. The supposedly nonmagnetic ZnO single crystal reference shows no significant magnetic features (black circles) [1].

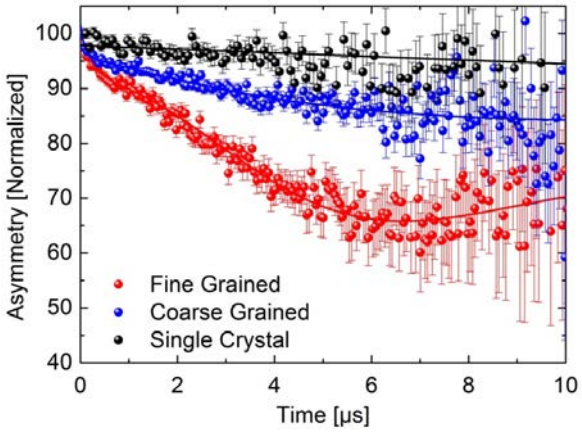

Figure 2: Averaged zero field μSR spectra for the single crystal (black dots), the coarse grained (blue dots), and the fine grained (red dots) ZnO sample. Plotted is the normalized detector asymmetry; the relaxing amplitude of the asymmetry is a measure for the magnetic volume fraction. The strongest relaxation is found for the fine grained sample (red dots), corresponding to a total magnetic volume fraction of about 35%. For the coarse grained sample (blue dots), the magnetic volume fraction is approx. 15%. The non-magnetic ZnO single crystal reference (black dots) shows no significant magnetic volume fraction [1].

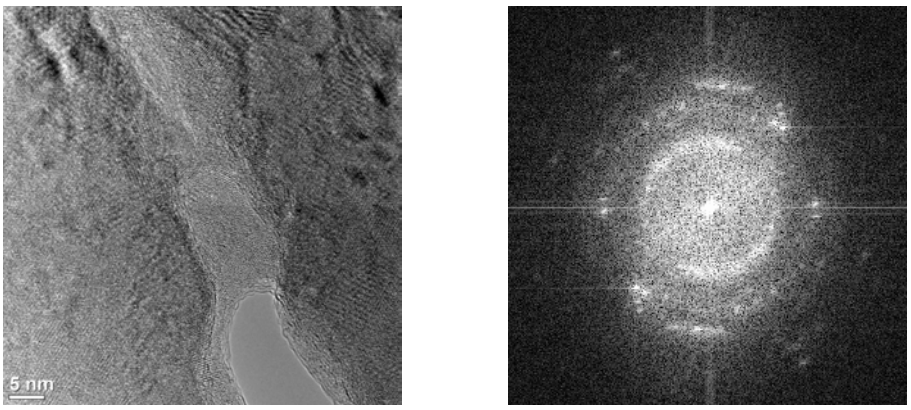

Figure 3. HRTEM micrograph of the grain boundary layer between $Nd_2Fe_{14}B$ grains and the respective FFT image (Nd_2O_3 oxide phase).

[1] B.B. Straumal, S.G. Protasova, A.A. Mazilkin, E. Goering, G. Schütz, P.B. Straumal and B. Baretzky, Beilstein J. Nanotechnol. 7, 1936 (2016)

[2] Th. Tietze et al., Scientific Reports 5, 8871 (2015)

Single Ion Molecular Magnets Adsorbed at Surfaces

Harald Brune

Institute of Physics, Ecole Polytechnique Fédérale de Lausanne (EPFL), CH-1015 Lausanne

Single molecule magnets are single molecules that exhibit magnetic remanence. In single ion molecular magnets, the magnetic center giving rise to magnetic remanence is a single atom. Quite often, these magnetic atoms are rare earth elements, as in the Tb phthalocyanine (Pc) double decker $TbPc_2$ [1, 2], Er bi-cyclooctatetraene (COT) $Er(COT)_2$ [3], Dy-metallocenium [4, 5], and in endofullerenes, such as $DySc_2N@C_{80}$ [6, 7]. However, also complexes containing single transition element atoms such as Fe may exhibit magnetic remanence [8]. Typically, these molecules are synthesized by chemical means and then either investigated in diluted powder bulk samples, or adsorbed onto surfaces.

We report on a novel way to create these molecules, namely on-surface-synthesis [9]. For this, we co-adsorb the organic ligands and the metal atoms under conditions where a majority forms the desired molecules. We first test the approach on known and already chemically synthesized molecules, such as $TbPc_2$. The morphology and the magnetic properties of the on-surface synthesized molecules are identical to the chemically synthesized ones. We then synthesize new molecules at surfaces that have not been synthesized by chemical means. Using tert-butyl-substituted phthalocyanine (tbu-2H-Pc) we create $Tb(tbu\text{-}Pc)_2$ on Ag(111) and find that also this molecule is a single-ion molecular magnet. We finally demonstrate the chemical robustness of on-surface synthesized $TbPc_2$ by exposing sub-monolayer islands of them on Ag(111) to air and then inserting them into UHV again. The atomic morphology as well as the magnetic properties are unchanged, proving the chemical protection of the central magnetic ion by the organic ligands [9].

[1] N. Ishikawa, M. Sugita, T. Ishikawa, S. Koshihara and Y. Kaizu, J. Am. Chem. Soc. **125**, 8694 (2003).

[2] C. Wäckerlin, F. Donati, A. Singha, R. Baltic, S. Rusponi, K. Diller, F. Patthey, M. Pivetta, Y. Lan, S. Klyatskaya, M. Ruben, H. Brune and J. Dreiser, Adv. Mater. **28**, 5195 (2016).

[3] L. Ungur, J. J. L. Roy, I. Korobkov, M. Murugesu and L. F. Chibotaru, Angew. Chem. Int. Ed. **53**, 4413 (2014).

[4] K. R. McClain, C. A. Gould, K. Chakarawet, S. J. Teat, T. J. Groshens, J. R. Long and B. G. Harvey, Chem. Sci. **9**, 8492 (2018).

[5] F. Guo, B. M. Day, Y. Chen, M. Tong, A. Mansikkamäki and R. A. Layfield, Science **362**, 1400 (2018).

[6] R. Westerström, J. Dreiser, C. Piamonteze, M. Muntwiler, S. Weyeneth, H. Brune, S. Rusponi, F. Nolting, A. Popov, S. Yang, L. Dunsch and T. Greber, J. Am. Chem. Soc. **134**, 9840 (2012).

[7] R. Westerström, A. C. Uldry, R. Stania, J. Dreiser, C. Piamonteze, M. Muntwiler, F. Matsui, S. Rusponi, H. Brune, S. Yang, A. Popov, B. Büchner, B. Delley and T. Greber, Phys. Rev. Lett. **114**, 087201 (2015).

[8] J. M. Zadrozny, D. J. Xia, M. Atanasov, G. J. Long, F. Grandjean, F. Neese and J. R. Long, Nat. Chem. **5**, 577 (2013).

[9] K. Diller, A. Singha, M. Pivetta, C. Wäckerlin, R. Hellwig, A. Verdini, A. Cossaro, L. Floreano, E. Vélez-Fort, J. Dreiser, S. Rusponi and H. Brune, RCS Adv. **9**, 34421 (2019).

Tuning electronic properties of 1D coordination polymers by the choice of the transition metal: Fe, Co and Ni

Aleš Cahlík[1], Christian Wäckerlin[1], Oleksander Stetsovych[1], Santhini Vijai Meena[1], Jesus Mendieta[1], Pingo Mutombo[1], Simon Pascal[2], Olivier Siri[2], Pavel Jelínek[1]

Institute of Physics, ASCR, v.v.i., Cukrovarnická 10, CZ-16253 Praha 6, Czech Republic
(corresponding author: A. Cahlík, e-mail: cahlik@fzu.cz)

[1] *Institute of Physics, ASCR, v.v.i., Cukrovarnická 10, CZ-16253 Praha 6, Czech Republic*

[2] *Aix Marseille Université, CNRS, CINaM UMR 7325, 13288, Marseille, France*

One-dimensional (1D) polymers are of particular interest due to their potential applications in the field of molecular electronics. The synthesis of nanomaterials at the solvent-free solid-vacuum interface has been emerging as a promising approach to obtain tailored low dimensional materials with atomic precision. One of the promising candidates are 1D coordination-polymers (CPs), that can be obtained on-surface by reaction between metal atoms and suitable linker bridges. [1,2] This approach allows a tuning of the electronic and spintronic properties of the wires depending on the nature of the metal center.

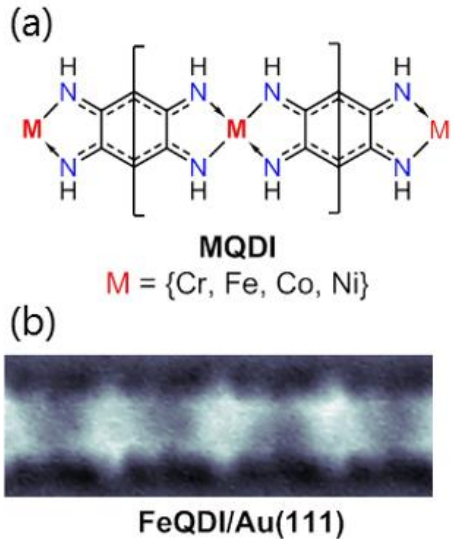

(a) On surface formation of structurally distinct four-fold coordinated **2**·M_2 (M=Cr, Fe, Co, Ni) wires by dehydrogenative metalation. (b) High resolution nc-AFM image of **2**·Fe_2 wires.

Here, we examine the formation and the electronic transport through 1D coordination polymers in ultrahigh vacuum at 5K using combined scanning tunneling and non-contact atomic force microscopies (STM/ nc-AFM). The polymers are synthesized in-situ by co-deposition of Fe, Co or Ni atoms and the quinonediimine (2,5-diamino-1,4-benzoquinone-diimine) ligand [3] onto Au(111). In all cases we could obtain wires with lengths over 100 nm. Submolecular resolution achieved with a CO-functionalized tip shows that for all coordination metals polymers are structurally equivalent - with a geometry consistent with the expected formal M(II) oxidation states. That implies dehydrogenation of the quinonediimine ligand.

The combination of STM and nc-AFM further allows for lifting and transport experiments due to the possibility to simultaneously measure the current, conductance and force gradient as a function of bias voltage and lifting height. We observe a distinct bandgap opening behavior depending on the incorporated metal element. While lifting of Fe and Ni wires leads to the opening of a band gap at heights of a few nanometers, the Co containing polymers do not

exhibit any gap opening even above 10 nm. In addition, we can demonstrate the possibility to modulate the conductance of these wires between highly conductive and non-conductive by increased bias voltage or upon light illumination.

[1] A. Shchyrba, C. Wäckerlin, J. Nowakowski, S. Nowakowska, J. Björk, S. Fatayer, J. Girovsky, T. Nijs, S. C. Martens, A. Kleibert, J. Am. Chem. Soc., 136, 9355–9363, (2014)

[2] F. Huttmann, N. Schleheck, N. Atodiresei, T. Michely, J. Am. Chem. Soc. (2017)

[3] S. Pascal, O. Siri, Coordination Chemistry Reviews, Volume 350, 178-195, (2017)

Active site representation in first-principles microkinetic models: Data-enhanced computational screening for improved methanation catalysts

M. Deimel, M. Andersen, and K. Reuter

Chair for Theoretical Chemistry and Catalysis Research Center, Technical University of Munich, D-85748 Garching, Germany
(corresponding author: M. Deimel, e-mail: martin.deimel@tum.de)

Reductionist first-principles microkinetic models have largely contributed to our trend understanding of transition metal (TM) and TM alloy catalysts. As a key enabling step towards computational screening of potential catalyst materials, these models draw much of their computational efficiency from simple thermochemical dependencies relying on only few descriptive quantities. Such scaling relations and Brønsted-Evans-Polanyi relations, linking adsorption energies with each other and with transition-state energies, respectively, reduce the required first-principles input to only a few adsorption energies of key reaction intermediates [1,2]. Notwithstanding, as these relations need to be established separately for every surface site and adsorbate, only a minimum number of adsorption sites are typically considered in existing such microkinetic models. This might jeopardize their predictive power by an overly simplistic representation of the active catalyst surface [3].

Here we address this issue by employing the recently established compressed-sensing approach 'sure independence screening and sparsifying operator' (SISSO) [4,5]. Once trained, this machine learning algorithm provides a descriptor for the quantitative prediction of adsorption energies of *all* involved reaction intermediates at *all* high-symmetry sites from a single density-functional theory calculation of the clean surface [6]. Exploiting this extensive adsorption energetics, refined microkinetic models considering multiple active sites come into reach [7]. As a showcase for this novel approach we revisit existing work screening TMs or binary TM alloys for their suitability as methanation catalysts on the basis of a less detailed microkinetic model [8]. Due to a variety of different possible surface terminations and a concomitantly large number of inequivalent high-symmetry sites, binary TM alloys generally offer a plethora of potential reaction pathways from the educts to the product. This richness is not adequately captured by reductionist microkinetic models that often even focus on only one fixed reaction pathway that is e.g. motivated by experimental findings for a specific catalyst. Indeed, our refined screening and mechanistic analysis reveals that the explicit consideration of hitherto neglected step and terrace sites yields new highly promising materials, which owe their high catalytic activity to previously not considered reaction pathways.

Support by the Leibniz Supercomputing Centre of the Bavarian Academy of Sciences and Humanities for providing computing time is gratefully acknowledged.

[1] J. K. Nørskov, F. Abild-Pedersen, F. Studt, and T. Bligaard, Proc. Natl. Acad. Sci. U.S.A. 108, 937 (2011)

[2] T. Bligaard, J. K. Nørskov, S. Dahl, J. Matthiesen, C. H. Christensen, and J. Sehested, J. Catal. 224, 206 (2004)

[3] K. Reuter, C.P. Plaisance, H. Oberhofer, and M. Andersen, J. Chem. Phys. 146, 040901 (2017)

[4] R. Ouyang, S. Curtarolo, E. Ahmetcik, M. Scheffler, and L. M. Ghiringhelli, Phys. Rev. Materials 2, 083802 (2018)

[5] R. Ouyang, E. Ahmetcik, C. Carbogno, M. Scheffler, and L. M. Ghiringhelli, J. Phys.: Mater. 2, 024002 (2019)

[6] M. Andersen, S. V. Levchenko, M. Scheffler, and K. Reuter, ACS Catal. 9, 2752 (2019)

[7] M. Andersen, C. P. Plaisance, and K. Reuter, J. Chem. Phys. 147, 152705 (2017)

[8] A. C. Lausche, A. J. Medford, T. S. Khan, Y. Xu, T. Bligaard, F. Abild-Pedersen, J. K. Nørskov, and F. Studt, J. Catal. 307, 275 (2013)

Assessing the proton affinity of individual surface OH groups with nc-AFM

Margareta Wagner,[1,2] Martin Setvin,[1] Michael Schmid, [1]
Bernd Meyer,[3] and Ulrike Diebold[1]

[1]Institute of Applied Physics, TU Wien, Wiedner Hauptstrasse 8-10/134, A-1040 Vienna, Austria
[2]Central European Institute of Technology (CEITEC), Brno University of Technology, Purkyňova 123, 612 00 Brno, Czech Republic
[3]Interdisciplinary Center for Molecular Materials and Computer-Chemistry-Center, Friedrich-Alexander-Universität Erlangen-Nürnberg, Nägelsbachstrasse 25, 91052 Erlangen, Germany

With non-contact AFM in an UHV environment, measuring the properties of individual surface sites has become possible [1-6]. Here we report a novel approach to determine the proton affinity (PA) -- the tendency to gain/lose a proton -- of individual surface hydroxyls. The $In_2O_3(111)$ surface has four different types of surface $O_S(\alpha–\delta)$ atoms within the unit cell [7], which makes it a convenient testbed for our method. When dosing water vapor at room temperature, the molecule dissociates at one particular location, resulting in a propeller-type configuration of three symmetrically equivalent O_WH and $O_SH(\beta)$ pairs [7]. By tip manipulation, the proton can be moved to other O_S atoms. Force-distance curves above the various hydroxyls are remarkably reproducible and in quantitative agreement with calculations involving a OH-terminated In_2O_3 tip. By using the same tip for calculations of force curves on a variety of gas phase molecules with a known PA, a calibration line is obtained; with the help of this scaling relation, PA values of 1487 ± 10 kJ/mol, 1558 ± 10 kJ/mol, and 1570 ± 10 kJ/mol are obtained for the $O_SH(\gamma)$, $O_SH(\delta)$ and $O_SH(\beta)$ groups, respectively.

Acknowledgements: This work was supported by the Austrian Science Fund (FWF), project T 749-N27 (Herta-Firnberg-Stelle, MW) and Z 250-N27 (Wittgenstein Prize, UD), as well as the German Research Foundation (DFG), Research Unit FOR 1878 (funCOS, BM). MW and UD also acknowledge funding under the Horizon 2020 Research and Innovation Programme under the Grant Agreement No 810626.

[1] Giessibl, F. J. The qPlus sensor, a powerful core for the atomic force microscope. *Rev. Sci. Instrum.* **90,** 011101–60 (2019).
[2] Lantz, M. A. *et al.* Quantitative measurement of short-range chemical bonding forces. *Science* **291,** 2580–2583 (2001).
[3] Sugimoto, Y. *et al.* Chemical identification of individual surface atoms by atomic force microscopy. *Nature* **446,** 64–67 (2007).
[4] Gross, L. *et al.* Measuring the charge state of an adatom with noncontact atomic force microscopy. *Science* **324,** 1428–1431 (2009).
[5] Onoda, J., Ondráček, M., Jelínek, P. & Sugimoto, Y. Electronegativity determination of individual surface atoms by atomic force microscopy. *Nature Comms.* **8,** 15155 (2017).

[6] Wagner, M. *et al.* Reducing the $In_2O_3(111)$ surface results in ordered Indium adatoms. *Adv. Mater. Interfaces* **1,** 1400289–6 (2014).
[7] Wagner, M. *et al.* Resolving the structure of a well-ordered hydroxyl overlayer on $In_2O_3(111)$: Nanomanipulation and Theory. *ACS nano* **11,** 11531–11541 (2017).

Accurate surface energies by van der Waals inclusive DFT calculations

S. Filimonov, M. Pidchenko

Faculty of Physics, Tomsk State University, 634050 Tomsk, Russia
(corresponding author: S. Filimonov, e-mail: filimon@phys.tsu.ru)

Density functional theory (DFT) calculations have been established as an indispensable tool for modeling properties of solid surfaces from first principles. Typical tasks for DFT in the field of surface science are calculations of the surface energy [1-4] and calculations of the adsorption and diffusion energies of atoms on surfaces [5-6]. To achieve better agreement with the experiment the surface energies are usually calculated with the local density approximation (LDA) for the exchange correlation energy, whereas a somewhat more sophisticated generalized gradient approximation (GGA) shows better performance in describing the interatomic bonding. This leads to a very uncomfortable situation when different properties of the same surface cannot be adequately treated at the same level of approximation. In the present work we show that the accuracy of the DFT-GGA calculations of the surface energy is substantially improved by taking dispersive van der Waals (vdW) interactions into account, thus making the GGA approximation suitable for distinct computational surface science tasks.

Calculations were performed with the Fritz-Haber-Institute ab initio molecular simulations (FHI-aims) code [7] using the generalized gradient approximation in the Purdue- Burke-Ernzerhof (PBE) parameterization [8]. DFT calculations were coupled with the many-body dispersion (MBD) method [9-10] to take into account dispersive vdW interactions.

The clean Si(001) and Si(111) surfaces were modeled with a symmetric periodic slab with two middle Si layers fixed in the bulk positions. The total energy of the system is given by

$$E = \mu_{Si} N_{Si} + 2A\gamma \quad (1)$$

and the surface energy γ can be found by linear approximation of the total energy E as a function of the number of Si atoms N_{Si} in the slab [10,11]. Other quantities in (1) are the surface area per unit cell A and the chemical potential of the bulk Si crystal μ_{Si}.

Calculation results for clean Si(001) and Si(111) surfaces are shown in Table 1. The second and third columns show the surface energy per unit area calculated in the present work with PBE+MBD method and in Ref. 4 with the LDA approximation. It is known that the LDA approximation gives better results for the surface energy compared to the PBE approximation. Good agreement of our results with the LDA results proves good performance of the PBE+MBD method in the surface energy calculations.

Table 1. Surface energy of clean Si(001) and Si(111) surfaces.

	Surface energy γ(eV/Å^2)		vdW contribution	
	present work	Ref. 4	γ_{vdW}(eV/Å^2)	γ_{vdW}(%)
Si(100)-1 × 1	0.148	0.147	0.013	8.8
Si(100)-c4 × 2	0.092	0.092	0.013	14.1
Si(111)- 1 × 1	0.112	0.124	0.012	11.1
Si(111)- 2 × 1	0.093	-	0.012	12.9

The last two columns show contribution of the vdW interactions to the surface energy. As can be seen the vdW interactions increase the surface energy of clean Si(001) and Si(111) surfaces by 0.012-0.013 eV/Å^2 thereby relative contribution of the vdW interactions to the surface energy varies from 8 to 13%, depending on the surface reconstruction.

In conclusion, the obtained results show that even in purely covalent materials like silicon, dispersive forces are playing substantial role and has to be taken into account when analyzing the structural and energetic properties of surfaces. Performance of the PBE based DFT calculations is improved by taking into account vdW forces, thus making it possible accurate treatment of both the surface energy and the adatom bonding and diffusion at surfaces within the same level of approximation for the exchange-correlation energy.

[1] D. Vanderbilt, Phys. Rev. Lett. 59, 1456 (1987)
[2] R.D. Meade, D. Vanderbilt, Phys. Rev. B 40, 3905 (1989)
[3] A.A. Stekolnikov, J. Furthmüller, F. Bechstedt, Phys. Rev. B 68, 205306 (2003)
[4] G.H. Lu et al., Surf. Sci. 588, 61(2005)
[5] A.P. Smith et al., J. Chem. Phys.102, 1044 (1995)
[6] A. van de Walle, M. Asta, P. Voorhees, Phys. Rev. B. 67, 041308 (2003)
[7] V. Blum et al. Comp. Phys. Comm., 180, 2175 (2009)
[8] P. Perdew, K. Burke, K. Ernzerhof, Phys. Rev. Lett., 77, 3865 (1996)
[9] A. Tkatchenko et al., Phys. Rev. Lett. 108, 236402 (2012)
[10] A. Tkatchenko, A. Ambrosetti, R.A. DiStasio Jr. J. Chem. Phys., 138, 074106 (2013)

Occupied and unoccupied electronic structure of the $BaTiO_3$-derived oxide quasicrystal

S. Förster[1], C.-T. Chiang[1,2], M. Ellguth[3], F. Schumann[1], C. Tusche[3,4], R. Kraska, and W. Widdra[1,3]

[1] *Martin-Luther-Universität Halle-Wittenberg, Halle, Germany*
(corresponding author: S. Förster, e-mail: stefan.foerster@physik.uni-halle.de)

[2] *Institute of Atomic and Molecular Sciences, Academia Sinica, Taipei, Taiwan*

[3] *Max-Planck-Institut für Mikrostrukturphysik, Halle, Germany*

[4] *Peter-Grünberg-Institut (PGI-6), Forschungszentrum Jülich, Jülich, Germany*

In solid state physics, the electronic structure is often explained by examples of periodic systems. In reality, quasicrystals of metallic alloys with aperiodic atomic structure are well-known, whereas their valence electronic structure is still under debate [1]. Moreover, only very recently their unoccupied electronic structure has been studied [2]. In this contribution, we present angle-resolved photoelectron spectroscopy on the occupied and unoccupied electronic structure of a two-dimensional oxide quasicrystal (OQC), which is formed from $BaTiO_3$ on Pt(111) [3,4].

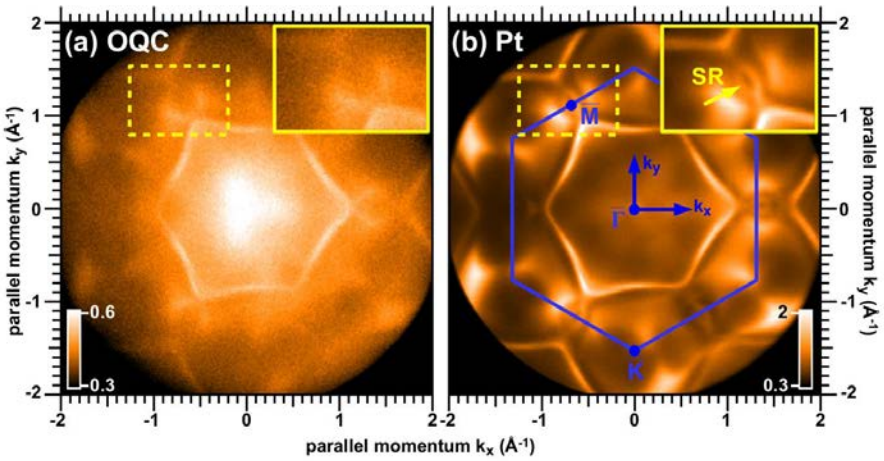

Figure 1: Fermi surface maps of the OQC and the bare Pt(111) surface measured by the momentum microscope [6].

The occupied valence bands are investigated by the momentum microscope with He I excitation [5], and the photoelectron distribution

over the whole hemisphere above the surface is mapped [6]. Exemplary the Fermi surface of the OQC and the bare Pt(111) are shown in Fig. 1. We find an enhanced density of states at the Fermi level originating from singly occupied Ti3d states. This emphasizes that the OQC structure provides a dodecagonal arrangement of atoms carrying an unpaired spin. Furthermore, we decomposed the energy-dependent photo-electron patterns according to symmetry considerations. As a results, clear dispersion of the oxygen 2p bands with a bandwidth of more than 0.5 eV at 5.2 eV below the Fermi level (E_F) can be identified. Moreover, localized oxygen 2p states are observed at around 4 and 6 eV below E_F, which are comparable to the O non-bonding and the Ti-O dpσ bands in bulk, respectively [7].

As preliminary studies on the unoccupied electronic states and their femtosecond dynamics, two-photon photoemission spectroscopy studies using a megahertz fiber laser system have been performed. With a pump and probe photon energy of around 3.9 and 1.7 eV, the n=1 and 2 image potential states on OQC are identified at around 3.5 and 3.6 eV above E_F.

Support by the Fonds zur Förderung der Wissenschaftlichen Forschung (projects S6204 and S6201), Royal Society (London), British Council (Vienna) and the European Union (ER-BCHRX-CT94-0571 and HCM Ψ_k) is gratefully acknowledged.

[1] V. A. Rogalev, O. Gröning, R. Widmer, J. H. Dil, F. Bisti, L. L. Lev, T. Schmitt, and V. N. Strocov, Nat. Comm. 6, 8607 (2015)

[2] M. Maniraj, A. Rai, S. R. Barman, M. Krajčí, D. L. Schlagel, T. A. Lograsso, and K. Horn, Phys. Rev. B 90, 115407 (2014)

[3] S. Förster, K. Meinel, R. Hammer, M. Trautmann, and W. Widdra, Nature 502, 215 (2013)

[4] S. Förster, S. Schenk, E. M. Zollner, O. Krahn, C.-T. Chiang, F. O. Schumann, A. Bayat, K.-M. Schindler, M. Trautmann, R. Hammer, K. Meinel, W. A. Adeagbo, W. Hergert, J. I. Flege, J. Falta, M. Ellguth, C. Tusche, M. DeBoissieu, M. Muntwiler, T. Greber, and W. Widdra, Phys. Status Solidi B, 1900624 (2019)

[5] C. Tusche, A. Krasyuk, and J. Kirschner, Ultramicroscopy 159, 520 (2015)

[6] C.-T. Chiang, M. Ellguth, F. O. Schumann, C. Tusche, R. Kraska, S. Förster, and W. Widdra, Phys. Rev. B 100, 125149 (2019)

[7] S. W. Robey L. T. Hudson, V. E. Henrichs, C. Eylem, and B. Eichhorn, Journal of Phys. Chem. Sol. 57, 1385 (1996)

Movable holder for a quartz crystal microbalance for exact doses in pulsed laser deposition

Giada Franceschi, Dieter Ingerle[1], Christina Streli[1], Michael Schmid, Ulrike Diebold, and Michele Riva

(corresponding author: G. Franceschi, e-mail: franceschi@iap.tuwien.ac.at)

Institute of Applied Physics, TU Wien, Vienna, Austria

[1] *Institute of Atomic and Subatomic Physics, TU Wien, Vienna, Austria*

Controlling the amount of material deposited by pulsed laser deposition (PLD) down to fractions of one Ångström is crucial for nanoscale technologies based on thin-film heterostructures. Because it is highly accurate, easily implemented, and cheap, the quartz crystal microbalance (QCM) is often the technique of choice for measuring growth rates with high precision. Commonly used ex-situ measurements are often not suitable for hygroscopic materials, are destructive, or entail multiple sample mounting, preparation, and characterization steps. In contrast, a QCM operates in vacuum and in situ. When applied to PLD, QCMs suffer from some limitations, however: QCM sensors are commonly fixed off to one side of the substrate, causing fast degradation of the quartz crystal, as it is constantly exposed to the ablated material. The positioning of the QCM is problematic also because of the pronounced directionality of the PLD plasma plume and its strong dependence on deposition parameters (e.g., background pressure, fluence): QCMs should ideally be placed at the same position as a substrate during growth.

Our design of a movable QCM holder (Figure 1) overcomes these issues. The holder is composed of two electrically insulated, flag-style sample plates in a double-decker geometry. It is compatible with standard UHV transfer arms, allowing easy transfer across UHV chambers and straightforward implementation (no bake-out required). The QCM is placed at the same position as the substrate during PLD growth, and it can be moved to a sample storage position when not needed. Its resonance frequency can be measured in vacuum before and after deposition by placing the holder in a stage that provides separate electrical contacts to the two plates of Figure 1, which, in turn, are in contact with the opposing faces of the crystal.

We tested the design by depositing manganese oxide. The stoichiometry of the manganese oxide film as determined with XPS was MnO_2. This information is required to translate the mass readings of the QCM into a growth rate of Mn in monolayers per laser pulse. The resulting rates are in good agreement with those obtained from independent x-ray fluorescence and x-ray reflectivity measurements. We show that determining precise cation deposition rates when growing from an oxidic PLD target can be useful to better understand

the surface properties of multicomponent oxide materials whose surface composition and atomic structure is tuned by PLD. We exemplify this for manganese oxide deposition on the (110)-oriented surface of $La_{0.8}Sr_{0.2}MnO_3$: The deposition rate of Mn cations determined by our QCM measurements allows us to establish quantitative relations between the composition-related surface reconstructions of $La_{0.8}Sr_{0.2}MnO_3$(110).

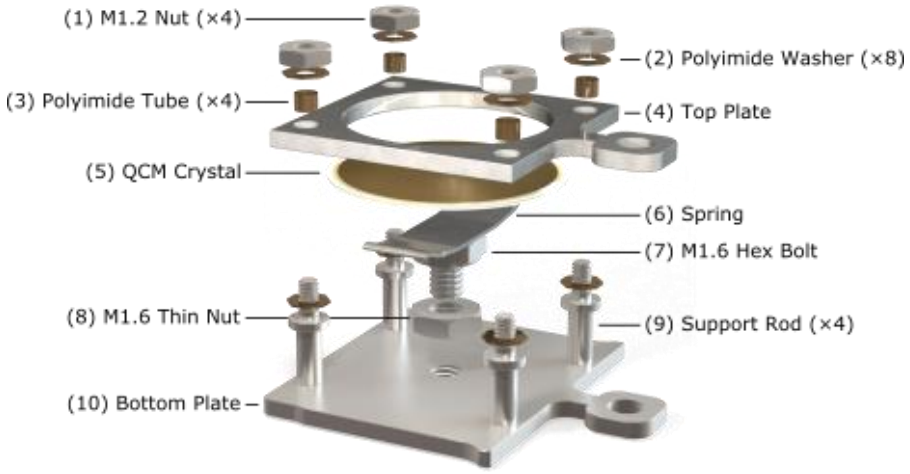

Figure 1. Exploded view of the QCM holder

Understanding pH and potential effects from ab-initio simulations of electrochemical interfaces using implicit solvation models

Nicolas G. Hörmann and Karsten Reuter

Chair of Theoretical Chemistry and Catalysis Research Center,
Technische Universität München,Germany

(corresponding author: Nicolas G. Hörmann, nicolas.hoermann@tum.de)

An in-depth, atomic-level characterization of solid-liquid interfaces is crucial for the design of a wide range of energy conversion systems such as electrocatalysts, batteries or fuel cells. Predictive-quality quantum mechanical (QM) simulations can make most valuable contributions to this end, but are challenged by the treatment of the liquid environment – even when relying on computationally most efficient approaches like semi-local density-functional theory (DFT). Traditionally, the electrochemical stability and activity at such interfaces has therefore been analyzed from charge-neutral DFT calculations, often considering only a very reduced set of interfacial degrees of freedom, e.g. only adsorbates that are chemically bound to the electrode surface.

Recently, it has been shown that an inclusion of mean-field solvation and electrolyte effects via hybrid QM/continuum models [e.g. the ENVIRON [1] module of Quantum ESPRESSO], allows to determine electrochemical properties with much better accuracy and at only marginally higher computational costs [2,3].

Here, it will be discussed how the explicit variation of electronic surface charges in such simulations allows to include the electrode potential explicitly giving access to fully grand canonical interface energetics [2]. This approach allows to determine nontrivial effects previously inaccessible to simulation, such as pH shifts of electrosorption peaks on the RHE scale or non-integer electrosorption valencies.

In order to understand better why the inclusion of electronic and electrolyte degrees of freedom are essential to the description of such effects we analyse in detail the electrosorption behaviour of H^+ and Cl^- on Pt. We show that a second order Taylor expansion of the grand canonical energetics decomposes into an energy contribution equivalent to the zero-net-charge energetics of the Computational Hydrogen Electrode, and into a double layer contribution only accessible in fully grand canonical simulations. The double-layer-related

contribution depends on the applied electrode potential and the adsorbate-induced change in work function as well as the interfacial capacitance; all three components are necessary to explain the non-trivial pH shifts of electrosorption peaks observed e.g. for H on Pt in grand canonical simulations.

Based on this analysis we will assess the general accuracy of ab-initio simulations of electrochemical interfaces as obtained with implicit solvation models and compare selected results to experiments and other simulations.

[1] www.quantum-environment.org
[2] Hörmann, Andreussi, Marzari, J. Chem. Phys. 150, 041730 (2019).
[3] Hörmann, Guo, Ambrosio, Andreussi, Pasquarello, Marzari, npj Computational Materials 5, 100 (2019)

The quest for magnons in ultra-thin nickel films

H. Ibach[1,2*] and C. M. Schneider[1,2]

[1]*Peter Grünberg Institut* (PGI-6), *Forschungszentrum Jülich, 52425 Jülich, Germany*

[2]*Jülich Aachen Research Alliance, Germany*
*h.ibach@fz-juelich.de

High momentum magnons in ultra-thin films have been studied successfully in the past using inelastic electron scattering (EELS) (see for example [1-5]). The studies focused on epitaxial films of cobalt and iron. In particular cobalt films grown on Cu(100) found much attention because of the nearly perfect match on the lattice constant of fcc cobalt and copper. Attempts to expand the studies onto nickel layers failed however (see e.g. [6]), although Ni grows well on Cu(100) and the stiffness of bulk magnons in cobalt and nickel is about the same [7-9]. We speculated that the reason for the failure is the small magnon/electron coupling in the case of nickel because of the small magnetic moment of nickel. The even more itinerant nature of the magnons in nickel compared to cobalt and iron might add to the smallness of the cross section for electron magnon scattering.
To explore this hypothesis we have studied electron energy loss spectra of Ni-films covered by a few atomic layers of cobalt with the idea that cobalt would provide the coupling to the scattering electrons whereas the spectra should reflect the exchange coupling between the Co-atoms as well as between the Ni-atoms below [10,11]. Since bulk magnons of cobalt and nickel have a similar stiffness one expects the magnon modes of the composite film to be reasonably well represented by the Heisenberg model with homogeneous exchange coupling constants.

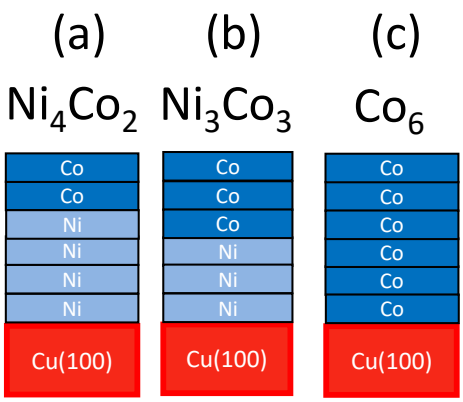

Fig.1. Some six-layer epitaxial systems studied in this work.

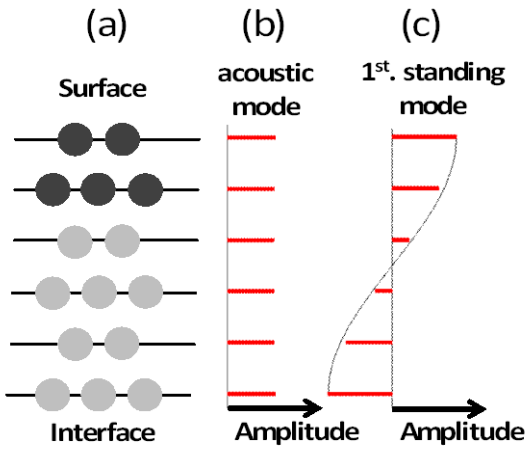

Fig. 2. Illustration of the acoustic and first standing magnon mode in a six-layer film.

Fig. 1 shows three six-layer films studied in this work, (a) Co_2Ni_4, (b) Co_3Ni_3, and (c) Co_6. As known from previous work [4] the Co_6 films exhibits an acoustic mode (Fig. 2b) and the first standing mode (Fig. 2c). A sample spectrum is shown in Fig. 3a. The acoustic mode is displays about the same intensity and nearly the same energy in the Co_3Ni_3 and the Co_2Ni_4 films; the standing mode is missing however (Fig. 3 and 4).

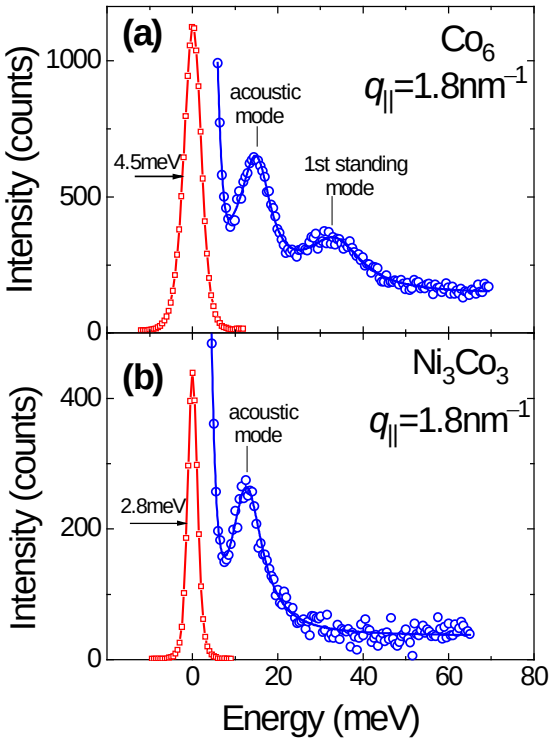

Fig. 6. Magnon spectra for Co_6 and Ni_3Co_3 films deposited on Cu(100). The spectra are corrected for the Bose-occupation number.

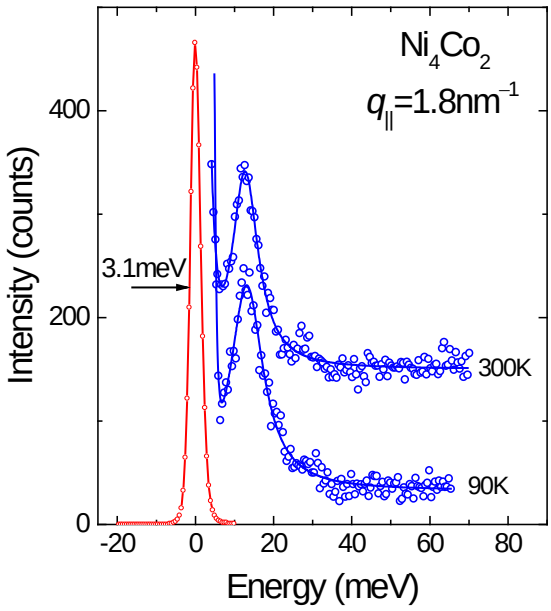

Fig. 7. Magnon spectra of a Ni_4Co_2 film corrected for the Bose occupation number at 300K and 90K. The acoustic mode is at the same energy at both temperatures.

The absence of a standing wave in spectra of Ni_3Co_3 and Ni_4Co_2 films (as well as the standing wave spectra of $Ni_{3/5}Co_{5/8}$ Ni-films) can be understood as resulting from a strong damping of standing waves at the interface to copper when the wave vector exceeds about $3nm^{-1}$ [12].

[1] R. Vollmer, M. Etzkorn, P. S. A. Kumar, H. Ibach, and J. Kirschner, Phys. Rev. Lett. **91**, 147201 (2003).
[2] E. Michel, H. Ibach, C. M. Schneider, D. L. R. Santos, and A. T. Costa, Phys. Rev. B **94**, 014420 (2016).
[3] E. Michel, H. Ibach, and C. M. Schneider, Phys. Rev. B **92**, 024407 (2015).
[4] J. Rajeswari, H. Ibach, and C. M. Schneider, Phys. Rev. Lett. **112**, 127202 (2014).
[5] K. Zakeri, Phys. Rep. **545**, 47 (2014).
[6] J. Rajeswari, Thesis, University of Duisburg, 2013.
[7] S. J. Pickart, H. A. Alperin, V. J. Minkiewicz, R. Nathans, G. Shirane, and O. Steinsvoll, Phys. Rev. **156**, 623 (1967).
[8] H. A. Mook and D. M. Paul, Phys. Rev. Lett. **54**, 227 (1985).
[9] R. N. Sinclair and B. N. Brockhouse, Phys. Rev. **120**, 1638 (1960).
[10] H. Ibach and C. M. Schneider, Phys. Rev. B **98**, 014413 (2018).
[11] H. Ibach and C. M. Schneider, Phys. Rev. B **99**, 184406 (2019).
[12] P. Buczek, A. Ernst, and L. M. Sandratskii, Phys. Rev. B **84**, 174418 (2011).

Revision of role of hydrogen bonding in self-ordering of partialy fluorinated phthalocyanines

P. Kocán, P. Matvija, P. Sobotík, I. Ošťádal, B. Pieczyrak[1], and L. Jurczyszyn[1]

Charles University, Faculty of Mathematics and Physics, Department of Surface and Plasma Science, V Holešovičkách 2, 180 00, Prague, Czech Republic
(corresponding author: P. Kocán, e-mail: pavel.kocan@mff.cuni.cz)

[1] *Instytut Fizyki Doswiadczalnej, Uniwersytet Wroclawski, pl. Maksa Borna 9, 50-204 Wroclaw, Poland.*

Hydrogen-like bonding between halogen and hydrogen atoms is widely accepted as the driving force in self-ordering process of various molecular layers. A proper understanding how the molecular periphery influences the self-ordering is crucial for formation of structurally and electronically well defined interfaces.

In our previous works we studied room-temperature behavior of F_0CuPC [1] and of F_{16}CuPC [2] molecules deposited on the Si(111)-Tl1×1 surface. We found that the F_0CuPC molecules form ordered structures at full monololayer (ML) coverage. At lower coverages, the ordering can be achieved locally by increasing the coverage using the electric field of a STM tip [1,3]. A completely different behavior was observed in the case of the F_{16}CuPC molecules, which have a strong tendency to form a 2D gas instead of an ordered close-packed (OCP) phase, which allowed to study molecular correlations within the gas phase by STM [2].

Here we focus on two molecular layers composed of phthalocyanines with possibility of stabilization by C-H...F hydrogen-like bonds: 1) chessboard-like structure forming binary mixture of F_{16}CuPC with F_0CuPC and 2) single-species F_8CuPC on the Si(111)-Tl1×1 surface. Size of ordered domains and their stability against the electric field of the STM tip are used to compare room-temperature stability of these structures and of the previously studied structures [1,2]. With help of DFT calculations we compare stability of the relaxed atomic structures of F_{16}CuPC + F_0CuPC, F_8CuPC, F_{16}CuPC and F_0CuPC molecules. The results show that the straightforward explanation of the process of self-ordering by hydrogen-like bonding is not acceptable in the studied case.

To probe the stability of ordered molecular layers of phthalocyanines with various fluorination on the Si(111)-Tl1×1 surface we introduce utilization of a strong electric field of the STM tip [1,3]. The dipoles induced by molecular adsorption are either attracted towards or repelled by the tip due to its high-gradient field. At room temperature we found tip-sample voltage threshold of voltage sufficient to stabilize the molecular close-packed structure in case

of the molecules with various fluorination. While F_{16}CuPC layer cannot be stabilized, F_0CuPC OCP structure is stable at sample voltage U_S < -1.7 V, binary mixture F_{16}CuPC+ F_0CuPC is stable at U_S < -1.0 V and the F_8CuPC layer is stable without the electric field. In case of hydrogen bonding responsible for stability of the layer, the binary mixture would be more stable than the F_8CuPC layer, because of more possible F...H contacts, in contrast to the observation.

Ab-initio calculations on extended lattices are used to distinguish molecule-substrate and intermolecular interactions. A systematic comparison of combinations of phthalocyanines with various fluorination allows to understand how the molecular periphery influences the intermolecular interaction. Results of the calculations confirm the higher stability in terms of cohesive energy of F_8CuPC molecular layer compared to F_{16}CuPC+ F_0CuPC binary mixture and support the conclusion that the process of self-ordering by hydrogen-like bonding is not acceptable in the studied case.

This work was supported by the Czech Science Foundation (Contract No. 16-15802S). DFT calculations reported in this work have been performed at the Interdisciplinary Center of Mathematical and Computational Modeling of the University of Warsaw within Grant No. GA73-20 and GB73-18. B.P. and L.J. acknowledge the support from the University of Wroclaw (Grant No. 1010/S/IFD/18).

[1] P. Matvija, F. Rozbořil, P. Sobotík, I. Ošťádal, B. Pieczyrak, L. Jurczyszyn, P. Kocán, Sci. Rep., 7, 7357 (2017)

[2] P. Matvija, F. Rozbořil, P. Sobotík, I. Ošťádal, P. Kocán, J. Phys. Chem. Lett., 8, 4268–4272 (2017).

[3] F. Rozbořil, I. Ošťádal, P. Sobotík, P. Kocán, Phys. Rev. E 99, 032110 (2019)

The TensErLEED Management Package: A new environment for analysis and calculation of LEED I(V) data

F. Kraushofer[1], M. Schmid[1], U. Diebold[1], L. Hammer[2], and M. Riva[1]

[1] *Institute for Applied Physics, TU Vienna, Austria*
(corresponding author: M. Riva, riva@iap.tuwien.ac.at)

[2] *Institute of Condensed Matter Physics, FAU Erlangen-Nürnberg, Germany*

Low-Energy Electron Diffraction (LEED) is a structure-sensitive technique commonly available in most surface science laboratories. Beyond the usual application as a tool to determine periodicity and degree of order of a surface phase, the method also gives access to the surface's crystallographic structure via a quantitative analysis of the modulation of beam intensities as a function of electron energy/voltage (LEED I(V)). This, however, requires complex full-dynamical intensity calculations as well as a time-consuming optimization of structural parameters minimizing the deviation between experimental and calculated $I(V)$ curves. The Erlangen program package TensErLEED [1] readily performs this task, but its required user input is almost prohibitively complex. This not only presents a significant hurdle for potential new users seeking to adopt the technique, but also carries a potential for human error even if the user has extended experience with the program.

We show that for most cases, the necessary TensErLEED input can be generated automatically by combining a handful of user parameters, a set of default values, and a structure file in a standard format. Based on this, we introduce a new package that greatly simplifies the use of TensErLEED and substantially reduces the amount of work and potential for errors, even for experienced users. Furthermore, functionality is enhanced by features like automatic detection of the surface symmetry, which can then be enforced during parameter optimization. To improve compatibility with modern data analysis software, output files from TensErLEED are automatically processed to supply $I(V)$ curves and optimized atom positions in standard file formats. Utilities for file conversion are supplied to ensure backwards compatibility with older data processed by TensErLEED.

The package is completed by a versatile utility for extracting experimental $I(V)$ spectra from a LEED video or a stack of LEED images. This combination of a powerful data acquisition tool and simplified data analysis will allow LEED I(V) to become a more easy-to-implement, mainstream technique in the future.

[1] V. Blum, K. Heinz, Computer Physics Communications 134 (2001) 392

Electroreduction of water on Mo_2C film electrodes affected by the presence of CO_2

Eva-Maria Wernig[1], Daniel Winkler, Christoph Griesser, Niusha Shakibi Nia, Haobo Li, Karsten Reuter, and Julia Kunze-Liebhäuser

Institut für Physikalische Chemie, Leopold-Franzens-Universität Innsbruck, 6020 Innsbruck, Austria (corresponding author: J. Kunze-Liebhäuser, e-mail: julia.kunze@uibk.ac.at)

The materials class of transition metal carbides (TMCs) has gained importance among electrocatalysts for reduction processes such as the hydrogen evolution reaction (HER) and the CO_2 reduction reaction (CO_2RR). In the CO_2RR, theoretical calculations [1] predict that TMCs are promising alternatives to Cu catalysts due to their ability of breaking the binding energy scaling relations for the corresponding reaction intermediates, which has been experimentally shown to result in less negative onset potentials for hydrocarbon formation on Mo_2C compared to Cu [2]. For a comprehensive understanding of the electrocatalytic properties of Mo_2C towards the CO_2RR and the competing HER in aqueous electrolytes, the present study merges materials science and interface analytics with electrochemistry to unravel the pathways of these complex reactions.

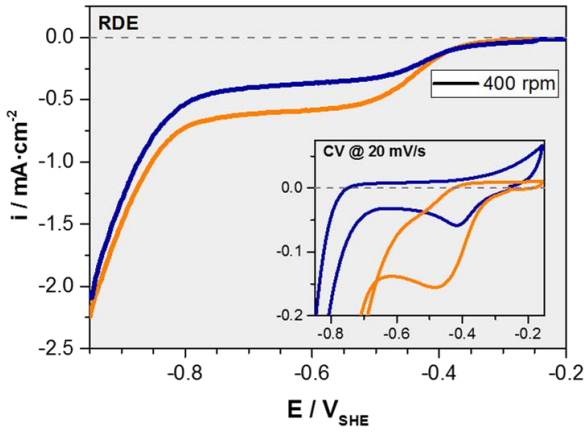

Figure 1: Rotating disc electrode (RDE) measurements compared to cyclic voltammograms (CV) in hanging meniscus configuration (inset) on Mo_2C in Ar and CO_2 saturated 0.1 M $NaClO_4$.

We report on the synthesis of Mo_2C films using direct carburization of polycrystalline Mo substrates through carbothermal conversion. Cyclic voltammetry, complemented by rotating ring disc electrode (RRDE) measurements (see Figure), was used to investigate the electrocatalytic activity of Mo_2C films towards the HER in the absence and presence of CO_2, while changes of the chemical composition at the surface were analyzed with ex-situ emersion X-ray photoelectron spectroscopy (XPS). Subtractively normalized interfacial Fourier transform infrared spectroscopy (SNIFTIRS) enabled the in-situ determination of reaction intermediates at the solid/liquid interface while gas chromatography was used for the detection of hydrogen. The activity of Mo_2C film electrodes towards the HER was observed to be enhanced in the presence of CO_2.

We find that proton and water reduction are separated processes at Mo_2C film electrodes under mildly acidic conditions. The proton reduction is strongly enhanced when CO_2 is present in the electrolyte. This can be understood by considering the surface pH, which is less altered with CO_2, and by taking into account the proton reduction mechanism, which is changed through the presence of CO_2.

Through correlation of the interface chemistry under polarization at certain potentials and theoretical calculations of the Pourbaix diagram, the stable phases at the interphase during proton and CO_2 reduction conditions can be determined. It is found that in the potential range of proton reduction, a two monolayer thick MoO_2 film covers the electrode. For use of Mo_2C as CO_2RR and HER catalyst, the Pourbaix diagram has to be taken into account, which shows that the potential and pH range, where this material can be used as a catalyst, is very limited.

[1] R. Michalsky, Y. J. Zhang, A. J. Medford, A. A. Peterson, *J. Phys. Chem. C* 118, 13026-13034 (2014).

[2] S. K. Kim, Y. J. Zhang, H. Bergstrom, R. Michalsky, A. Peterson, *ACS Catal.* 6, 2003-2013 (2016).

Epitaxial vanadium dioxide – material for anisotropic switchable thin films

F. Ligmajer[1,2], P. Kepič[1], and T. Šikola[1,2]

(corresponding author: F. Ligmajer, e-mail: filip.ligmajer@ceitec.vutbr.cz)

[1] *Central European Institute of Technology, Brno University of Technology, Purkynova 123. 612 00 Brno, Czech Republic*

[2] *Institute of Physical Engineering, Faculty of Mechanical Engineering, Brno University of Technology, Technicka 2. 616 69 Brno, Czech Republic*

Metasurfaces and metamaterials are artificially nanostructured 2D and 3D structures with optical properties derived from their subwavelength building blocks (meta-atoms) rather than from the constituent material [1]. Careful engineering of the size and shape of the underlying nanostructures can thus result in an artificial electromagnetic space and subsequent propagation of light in unprecedented ways [2]. One of the contemporary challenges of this field is the issue of metamaterials' tunability and switching. Current approaches involve mechanical reconfigurability, modulation of charge-carrier density or introduction of phase-change materials, i.e. materials which can undergo some structural phase change related to the respective change of the optical properties [3]. Vanadium dioxide (VO_2) is one of the two most prominent phase change materials used today, either as a switchable substrate layer underneath the meta-atoms, or as the material forming the nanostructured meta-atoms themselves.

In this contribution we will show how carefully selected combination of monocrystalline substrate with the deposition conditions can lead to creation of thin VO_2 films with engineered degrees of symmetry. Specifically, utilization of monocrystalline sapphire substrates which were cut along particular crystal faces results in formation of VO_2 nanobeams along favourable crystallographic directions. Such nanobeam layers can be utilized for switchable polarizing elements or photonic modulators.

This work was supported by the TACR programme National Centre of Competence (Grant Nr. TN01000008 – Centre of electron and photon optics). Access to the CEITEC core facilities was supported by the Ministry of Education, Youth and Sports of the Czech Republic under the projects CEITEC 2020 (LQ1601) and CEITEC Nano (LM2015041).

[1] M. Kadic, G. W. Milton, M. van Hecke and M. Wegener, Nat. Rev. Mats 1, 198 (2019)

[2] M. L. Tseng et al., Adv. Opt. Mat. 6, 1800554 (2018)

[3] A. M. Shaltout, V. M. Shalaev, M. L. Brongersma, Science 364, 648 (2019)

How to clean a sample when sputtering is not possible because the sample has only one atomic layer?

A. Niggas[1], J. Schwestka[1], S. Creutzburg[2], T. Gupta[3],
B. C. Bayer-Skoff[3], F. Aumayr[1], and R. A. Wilhelm[1,2]

(corresponding author: A. Niggas, e-mail: niggas@iap.tuwien.ac.at)

[1] *Institute of Applied Physics, TU Wien, 1040 Vienna, Austria*
[2] *Institute Ion Beam Physics and Materials Research, Helmholtz-Zentrum Dresden-Rossendorf, Dresden 01328, Germany*
[3] *Institute of Materials Chemistry, TU Wien, 1040 Vienna, Austria*

In recent years interest in two-dimensional materials has experienced a strong rise and they have been a hot topic ever since the discovery of a single layer graphene in 2004 [1]. As they entail promising properties for future devices, a great effort was put into research for tunnelling devices, tuneable light-emitting diodes and molecular sieving possibilities [2-4]. However, two-dimensional materials have not only good prospects in regard to applications but are also interesting for fundamental research: We study ion-solid interaction where 2D materials come with the possibility of ion transmission so that ions can still be detected after the interaction with the material for instance [5].

One major issue concerning atomically thin materials is handling contaminations. Graphene for example is known to be hosting many contaminations mostly in the form of hydrocarbons, water and residuals from production and transfer processes [6]. In the case of a one-layer material, popular cleaning techniques like sputtering are detrimental to material stability, so other techniques need to be addressed.

We study the interaction of highly charged ions and two-dimensional materials. The ions (Xe^{1+} to Xe^{44+}) are produced in an electron beam ion source (EBIS) and individual charge states are extracted with kinetic energies in the range of 1-400 keV. After transmission through the sample, the exit charge states of the ions are separated by means of a pair of deflection plates. Additionally, an electron emission statistics setup detects the yield of emitted electrons. Coincidence measurements of transmitted ions and emitted electrons are possible and also allow determination of the time of flight of the incident projectiles and hence determination of the energy loss within the interaction [7,8].

Here, we want to present two techniques to clean our samples *in situ* before and during measurements based on presented possibilities in [9]. Heating and laser annealing both will be discussed regarding achieved cleaning results. Cleaned samples were analysed with ion beam spectroscopy and atomically resolved (scanning) transmission electron microscopy (S)TEM.

STEM measurements confirm our results and indeed show clean areas surrounded by areas with thick contamination. The latter are invisible for our ion beam spectroscopy, since ions get stuck or are transmitted with large energy loss and hence significantly longer time of flights which can be discriminated in our analysis (cf. figure 1).

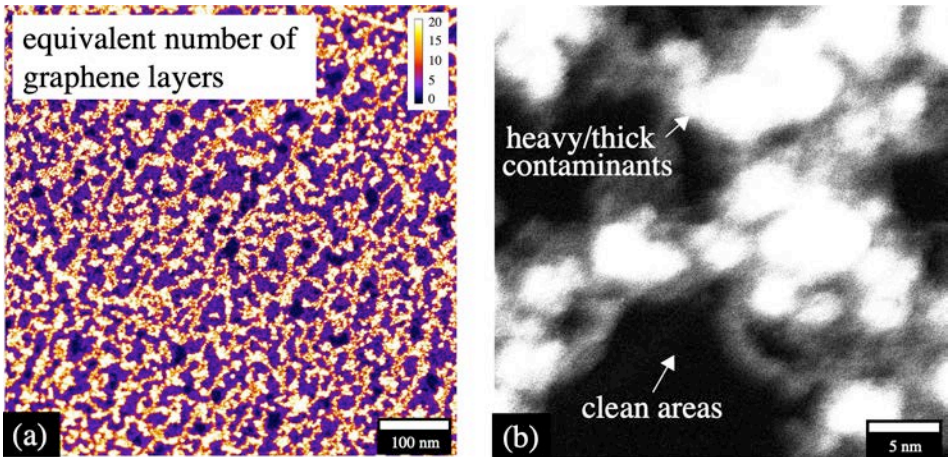

Figure 1 - STEM images of a single layer of graphene after cleaning procedure. The colour code in (a) shows the thickness of the sample in equivalent numbers of graphene layers. In (b) clean areas and areas with heavy/thick contamination are marked.

Finally, a comparison of measurements with cleaned samples to ones performed prior to the installation of cleaning procedures will complement this contribution.

Support by the Austrian Science Fund (FWF) is greatly acknowledged (project Y 1174-N36).

[1] K. Novoselov, A. Geim, S. Morozov, D. Jiang, Y. Zhang, S. Dubonos, I. Grigorieva, and A. Firsov, Science 306, 666 (2004)

[2] K. Novoselov, A. Mishchenko, A. Carvalho, and A. Castro Neto, Science 353, 461 (2016)

[3] F. Withers, O. Del Pozo-Zamudio, A. Mishchenko, A. Roney, A. Gholinia, K. Watanabe, T. Taniguchi, S. Haigh, A. Geim, A. Tartakovskii, and K. Novoselov, Nature Materials 14, 301 (2015)

[4] J. Abraham, K. Vasu, C. Williams, K. Gopinadhan, Y. Su, C. Cherian, J. Dix, E. Prestat, S. Haigh, I. Grigorieva, P. Carbone, A. Geim, and R. Nair, Nature Nanotechnology 12, 546 (2017)

[5] E. Gruber, R. Wilhelm, R. Pétuya, V. Smejkal, R. Kozubek, A Hierzenberger, B. Bayer, I. Aldazabal, A. Kazansky, F. Libisch, A. Krasheninnikov, M. Schleberger, S. Facsko, A. Borisov, A. Arnau, and F. Aumayr, Nature Communications. 7, 13948 (2016)

[6] Y.-C. Lin, C.-C. Lu, C.-H. Yeh, C. Jin, K. Suenaga, and P.-W. Chiu, Nano Letters 12, 414 (2012)

[7] J. Schwestka, D. Melinc, R. Heller, A. Niggas, L. Leonhartsberger, H. Winter, S. Facsko, F. Aumayr, and R. Wilhelm, Review of Scientific Instruments 89, 085101 (2018)

[8] J. Schwestka, A. Niggas, S. Creutzburg, R. Kozubek, R. Heller, M. Schleberger, R. Wilhelm, and F. Aumayr, The Journal of Physical Chemistry Letters 10, 4805 (2019)

[9] M. Tripathi, A. Mittelberger, K. Mustonen, C. Mangler, J. Kotakoski, J. Meyer, and T. Susi, Physica Status Solidi – Rapid Research Letters 11, 1700124 (2017)

Laser-induced analysis of the deuterium retention in Ta and W

J. Oelmann, D. Zhao[1], S. Mittelmann[2], D. Wu[3], E. Wüst, S. Brezinsek, S. Dickheuer, R. Krug, A. Kreter, and Ch. Linsmeier

Forschungszentrum Jülich GmbH, Institut für Energie- und Klimaforschung – Plasmaphysik, 52425 Jülich, Germany
(corresponding author: J. Oelmann, e-mail: j.oelmann@fz-juelich.de)

[1] *Southwestern Institute of Physics, Chengdu, Sichuan, 610041, China*

[2] *Institut für Laser- und Plasmaphysik, Heinrich-Heine-Universität Düsseldorf, Germany*

[3] *Key Laboratory of Material Modification by Laser, Ion and Electron Beams, Dalian University of Technology, China*

Laser-based techniques like Laser-Induced Breakdown Spectroscopy (LIBS) [1] enable for preparation free characterisation of material surfaces with a possible in-situ application in fusion devices like ITER or Wendelstein 7-X. The quantitative determination of hydrogen (H) and deuterium (D) retention in first wall materials like tungsten (W) is from particular interest, for example to analyze plasma-wall interactions and the plasma confinement [2].

In this study, we use a lab set-up combining LIBS and gas analysis after the ablation (Laser-Induced Ablation - Quadrupole Mass Spectrometry: LIA-QMS) [3], which simplifies the quantification process and reduces its uncertainties. Tantalum (Ta) and W samples were exposed to a D plasma in the linear plasma device PSI-2 [4] with a total fluence of up to 5.5×10^{25} D ions/m^2. The samples are placed in the maximum of the ion flux of a hollow plasma profile. A langmuir probe measures the radial gradient of the flux. The laser-based techniques are applied to analyze the retention of D depending on the ion fluence and the material. For W and Ta, the main major part of the detected deuterium is found in the first 30 nm and 50 nm of the sample, respectively, whereas studies with exposed carbon showed significant retention up to several μm [5]. The amount of retained D scales as the square root of the fluence, which is in good agreement with literature data for W [6, 7]. The quantitative LIA-QMS results are compared to Thermal Desorption Spectroscopy (TDS) and Nuclear Reaction Analysis (NRA) of the samples.

The LIBS measurement using this set-up with a pulse durations of $\tau = 35$ ps laser are compared to analyses of the same samples using systems with a $\tau = 8$ ns laser from Dalian University of Technology and a sub $\tau = 10$ fs laser from Heinrich-Heine-Universität Düsseldorf. Hence, the influence of desorption due to the thermal penetration depth of the

lasers is examined to gain a deeper understanding of the laser-induced ablation process. Moreover, this comparison is accounted to find the optimal pulse duration for an in-situ application of laser-based techniques in a fusion device with high detection limit of the measured D_α signal.

An alternative approach to increase the detection limit in ex-situ analysis is to use a second laser pulse to heat the plasma, which is formed in the laser-induced ablation process, called Double Pulse (DP)-LIBS [8]. The setup for this technique using a Nd:YAG laser with simultaneously available pulses of the wavelengths 1064 nm, 532 nm and 355 nm is presented and first results are shown.

[1] R. Noll, Springer Berlin Heidelberg (2012)
[2] C. Li, et al., Physica Scripta T170, 014004 (2017)
[3] J. Oelmann, et al., Spectrochimica Acta - Part B Atomic Spectroscopy 144, 38–45 (2018)
[4] A. Kreter, et al., Fusion Science and Technology 68, 8-14 (2015)
[5] D. Youchison, et al., Nuclear Materials and Energy 17, 123–128 (2018)
[6] T. Venhaus, et al., Journal of Nuclear Materials 290-293, 505-508 (2001)
[7] R.P. Doerner, et al., Nuclear Materials and Energy 9, 89–92 (2016)
[8] R. Hai, et al., Fusion Engineering and Design 89, 2435–2439 (2014)

Methods for exposing single-crystal metal-oxide samples to liquid/high pressure with preparation and characterization in UHV.

J. Pavelec, C. Kovacs, F. Kraushofer, F. Mirabella, J. Xu, J. Balajka, M. Schmid, U. Diebold, and G.S. Parkinson

Institute of Applied Physics, Vienna University of Technology, A-1040 Wien, Austria
(corresponding author: J. Pavelec, e-mail: pavelec@iap.tuwien.ac.at)

The importance of bridging the pressure gap in studies of model catalysts has been recognized for decades. The investigation of surfaces under ambient conditions still remains a challenge due to the restricted number of experimental techniques available and a high risk of contamination.

The poster will briefly present the design of two working instruments for tackling the pressure gap in surface science: An apparatus for dosing liquid water in ultrahigh vacuum [1] and a high-pressure cell [2]. The third presented instrument is currently under development: An electrochemical cell with in-situ infrared reflection absorption spectroscopy (IRAS) and differential electrochemical mass spectroscopy (DEMS). It utilizes experience gained during developing first two working instruments.

The first instrument is an apparatus for dosing liquid water in ultrahigh vacuum [1,2]. This allows dosing ultrapure liquid water on the surface of a sample (typically a single crystal) without exposure to air. The apparatus is coupled to an existing surface-science chamber, which enables reproducible sample preparation and sample characterization by UHV-based analytical techniques. First the water is condensed to a small cryostat, forming ultrapure ice. The ice is held at cryogenic temperature, which reduces its vapor pressure to the UHV range. A single crystalline sample is moved below the ice inside a small UHV volume. Upon warming, the ice melts and forms a liquid droplet, which drops onto the sample. The small chamber is then evacuated by cryopump, and sample transferred to the UHV setup for post characterization by STM, LEIS, LEED, XPS. The case study of Fe_3O_4 (001) surface exposed to water is shown [3].

The second presented instrument is a novel design for a high-pressure cell, which is connected to a LT STM/Q+AFM UHV system. The setup allows to prepare single metal oxide samples under UHV conditions and transfer them to the cell. It allows us to study reaction processes occurring on UHV-prepared metal-oxide single crystals samples at pressures up to 1 bar and temperatures up to 500 °C. In our setup, only the sample surface and the inner surface of a quartz tube are exposed to the gas at elevated temperature, which minimizes contamination. The maximum operational temperature is currently limited by quartz purity.

The sealing is provided by the optically flat polished surface on the quartz tube, which is pressed (load of 20-80N) onto the sample surface. A case study of the Fe_3O_4 (001) surface exposed to water vapor is presented. Surface exposed to water vapor exhibits same features as the surface exposed to liquid water [3].

The third presented instrument is a UHV-compatible electrochemical flow cell, which is to be combined with in-situ DEMS and IRAS. Electrochemical surface science is relatively well established, but studies involving metal-oxide single crystals remain rare, and best practices for UHV-to-electrolyte transfer are still being established. Here, we focus on the development of sample transfer and measurement techniques. To speed up the design process and optimize the cell performance, we have performed numerical simulations utilizing the program COMSOL Multiphysics. In particular, the simulations allow us to optimize the thickness of the flow cell, which has a major impact on IRAS and the electrochemical cell performance. Further, the residence time in the cell is also optimized to improve DEMS detection. The simulations focus on mass transport through the cell, as well as the reaction at the catalytic interface. Finally, charge transport is studied to optimize the position and shape of the counter and reference electrodes. Crucially, the transfer must be made without exposure to air. Here we would utilize the experience gained on apparatus for dosing liquid water in UHV and high-pressure cell.

Support by the FWF funding (START award Y847-N20) is gratefully acknowledged.

[1] J. Balajka, J. Pavelec , M. Komora, M. Schmid, U. Diebold (2018). "Apparatus for dosing liquid water in ultrahigh vacuum." Review of Scientific Instruments 89(8): 083906.

[2] J. Balajka, M.A. Hines, W. DeBenedetti, M. Komora, J. Pavelec, M. Schmid, U. Diebold (2018). "High-affinity adsorption leads to molecularly ordered interfaces on TiO2 in air and solution." Science 361(6404): 786-789.

[3] F. Kraushofer, F. Mirabella, J. Xu, J. Pavelec, J. Balajka, M. Müllner, N. Resch, Z. Jakub, J. Hulva, M. Meier, M. Schmid, U. Diebold and G. S. Parkinson (2019). "Self-limited growth of an oxyhydroxide phase at the Fe3O4(001) surface in liquid and ambient pressure water." The Journal of Chemical Physics 151(15): 154702.

Design of an IRAS Setup to Investigate Adsorbates on Metal-Oxide Single Crystals

D. Rath, J. Pavelec, G. S. Parkinson, M. Schmid, U. Diebold

Institut für Angewandte Physik, Technische Universität Wien, A-1040 Wien, Austria
(corresponding author: D. Rath, e-mail: rath@iap.tuwien.ac.at)

A major goal of science has always been to transfer and apply the results of basic research to real systems. Especially chemists and physicists follow sometimes the same goal but with completely different methods. A technique capable of connecting this two academic fields is IRAS (**I**nfrared **R**eflection **A**bsorption **S**pectroscopy). This technique is based on the measurement of infrared radiation reflected on a substrate. Vibrational modes of molecules adsorbed at a surface modify the dielectric properties at the resonance frequency, and, thereby, the intensity of the reflected IR radiation. As a consequence, determination of the type of molecule and the bond to the surface is possible. The challenge to investigate molecules on oxide surfaces is a weaker signal compared to metal surfaces [1]. Therefore, it is important to give special treatment to the throughput of the system. The aim of the newly developed IRAS system GRISU (**GR**azing incident **I**nfrared absorption **S**pectroscopy **U**nit) is to improve the efficiency of the system to enable investigations in the research field of single atom catalysis.

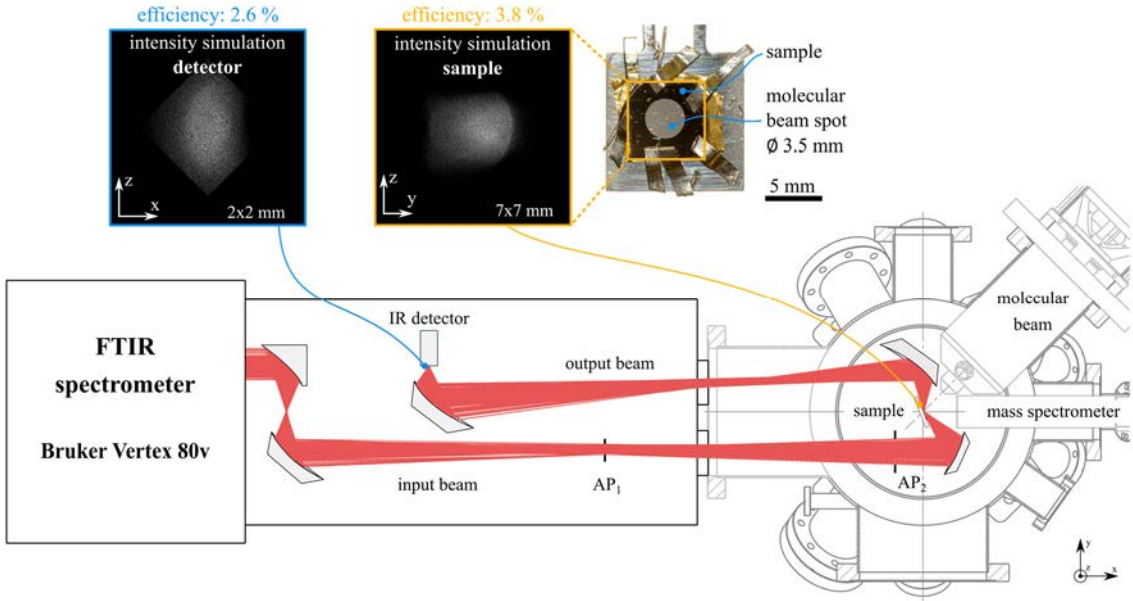

Figure 1.: (top) Simulated intensity distribution on the detector and the sample. (bottom) Schematic illustration of the IRAS setup GRISU. The main parts of the system are a FTIR spectrometer (left side of the image) one parabolic mirror, four elliptical mirrors, an MCT detector and the TPD chamber. Additionally, the optical system is equipped with two apertures to control the illumination shape on the sample and the incidence angle range on the sample, respectively.

GRISU is an optical system combining the commercially available FTIR spectrometer Bruker Vertex 80v with an UHV chamber [2]. This system features one parabolic mirror directly at the spectrometer output and four elliptical mirrors. Two of these elliptical mirrors are in the UHV

chamber and are used to illuminate the sample or collect the reflected radiation, respectively. Due to the geometry of the chamber it is necessary to design a system with a large distance of about 1 m between spectrometer and chamber. In our design, a large fraction of the beam intensity is focused to the 3.5 mm big molecular beam spot [3] on the sample. The small focal spot (3 mm) of the system is achieved by the shorter distance between mirror and sample of 60 mm. A beam shaping aperture is necessary to control the background signal originating from the surrounding area of the molecular beam spot.

The incidence angle range of the IR radiation on the sample is also an important factor. This is shown by calculations based on references [4, 5]. The band inversion at the Brewster angle requires a restriction of the angle range either to the left or right side of the Brewster angle, different for different substrates. In our IRAS system, this angle range limitation is realised by the second aperture AP_2.

The simulated system (done with a ray tracing program) shows an efficiency of 2.6 % of all IR radiation reaching the detector. Compared to a commercially available system with two parabolic mirrors with a focal length of 500 mm, this is higher by a factor of about 60. Compared to a system with two parabolic mirrors with 180 mm focal length the efficiency is increased by a factor of about 10. Reflective losses on the mirrors and absorption by the windows are not included in any of these simulations, and the sample is assumed to be a perfect mirror.

Furthermore, the compact design requires just one CF 150 flange on the UHV chamber. Optimised incidence angles for different materials in the range from 49 ° to 85 ° are possible. The ability to shape the illumination spot and the focus spot diameter of 3 mm provide a good reduction of the background signal originating from the area surrounding the molecular beam spot.

[1] Jürgen Kattner and Helmuth Hoffmann. “External reflection spectroscopy of thin films on dielectric substrates”. Handbook of vibrational spectroscopy (2002).

[2] Jiri Pavelec. “Surface chemistry setup and adsorption of CO_2 on Fe_3O_4(001)”. PhD thesis. TU Wien, 2019.

[3] Jiri Pavelec et al. “A multi-technique study of CO_2 adsorption on Fe_3O_4 magnetite”. J. Chem. Phys. 146 (2017), 014701.

[4] David C Langreth. “Macroscopic approach to the theory of reflectivity”. Phys. Rev. B 39 (1989), 10020.

[5] RG Tobin. “Asymmetric lines and background shifts in reflection-absorption infrared spectroscopy”. Phys. Rev. B, 45 (1992), 12110.

Detecting Tiny Cation Nonstoichiometry in Complex Oxide Films

Michele Riva, Giada Franceschi, Michael Schmid, and Ulrike Diebold

Institute of Applied Physics, TU Wien, Austria

(corresponding author: M. Riva, e-mail: riva@iap.tuwien.ac.at)

The rise of semiconductor-based electronics has gone hand in hand with the technological advancements allowing to reproducibly prepare materials with exceptionally small concentration of defects. A similar control of defects and composition is the key to making all-oxide electronics a reality, allowing to fully exploit the multitude of functionalities of these materials. Precise tuning of the oxide composition, however, requires the development of reliable tools to detect cation nonstoichiometry with extreme sensitivity: We develop an unconventional method based on STM that pushes down this detection limit by at least one order of magnitude [1].

We take advantage of the well-controlled surface reconstructions of $SrTiO_3$(110), and use the established relation between those reconstructions and the surface composition to assess the cation excess deposited in PLD-grown $SrTiO_3$(110) films. We demonstrate that a $< 0.1\%$ change in cation non-stoichiometry is detectable by our approach, and show that, for thin films that accommodate all the nonstoichiometry at the surface, our method has no fundamental detection limit.

[1] M. Riva, G. Franceschi, Q. Lu, M. Schmid, B. Yildiz, and U. Diebold, Phys. Rev. Mater. 3, 043802 (2019)

Solar Wind Sputtering Investigations on Planetary Mineral Analogues

P.S. Szabo, H. Biber, N. Jäggi[1], M. Brenner, D. Weichselbaum, M. Wappl, M.V. Moro[2], A. Niggas, R. Stadlmayr, D. Primetzhofer[2], A. Nenning[3], A. Mutzke[4], M. Sauer[5], J. Fleig[3], A. Foelske-Schmitz[5], K. Mezger[6], H. Lammer[7], A. Galli[1], P. Wurz[1], and F. Aumayr

Institute of Applied Physics, TU Wien, 1040 Vienna, Austria
(corresponding author: P.S. Szabo, e-mail: szabo@iap.tuwien.ac.at)

[1] *Physics Institute, University of Bern, 3012 Bern, Switzerland*

[2] *Department of Physics and Astronomy, Uppsala University, Ångströmlaboratoriet, 752 37 Uppsala, Sweden*

[3] *Institute of Chemical Technologies and Analytics, TU Wien, 1060 Vienna, Austria*

[4] *Max Planck Institute for Plasma Physics (IPP), 17491 Greifswald, Germany*

[5] *Analytical Instrumentation Center, TU Wien, 1060 Vienna, Austria*

[6] *Institute of Geological Sciences, University of Bern, 3012 Bern, Switzerland*

[7] *Space Research Institute, Austrian Academy of Sciences, 8042 Graz, Austria*

Planets, moons and asteroids that are not protected by a significant atmosphere are strongly exposed to the so-called space weathering effects. Here sputtering by solar wind ions plays an important role [1]. Together with electron-stimulated desorption, UV photon-stimulated desorption and micrometeorite impacts, it affects the surfaces of rocky bodies severely [2]. Their optical properties are changed and surface atoms are emitted to form a thin atmosphere, a so-called exosphere [3]. Understanding both these effects is of great interest for remote investigations in planetary science. Spectroscopy of the light reflected at the surface as well as analyzing the exosphere's composition allow probing the surfaces of planets and moons without performing an expensive spacecraft landing. Exosphere analysis, for example, is an important scientific goal for ESA's BepiColombo mission, which has recently launched to Mercury.

In order to correctly interpret remote analysis results, laboratory experiments with analogue minerals are essential. Especially for solar wind sputtering, knowledge of the occurring effects is still lacking and sputtering estimations mostly rely on TRIM simulations [4]. For example, changes in the surface composition resulting from preferential sputtering or effects that go beyond the kinetic sputtering from the ion-induced collision cascade need to be better understood.

For this reason, we have investigated sputtering of the pyroxene minerals wollastonite $CaSiO_3$ and augite (Ca, Mn, Fe)SiO_3, which are expected to make up a large part of the surfaces of Moon and Mercury [5]. Thin films of these materials were deposited on Quartz Crystal Microbalances (QCM) to allow in-situ real time sputtering yield measurements [6]. These targets were irradiated with different ion species at energies corresponding to 1 keV/amu representative for the solar wind, which contains about 96% H^+, 4% He^{2+} and minor contributions from heavier multiply charged ions [7].

Kinetic sputtering yields were measured for different ions at varying energies. Based on these findings adapted input parameters for simulations with the software SDTrimSP were defined [8], which consistently reproduce measured sputtering yields. Potential sputtering, which enhances the erosion of insulating surfaces by multiply charged ions, was especially investigated for He^{2+} and Ar^{q+} ($q \leq 8$). Linearly increasing sputtering yields with potential energy as well as strong decreases with ion doses were found. The latter effect could be connected to a preferential O depletion from potential sputtering by modelling the surface composition changes [9].

Based on these findings, the total effect of solar wind sputtering on pyroxene minerals was estimated. Due to the small H^+ sputtering yields, He^{2+} becomes more important. Especially its potential sputtering contribution will cause more release into the exosphere as well as significantly reducing the surface O content. These results agree with previous models (see for example [10, 11]), which gives a consistent view on solar wind sputtering effects from laboratory experiments to model predictions.

Financial support has been provided by the Austrian Science Fund FWF (Project No. I 4101-N36) and by KKKÖ (Commission for the Coordination of Fusion research in Austria at the Austrian Academy of Sciences - ÖAW) as well as the Swiss National Science Foundation Fund (200021L_182771/1). Support by VR-RFI (contracts #821-2012-5144, #2017-00646_9 & 2018-04834) and the Swedish Foundation for Strategic Research (SSF, contract RIF14-0053) supporting operation of the accelerator at Uppsala University is gratefully acknowledged.

[1] B. Hapke, J. Geophys. Res.: Planets 106, 10039 (2001)
[2] R. A. Killen, et al., Space Sci. Rev. 132, 433 (2007)
[3] P. Wurz, et al., Icarus 191, 486 (2007)
[4] J. F. Ziegler, M. D. Ziegler, J. P. Biersack, Nucl. Instr. Methods Phys. Res. B 268, 1818 (2010)
[5] P. Wurz, J. A. Whitby, U. Rohner, J. A. Martín-Fernández, H. Lammer, C. Kolb, Planet. Space Sci. 58, 1599 (2010)
[6] G. Hayderer, M. Schmid, P. Varga, H. P. Winter, F. Aumayr, Rev. Sci. Instrum. 70, 3696 (1999)
[7] C. T. Russell, J. G. Luhmann, R. J. Strangeway, Space Physics: An Introduction, Cambridge University Press (2016)
[8] A. Mutzke, R. Schneider, W. Eckstein, R. Dohmen, K. Schmid, U. v. Toussaint, G. Badelow, IPP-Report (2019)
[9] P. S. Szabo, et al., Icarus 314, 98 (2018)
[10] H. Hijazi, et al., J. Geophys. Res.: Planets 122, 1597 (2017)
[11] S. T. Alnussirat, et al., Nucl. Instrum. Methods Phys. Res. B 420, 33 (2018)

SAES CapaciTorr and NEXTorr Pumps Vacuum Excellence in a compact package for your Surface Science system

- Ideal solution to achieve 10^{-10} – 10^{-8} Pa
- Extremely compact and low-weight, perfect fit for complex and crowded UHV systems (XPS, STM, AFM, AES, ARPES, LEEM/PEEM,…)
- Utmost pumping speed for H_2
- High pumping speed for all active gases
- No need of power for operation
- Keep pumping even in case of power failures

CapaciTorr & NEXTorr pumps:
up to 3500 l/s (H_2) in less than 7 kg

www.saesgroup.com
neg_technology@saes-group.com

making innovation happen, together

saes group

Thursday

Molecular motor at the frontier of classical motion and quantum tunneling

S. Stolz[1,2], O. Gröning[1], J. Prinz[1,2], H. Brune[2], and R. Widmer[1]

[1] *Empa, Swiss Federal Laboratories for Materials Science and Technology, 8600 Dübendorf, Switzerland*
(corresponding author: R. Widmer, e-mail:roland.widmer@empa.ch)

[2] *Institute of Condensed Matter Physics, Station 3, EPFL, 1015 Lausanne, Switzerland*

In his seminal 1959 lecture "There's Plenty of Room at the Bottom", Richard Feynman envisioned the downscaling of information storage and machines to atomic dimensions [1]. Both challenges were eventually met, first by writing information by positioning single atoms on a nickel surface in 1990 [2], then by the realization of the first artificial, light-driven molecular machine in 1999 [3]. To this day, however, most synthetic molecular machines, while driven by quantum processes such as light absorption and bond reconfiguration, exhibit classical motion only [4,5].

We have realized and investigated a molecular motor, which converts non-directional, stochastic input stimuli into highly directional rotation and operates at the frontier between classical motion and quantum mechanical tunneling. It consists of a single acetylene (C_2H_2) rotor anchored to a chiral atomic cluster that acts as stator and is provided by a PdGa(111) surface as sketched in Figure 1. By breaking spatial inversion symmetry, the stator defines the unique sense of rotation. We have studied the electronically and thermally activated (5-25 K) motion of this motor by scanning tunneling microscopy (STM). While the thermally activated motion is non-directed, as dictated by the 2nd law of thermodynamics, inelastic electron tunneling (IET) through C_2H_2 triggers a rotation with the degree of directionality depending on the magnitude of the STM bias voltage.

Below 17 K and 30 mV bias voltage, a constant rotation frequency is observed which bears fundamental characteristics of quantum tunneling. The high directionality, exceeding 97%, implicates the combination of quantum and non-equilibrium processes in this regime, being the hallmark of macroscopic quantum tunneling [6].

The acetylene on PdGa(111) motor therefore pushes molecular machines to their extreme limits, not just in terms of size, but also regarding structural precision, degree of directionality, and crossover from classical motion to quantum tunneling. This ultra-small motor thus opens the possibility to investigate in-operando effects and origins of energy dissipation during tunneling events, and ultimately energy harvesting at atomic scales.

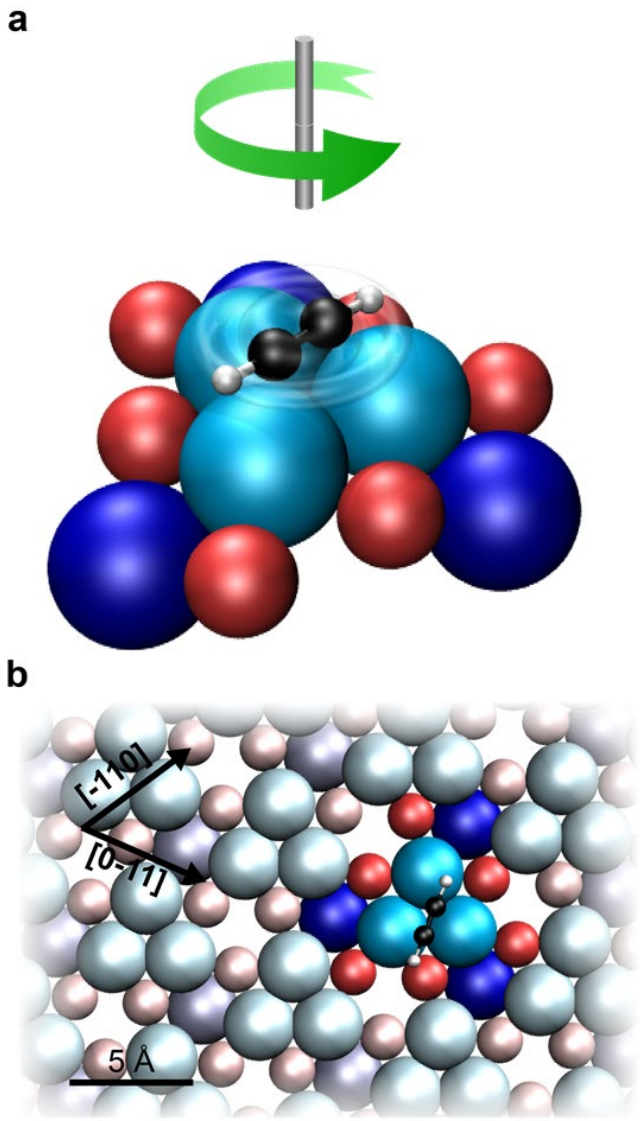

Figure 1: Acetylene rotation on the PdGa:A(-1-1-1)Pd_3 surface.

a Sketch of the acetylene on Pd_3 motor. **b** Atomic structure of the PdGa:A(-1-1-1)Pd_3 surface with the PdGa cluster acting as stator highlighted in saturated colors. The acetylene rotor is depicted in one of its three equivalent adsorption configurations. The top-layered Pd trimers (z = 0 Å) are depicted in bright blue, the second layered Ga trimers (z = -0.85 Å) in red and the third layered single Pd atoms (z = -1.61 Å) in dark blue. (Please refer to the electronic version for colors)

Support by the Swiss National Science Foundation is gratefully acknowledged.

[1] Feynman, R. P. There's Plenty of Room at the Bottom. (1959).

[2] Eigler, D. M. & Schweizer, E. K. Positioning single atoms with a scanning tunnelling microscope. *Nature* **344**, 524–525 (1990).

[3] Koumura, N., Zijlstra, R. W. J., van Delden, R. A., Harada, N. & Feringa, B. L. Light-driven monodirectional molecular rotor. *Nature* **401**, 152–155 (1999).

[4] Salma Kassern, T. van L., Anouk S. Lubbe, M. R. W. & Ben L. Feringa, D. A. L. Artificial molecular motors. *Chem Soc Rev* **46**, 2592–2621 (2017).

[5] Pezzato, C., Cheng, C., Stoddart, J. F. & Astumian, R. D. Mastering the non-equilibrium assembly and operation of molecular machines. *Chem. Soc. Rev.* **46**, 5491 (2017).

[6] Caldeira, A. O. & Leggett, A. J. Influence of Dissipation on Quantum Tunneling in Macroscopic Systems. *Phys. Rev. Lett.* **46**, 211–214 (1981).

The dynamic nature of CO adlayers on Pt(111) electrodes

J. Wei,[1,2] R. Amirbeigiarab,[1] Y.X. Chen,[2] S. Sakong,[3] A. Gross,[3] O.M. Magnussen[1]

Institute of Experimental and Applied Physics, Kiel University, Kiel 24098, Germany ia (corresponding author: O.M. Magnussen, e-mail: magnussen@physik.uni-kiel.de)

[1] *Institute of Experimental and Applied Physics, Kiel University, Kiel 24098, Germany*

[2] *Hefei National Laboratory for Physical Sciences at Microscale, University of Science and Technology of China, Hefei 230026, China*

[3] *Institute of Theoretical Chemistry, Ulm University, Albert-Einstein-Allee 11, 89081 Ulm, Germany*

The interaction of CO with metal surfaces is a major topic in electrocatalysis as well as in gas phase heterogeneous catalysis. CO is an important intermediate or poison in many catalytic reactions, such as electrochemical CO_2 reduction or electrode reactions in low-temperature fuel cells, and its interaction with platinum electrodes has accordingly received much attention. In particular, CO adlayers on Pt(111) are arguably the most extensively studied model system for electrochemical CO adsorption and oxidation [1]. The potential-dependent structure and dynamics of these adlayers are complex and still controversial. While at the negative limit of the double layer potential range the presence of a close-packed (2 × 2)-3CO adlayer is well established, a coherent picture in the pre-oxidation range is still lacking. Specifically, *in situ* STM observations reported in the presence of CO in solution additional transient CO_{ad} adlayer structures, namely a (2 x 2)-4CO and a (1 x 1)-CO adlayer, which were assigned to adsorbate structures where every Pt surface atom is occupied by a CO_{ad} in an atop or near-atop site [2]. The presence of such phases is highly surprising as it would imply that the CO_{ad} surface coverage (i) can be much higher than reported in all previous electrochemical or gas phase studies and (ii) transiently increases during pre-oxidation, contrary to the expected coverage decrease.

To resolve this mystery, we here employ in situ high-speed scanning tunneling microscopy for studying the surface phase behavior in CO-saturated 0.1 M H_2SO_4 on the millisecond time scale. At potentials near the onset of CO pre-oxidation local fluctuations in the (2 × 2)-CO adlayer are observed, which increase towards more positive potentials. Above 0.20 V (vs. Ag/AgCl), this leads to an adlayer where CO_{ad} apparently reside on every top site, but still exhibit a (2 × 2) superstructure modulation. We interpret this observation as a dynamic effect, caused by a small number of highly mobile point defects in the (2 × 2)-CO adlayer. In this scenario, the variations in CO_{ad} brightness within the apparent (1 x 1) phase reflect different probabilities for the molecules to reside in these sites. Specifically, our data indicate the coexistence of a rather static primitive (2 × 2) CO sublattice with highly dynamic CO on the

residual atop sites. Density functional theory calculations support this interpretation. They show that the CO lattice near such defects relaxes into a local (1 × 1) arrangement, which can rapidly propagate across the surface. This behavior resembles the "door-opening" mechanism, proposed recently to explain the fast diffusion of O_{ad} on a fully CO-covered Ru(0001) surface [3]. Also here, local density fluctuations in the CO_{ad} adlayer intermittently create O_{ad} diffusion pathways with low activation energy. The proposed mechanism enables a high CO_{ad} surface mobility during CO pre-oxidation, even in the presence of ordered adlayers of high packing density and thus ensures effective mixing of CO_{ad} and OH_{ad} on the electrode surface.

J.W. gratefully acknowledges the funding by China Scholarship Council (CSC), the National Natural Science Foundation of China (No. 21473175 and No. 21832004), and the 973 Program of the Ministry of Science and Technology (No. 2015CB932).S.S. and A.G. acknowledge support by the Baden-Württemberg Foundation through the project MSMEE within the High-Performance Computing II program and computer time through bwHPC and the German Research Foundation (DFG), grant number INST 40/467-1 FUGG.

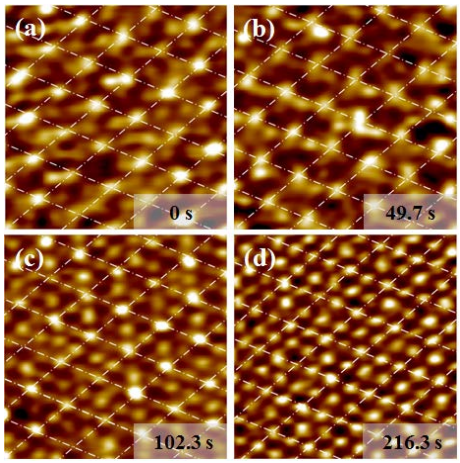

Figure 1. Potential-dependent structure of the CO adlayer on Pt(111) in CO-saturated 0.1 M H_2SO_4 solution. Video-STM images (3 nm × 3 nm) were recorded at (a) -0.10 V, (b) 0.12 V, (c) 0.20 V, and (d) 0.30 V and shoe gradual deviations from the (2 × 2) symmetry with increasing potential, resulting in a modulated (1 × 1) structure at the most positive potentials.

[1] N. Marković, P. Ross Jr, *Surface Science Reports* **2002**, *45*, 117-229

[2] C. Jung, B. Ku, J. Kim, C. K. Rhee, *Chemical Communications* **2006**, 2191-2193; b) C. Jung, J. Kim, C. K. Rhee, *Langmuir* **2007**, *23*, 9495-9500.

[3] A.-K. Henß, S. Sakong, P. K. Messer, J. Wiechers, R. Schuster, D. C. Lamb, A. Groß, J. Wintterlin, *Science* **2019**, *363*, 715-718

Adsorption of Carboxylic Acids on Magnetite Surfaces

Marcus Creutzburg[1,2], Heshmat Noei[1], Björn Arndt[1,2], Vedran Vonk[1], Elin Grånäs[1], Kai Sellschopp[3], Gregor Vonbun-Feldbauer[3], Andreas Stierle[1,2]

[1]*Deutsches Elektronen-Synchrotron (DESY), Notkestraße 85, 22607 Hamburg, Germany (corresponding author: A. Stierle, e-mail: andreas.stierle@desy.de)*

[2]*Department of Physics, University of Hamburg, Jungiusstraße 9, 20355 Hamburg, Germany*

[3]*Institute of Advanced Ceramics, Hamburg University of Technology, Denickestraße 15, 21073 Hamburg, Germany*

The adsorption behavior of carboxylic acids on magnetite surfaces is important for a fundamental understanding of oxide / organic interfaces, playing a decisive role for the mechanical properties of hierarchical materials composed of oleic acid stabilized magnetite nanoparticles [1,2]. Further on, formic acid is an important intermediate in the water gas shift reaction, catalyzed by magnetite. For both molecules the adsorption geometry and energetics on magnetite surface is largely unknown. We combine various surface sensitive methods such as Fourier transform infrared reflection absorption spectroscopy (FTIRRAS), scanning tunneling microscopy, x-ray photo emission, as well as surface x-ray diffraction to elucidate the structural and electronic properties of such organic / oxide interfaces. The experimental results are complemented by ab initio density functional theory calculations. We have investigated the room temperature adsorption of formic acid as well as oleic acid on the Fe_3O_4 (001) and (111) surfaces. Formic acid acts here as small probe molecule with the same end group as oleic acid. We find a distinctly different adsorption behavior for the different magnetite terminations: on the (001) surface, formate is formed in bridging bidentate geometry [3,4]. In addition the near surface cations undergo an adsorption driven structural rearrangement, re-establishing bulk stoichiometry, as compared to the oxygen rich clean surface with subsurface cation vacancy reconstruction [5,6]. On the Fe tet_1 terminated (111) surface, formic acid adsorbs in a quasi-bidentate geometry, as well as in a chelating bidentate configuration [7]. We find that the adsorption of the longer chained oleic acid molecules also differs on both surfaces, as well as compared to that of formic acid: on both surfaces non-dissociated oleic acid molecules are observed, but on the (111) surface a higher fraction of upstanding molecules is present.

This work was funded by the Deutsche Forschungsgemeinschaft (DFG, German Research Foundation)– Projektnummer 192346071–SFB 986.

[1] A. Dreyer, A. Feld, A. Kornowski, E. D. Yilmaz, H. Noei, A. Meyer, T. Krekeler, C. Jiao, A. Stierle, V. Abetz, H. Weller, G. A. Schneider, Organically linked iron oxide nanoparticle supercrystals with exceptional isotropic mechanical properties, Nature Materials 15, (2016) 522.
[2] B. Domènech, A. Plunkett, M. Kampferbeck, M. Blankenburg, B. Bor, D. Giuntini, T. Krekeler, M. Wagstaffe, H. Noei, A. Stierle, M. Ritter, M. Müller, T. Vossmeyer, H. Weller, G. A. Schneider, Modulating the mechanical properties of supercrystalline nanocomposite materials via solvent-ligand interactions, Langmuir (2019), doi: 10.1021/acs.langmuir.9b01938.
[3] [1] B. Arndt, K. Sellschopp, M. Creutzburg, E. Grånäs, K. Krausert, V. Vonk, S. Müller, H. Noei, G. Vonbun-Feldbauer, A. Stierle, Carboxylic acid induced near-surface restructuring of a magnetite surface, Communications Chemistry 2, 92 (2019).
[4] O. Gamba, H. Noei, J. Pavelec, R. Bliem, M. Schmid, U. Diebold, A. Stierle, G.S. Parkinson, Adsorption of Formic Acid on the Fe_3O_4 (001) Surface, J. Phys. Chem. C 119 (2015) 20459.
[5] R. Bliem, E. McDermott, P. Ferstl, M. Setvin, O. Gamba, J. Pavelec, M. A. Schneider, M. Schmid, U. Diebold, P. Blaha, L. Hammer, G.S. Parkinson, Subsurface cation vacancy stabilization of the magnetite (001) surface, Science 346, (2015) 1215.
[6] B. Arndt, R. Bliem, O. Gamba, J. E.S. van der Hoeven, H. Noei, U. Diebold, G. S. Parkinson, A. Stierle, Atomic structure and stability of magnetite Fe_3O_4(001): An X-ray view, Surface Science, 653 (2016) 76.
[7] M. Creutzburg, K. Sellschopp, B. Arndt, E. Grånäs, G. Vonbun-Feldbauer,H. Noei, Andreas Stierle, in preparation.

Local environment defines reactivity of model single-atom catalysts: Ir and Rh on Fe_3O_4(001)

Zdenek Jakub[1], Jan Hulva[1], Matthias Meier[1, 2], Roland Bliem[1], Florian Kraushofer[1], Martin Setvin[1], Cesare Franchini[2], Michael Schmid[1], Ulrike Diebold[1], Gareth S. Parkinson[1]

[1]Institute of Applied Physics, TU Wien, 1040 Wien, Austria
(corresponding author: jakub@iap.tuwien.ac.at)

[2]Center for Computational Materials Science, Faculty of Physics, University of Vienna, 1090 Wien, Austria

The development of single-atom catalysts (SACs) was originally motivated by saving of the precious metal, but an equally intriguing characteristic of the ideal SAC is potentially high selectivity due to the high number of identical active sites. The coordination of the active metal center is known to play a crucial role in homogeneous catalysis, and on my poster, I will demonstrate that similar effects can be observed on two model single atom catalysts: Ir_1 and Rh_1 on Fe_3O_4(001). Using scanning tunneling microscopy (STM), noncontact atomic force microscopy (nc-AFM), temperature programmed desorption (TPD), x-ray photoemission spectroscopy (XPS) and DFT calculations, we show that the coordination of single Ir_1 and Rh_1 adatoms can vary depending on preparation, and that the local environment has dramatic consequences for the ability of the catalyst to adsorb CO, and to form CO_2 via a Mars-van-Krevelen mechanism.

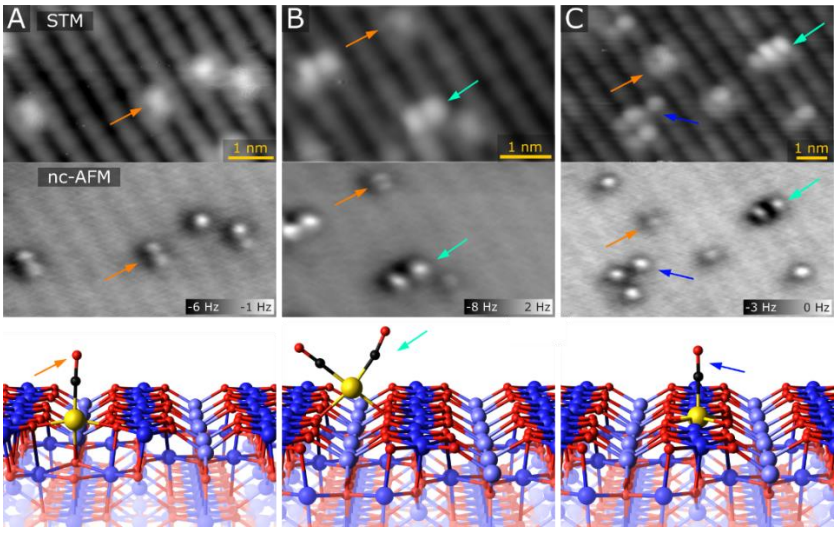

As deposited at room temperature, the M_1 (M = Ir, Rh) adatoms take 2-fold coordination to the surface oxygen atoms. Upon annealing, they incorporate into the first surface layer (5-fold coordinated adatoms), and then further into the subsurface (6-fold coordinated atoms). All the three cases feature a stable single M_1 adatom very close to the surface, but comparison of their CO adsorption properties reveals striking differences. The 2-fold adatoms can form both monocarbonyls (M_1CO, panel A in Fig.) and dicarbonyls ($M_1(CO)_2$, panel B), whereas the 5-fold can only form monocarbonyls (panel C). This behavior can be rationalized by analogy to simple coordination chemistry, which predicts the preference of square-planar geometry of the carbonyls formed by CO adsorption on the 2-fold adatom. Such geometry can be formed either

by adsorbing two CO molecules, or by adsorbing a single CO and forming an additional bond to the subsurface oxygen. In case of the 5-fold adatom, adsorption of a single CO molecule completes the octahedral geometry and adsorption of an additional CO is strongly unfavourable. The 6-fold atoms are subsurface and coordinatively saturated, and thus inactive for CO adsorption.

Reactivity measurements on Rh_1 and Ir_1 adatoms reveal that while the Rh and Ir carbonyls form the same geometrical structures, the relative differences in their stability lead to distinct structural changes taking place during the TPD experiment. Based on these experiments, we discuss the effect of the local surroundings of the the mono- and dicarbonyls, and attempt to identify the species likely responsible for the CO oxidation activity via a Mars-van-Krevelen pathway. Lastly, I will demonstrate that exposure or the 2-fold Rh_1 to O_2 leads to rapid clustering, and the resulting Rh_xO_y clusters catalyze CO oxidation via a Langmuir-Hinshelwood mechanism below room temperature.

This work clearly demonstrates that small differences in coordination and local environment can have dramatic effect on the catalytic properties of single atoms. Some of these effects can be well explained by analogy to coordination chemistry, validating the conceptual link between the fields of single-atom- and homogeneous catalysis.

Near-surface iron diffusion in magnetite

S. Tober[1,2], V. Vonk[1], D. Lott[3], L. Voggler[4], H. Hutter[4], S. Mattauch[5] and A. Stierle[1,2]

1 DESY NanoLab, Deutsches Elektronen-Synchrotron (DESY), D-22607 Hamburg, Germany

(corresponding author: V. Vonk, e-mail: vonk@desy.de)

2 Physics Department, University of Hamburg, D-20355 Hamburg, Germany

3 Helmholtz Zentrum Geesthacht, D-21502 Geesthacht, Germany

4 Institute of Chemical Technologies and Analytics, TU Wien, A-1060 Vienna, Austria

5 Jülich Centre for Neutron Science (JCNS) at the Heinz Maier-Leibnitz Zentrum (MLZ), Germany

Magnetite is a material which has been studied for a long time, one could say ages, and which has reentered the focus of attention for its catalytic properties. In general, chemical reactions take place at the surfaces of condensed matter and therefore it is appropriate to use well-established surface science techniques. Combined efforts of different groups have recently led to the solving of the atomic structure of the $Fe_3O_4(001)$ surface, which included the discovery of a so-called subsurface cation vacancy stabilization mechanism [1,2]. It is unclear for the moment how this particular mechanism could play a role in the case of non-vacuum conditions, especially the oxygen chemical potential, which are typically encountered in catalytic applications. One important ingredient for obtaining a more thorough insight is by gaining detailed information about the near-surface cation mobility, especially in the catalysis-relevant temperature-range of 400-800 K.

We report on experiments, which allow us to quantify the near-surface cation diffusion in Fe_3O4 at temperatures between 470K and 770 K. Thin homoepitaxial films of magnetite, grown using isotopically labeled ^{57}Fe, were investigated by neutron reflectivity and time of flight secondary ion mass spectrometry. By heating the thin films in vacuum to different temperatures for a well-defined time and determining the ^{57}Fe distribution along the surface normal (see Fig. 1), the diffusion lengths are obtained. For the investigated temperature range, diffusion constants of the order of $10^{-20} m^2/s$ are deduced. These results are important in view of near-surface mass transport induced by oxygen chemical potential differences occurring when magnetite is exposed to different gas atmospheres or by adsorbates.

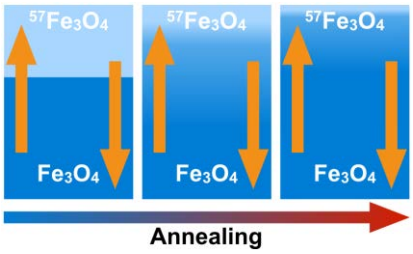

Fig. 1 Schematic of the studied cation diffusion in thin homoepitaxial films.

The detailed growth recipe of homoepitaxial films will be presented. LEED and AES (see Fig. 2) allow to follow the quality of the film's surface structure. Neutron reflectivity (NR) measurements (see Fig. 3) are used to probe the sharpness of the interface between the isotopically labeled film and the underlying substrate. The neutron scattering contrast due to the interface gradually disappears when annealing step-wise up to 770 K, which comes about

by the $^{56}Fe/^{57}Fe$ exchange between bulk and film. These experiments are complemented by TOF-SIMS sputter-profiles, which show excellent agreement with the NR results.

The obtained experimental results indicate that the activation barrier for diffusion is much lower at these relatively low temperatures than at temperatures above 800K. This can be partly explained by the fact that the cation vacancy-concentration in magnetite decreases with increasing temperature [3]. Our results [4] are discussed in view of this diffusion mechanism, which has hitherto not been experimentally verified for temperatures lower than 800 K.

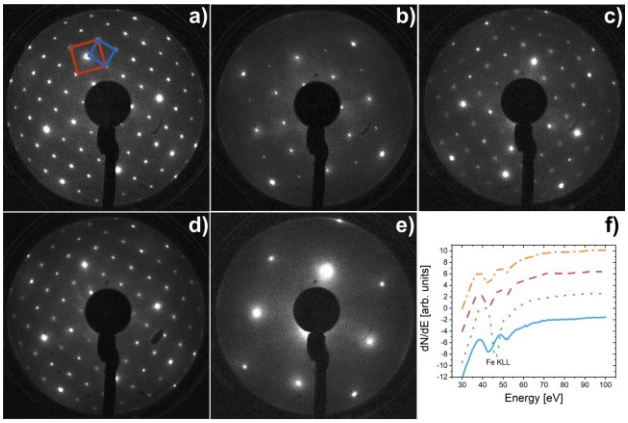

Fig 2. LEED and AES of the homoepitaxial $^{57}Fe_3O_4$ films on $^{56}Fe_3O_4(001)$. a) The clean surface, showing the $\left(\sqrt{2}\times\sqrt{2}\right)R45°$ reconstruction. After growth of approx.. 20 nm thin films at temperatures b) RT, c) 420 K and d) 520K. e) Pure Fe film grown at RT. F) AES spectra showing Fe.

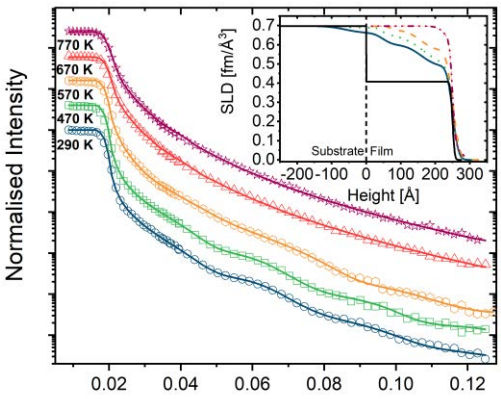

Fig 3. Neutron reflectivity measurements and fits of the homoepitaxial thin films systems after annealing to different temperatures. After growth, there is still a relatively well-defined interface between the isotopically labeled thin film and the substrate, as seen by the finite thickness oscillations. After gradually annealing the films to higher temperature, the thikness oscillation become less pronounced, which indicates the exchange of ^{57}Fe from the film with ^{56}Fe from the substrate.

This work is based upon experiments performed at the MARIA instrument operated by JCNS at the Heinz Maier-Leibnitz Zentrum (MLZ), Garching, Germany. Funded by the Deutsche Forschungsgemeinschaft (DFG, German Research Foundation) – Projektnummer 192346071 – SFB 986.

[1] R. Bliem, E. McDermott, P. Ferstl, M. Setvin, O. Gamba, J. Pavelec, M. A. Schneider, M. Schmid, U. Diebold, P. Blaha, L. Hammer, and G. S. Parkinson, Science 346, 1215 (2014)

[2] B. Arndt, R. Bliem, O. Gamba, J. E. van der Hoeven, H. Noei, U. Diebold, G. S. Parkinson, and A. Stierle, Surface Science 653, 76 (2016).

[3] R. Dieckmann and H. Schmalzried, Berichte der Bunsengesellschaft für physikalische Chemie 81, 344 (1977).

[4] Steffen Tober, Marcus Creutzburg, Björn Arndt, Konstantin Krausert, Stefan Mattauch, Alexandros Koutsioubas, Sabine Pütter, Amir Syed Mohd, Lukas Volgger, Herbert Hutter, Heshmat Noei, Vedran Vonk, Dieter Lott, and Andreas Stierle (submitted).

Control of charge transfer into organic molecules on ultrathin MgO(001) films

P. Hurdax, M. Hollerer, L. Egger, G. Koller, M. Ramsey, and M. Sterrer,

Institut für Physik, Universität Graz, A-8010 Graz, Austria
(corresponding author: M. Sterrer, e-mail: martin.sterrer@uni-graz.at)

Charge transfer processes on ultrathin, supported oxide films have received increasing attention in recent years because of the possibility to control the charge state of adsorbates or the direction of catalytic reactions. The main driving force for the occurrence of charge transfer in these systems is the reduction of the substrate work function induced by deposition of the oxide film in combination with an adsorbate with high electron affinity. While previous studies have focused on the charging of metal atoms (e.g. Au) or small molecules (e.g. O_2, NO_2), we have recently extended these investigations into charge transfer processes into large organic molecules. In this contribution, we present results on the adsorption and charging of pentacene (5A) and tetraphenylporphyrin (2H-TPP) on ultrathin MgO(001) films supported on Ag(001). By combing scanning tunneling microscopy and photoemission spectroscopy and tomography, we identify and quantify charge transfer into the organic monolayer film. In addition, we show that by variation of the work function and the MgO thickness it is possible to drive the system into a state where no charge transfer occurs. In the case of 2H-TPP, charge transfer also appears to strongly influence the self-metalation of 2H-TPP to Mg-TPP. Thus, our investigations lay the basis for the ultimate control of charge transfer, and the related chemistry, on ultrathin oxide film systems.

Interface oxygen induced internal structures of ultrathin MgO islands grown on Ag(100) observed with STM

L. Savio[1], M. Smerieri[1], L. Vattuone[1,2], S. Tosoni[3], M. Rocca[1,2]

Dipartimento di Fisica, Università di Genova, 16146 Genova, Italy
(corresponding author: M. Rocca, e-mail: rocca@fisica.unige.it)

[1] *IMEM -CNR UOS Genova, Via Dodecaneso 33, 16146 Genova, Italy*

[2] *Dipartimento di Fisica, Università di Genova, Via Dodecaneso 33, 16146 Genova, Italy*

[3] *Dipartimento di Scienza dei Materiali, Università Milano Bicocca, Via R. Cozzi 55, 20125 Milano, Italy*

The small mismatch, as well as the simple cubic structure, make supported ultrathin MgO films a model system for the understanding of the electronic and catalytic properties of oxide films [1], oxide-supported metal nanoclusters [2-5], as well as of the magnetic properties of isolated adatoms [6]. For this reason this system has been at the focus of research for the past decades. We recently demonstrated by scanning tunnelling microscopy (STM) [7,8] that nearly perfectly uniform MgO films as well as MgO islands with square shape can be grown by reactive deposition at 773 K on Ag(100). The outcome is dictated by the cooling rate of the sample after film growth, which allows to reach the thermodynamically favoured state at sufficiently low cooling rate.

At lower growth temperature, T_g , the islands show a more irregular shape with wavy borders. Some islands show in addition dark fractal features in their interior when imaged under non topographic conditions. Though reported frequently [9], such features are so far unexplained.

In order to understand their origin, we reinvestigated MgO submonolayers grown by reactive deposition on Ag(100) for sample bias voltages from +4 to -4 V.

At T_g = 450 K most islands appear uniformly flat. Most of them protrude off the Ag plane for all bias values, while others have a negative apparent height when imaged under non topographic conditions. Notably, the apparent height at large *positive* sample bias (when topographic conditions are met) is the same for all islands and consistent with a single MgO monolayer.

At T_g = 500 K the landscape looks different. Some islands look still uniformly flat while others show dark fractal features in their interior under non topographic conditions. Under topographic conditions, met in this case at *negative* sample bias, the islands protrude off the Ag plane by a height consistent with one MgO monolayer.

One possible reason for these phenomena is the accumulation of additional oxygen at the interface between silver and the oxide, which we inferred previously from X ray photoemission spectroscopy [7,8]. To prove this hypothesis, we performed density functional theory (DFT) simulations of the STM images for MgO monolayers and bilayers in presence and in absence of interface oxygen at different sample bias. We find that indeed interface oxygen has an important influence on the density of states and hence on the apparent height. In particular, its presence reverts the conditions at which topographic imaging is achieved.

Our results allow to assign the most common kinds of islands.

At a growth temperature of 450 K there is little interface oxygen accumulation. The MgO islands have monolayer height above the Ag plane, but some of them may have a second layer excavated in the Ag plane. Topographic imaging conditions are reached at large positive sample bias.

At a growth temperature of 500 K, we find again monolayer islands on top of the Ag plane and partially embedded bilayer islands but in this case additional oxygen is present at the interface with the silver substrate. For the monolayer islands such oxygen accumulates close to the centre of the islands and causes the fractal indented structures. For the bilayer islands the interface oxygen is more uniformly distributed and its only effect is to change the bias dependence of the images which reach topographic conditions at negative sample bias. Under non topographic conditions areas with a higher interface oxygen concentration appear thereby darker and become topographic at higher negative bias values.

[1] Y. Martynova, S. Shaikhutdinov, H.J. Freund, Chemcatchem, 5, 2162 (2013)

[2] G. Barcaro, A. Fortunelli, A. Journal of Chemical Theory and Computation, 1, 972 (2005)

[3] F.R. Negreiros, G. Barcaro, Z. Kuntova, G. Rossi, R. Ferrando, A. Fortunelli, Surf. Sci., 605, 483 (2005)

[4] M. Smerieri, J. Pal, L. Savio, L. Vattuone, R. Ferrando, S. Tosoni, L. Giordano, G. Pacchioni, M. Rocca, The Journal of Physical Chemistry Letters 6, 3104 (2015)

[5] L. Savio, M. Smerieri, J. Pal, E. Celasco, M. Rocca, L. Vattuone , J. Phys. Chem C in press (2019)

[6] W. Paul, K. Yang, S. Baumann, N. Romming, T. Choi, C.P. Lutz, J.H.Heinrich, *Nature Physics* 13, 403 (2017)

[7] J. Pal, M. Smerieri, E. Celasco, L. Savio, L. Vattuone, M. Rocca, *Phys. Rev. Lett. 112*, 126102 (2014).

[8] J. Pal, M. Smerieri, E. Celasco, L. Savio, L. Vattuone, R. Ferrando, S. Tosoni, L. Giordano, G. Pacchioni, M. Rocca, *The Journal of Physical Chemistry C*, *118*, 26091 (2014)

[9] S. Schintke, S. Messerli, M. Pivetta, F. Patthey, L. Libioulle, M. Stengel, A. De Vita, W.D. Schneider, *Phy. Rev. Lett. 87* (2001)

Accuracy in the theory of oxides – the many phases of ZrO_2

F. Mittendorfer, W. Mayr-Schmölzer, J. Planer, J. Redinger, and A. Grüneis[1]

Institut of Applied Physics and Center for Computational Materials Science, Vienna University of Technology, A-1040 Wien, Austria
(corresponding author: F. Mittendorfer, e-mail: Florian.Mittendorfer@tuwien.ac.at)

[1] *Institute for Theoretical Physics, Vienna University of Technology, A-1040 Wien, Austria*

In the recent years, ab-initio modelling has been established as a complementary approach to experimental catalysis research. Especially density functional theory (DFT) based approaches usually allow to determine reliable structural models for model systems of a few hundred atoms. Yet the accuracy of the predicted energies can strongly depend on the choice of the exchange-correlation method. High-level many-electron approaches, e.g. in the framework of the ACFDT-RPA, can offer reference values for systems where the common semi-local exchange correlation functionals fail, such as the adsorption of CO on transition metal surfaces [1] or the adsorption of a superoxo O_2^- species on an oxide perovskite surface [2].

In this presentation I will discuss our recent results [3] on the accuracy of DFT approaches and beyond for the description of the phase stabilities of zirconia (ZrO_2). ZrO_2 has been studied extensively experimentally due to its technological relevance, including applications for catalysis, gas sensors or solid oxide fuel cells. Yet ZrO_2 displays a variety of crystallographic bulk phases as a function of temperature, pressure or film thickness [4], and consequently theoretical approaches have to be able to capture subtle difference for a correct quantitative description. I will show that commonly used DFT functionals severely overestimated energetic difference between the monoclinc ground state and the high-termperature cubic and monoclinic phase, and even predict new meta-stable phases. Only high-level approaches like the RPA or quantum-chemical coupled cluster methods (CCSD(T)) allow to establish the correct order and to obtain a good quantitative agreement with the experimental data. In addition, also the size of the zero point energy corrections strongly depends on the quality of the theoretical description.

Support by the Fonds zur Förderung der Wissenschaftlichen Forschung (project SFB FOXSI:F45) is gratefully acknowledged.

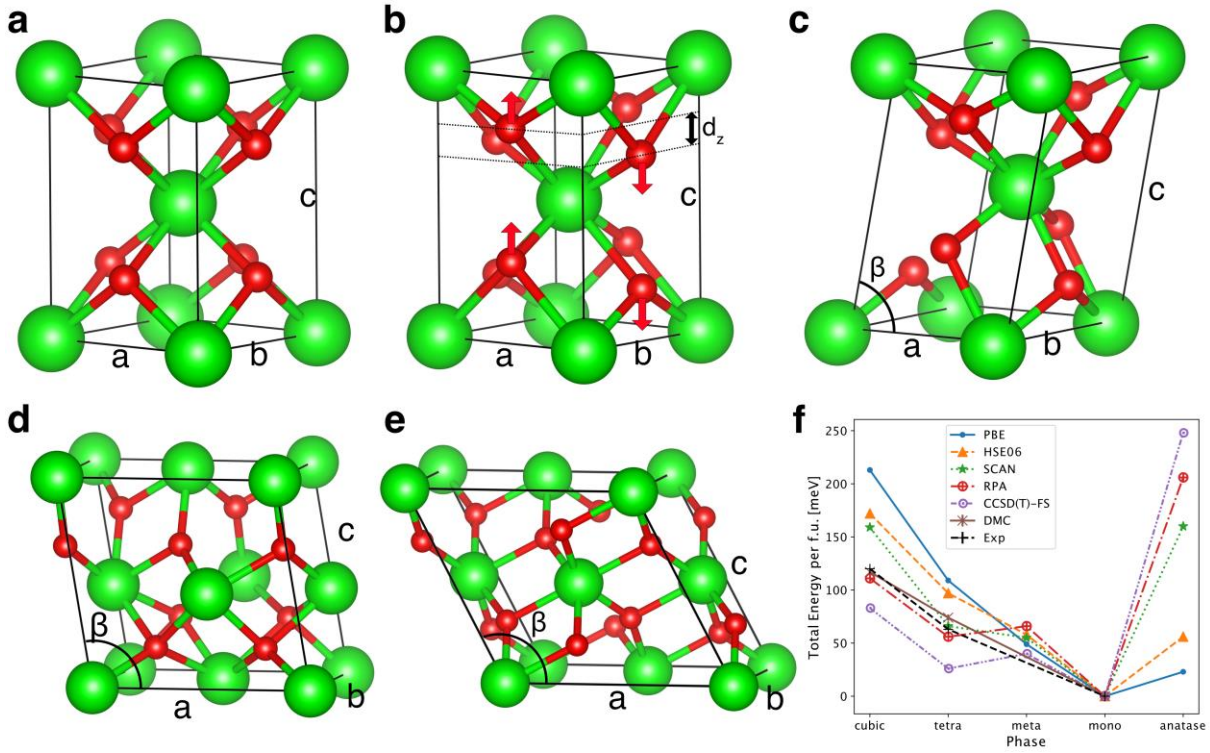

Fig.1. (a-e) Common phases of ZrO_2: cubic, tetragonal, metamonoclinc, monoclinic, anatase (f) phase diagram.

[1] L. Schimka, J. Harl, A. Stroppa, et al.; Nat. Mater. 9, 741 (2010)
[2] D. Halwidl, W. Mayr-Schmölzer, M. Setvin, et al.; J. Mat. Chem. A 6, 5703 (2018)
[3] W. Mayr-Schmölzer, et al. *submittet (2019)*
[4] P. Lackner, Z. Zou, S. Mayer, et al., Surf. Sci. 679, 180 (2019)

Acoustic surface plasmon on Ni(111)

V. M. Silkin[1,2,3], G. Benedek[1,4], I. V. Silkin[5], E. V. Chulkov[1,2,6], and P. M. Echenique [1,2,6]

[1]*Donostia International Physics Center, 20018 San Sebastian, Spain*
(corresponding author: V. M. Silkin, e-mail: waxslavas@ehu.es)

[2]*Departamento de Física de Materiales, Facultad de Ciencias Químicas, Universidad del País Vasco/Euskal Herriko Unibertsitatea, 20080 San Sebastián, Spain*

[3]*IKERBASQUE, Basque Foundation for Science, 48013 Bilbao, Spain*

[4]*Dipartimento di Scienza dei Materiali, Universitá degli Studi di Milano-Bicocca, Milano, Italy*

[5]*Tomsk State University, 634050 Tomsk, Russia*

[4]*Material Physics Center MPC, Centro Mixto CSIC-UPV/EHU, 20018 San Sebastian, Spain*

In metals a long range Coulomb interaction between electrons manifests itself in the form of plasma oscillations. At metal surfaces a well known example of collective electron behaviour is a surface plasmon [1]. These excitations were intensively studied during several decades.

Some time ago it was predicted that at some metal surfaces besides the convention surface plasmons the coexistence of quasi two-dimensional (2D) surface state and underlying three-dimensional electron gas leads to formation of a novel low-energy collective electronic excitation [2]. This mode, called acoustic surface plasmon (ASP), has characteristic acoustic-like dispersion, i.e., a linear dispersion at small wave vectors with the sound velocity being very close to the Fermi velocity of the 2D surface state band. The first experimental evidence of ASP on a metal surface, Be(0001), was obtained with high-resolution electron-energy loss spectroscopy (HREELS) [3]. Similar observations have then been reported in Cu(111) [4], Au(111) [5-7], and other systems [8-10]. A key feature of these systems is the presence at the Fermi level of a shallow surface band with a binding energy in a few 100 meV range. A similar surface state exists on the (111) surface of ferromagnetic Ni as well. On this surface it crosses the Fermi level for the electrons in the majority spin channel only.

In the present contribution we report on the calculation results for surface response function of the Ni(111) surface based of a model potential that takes into account the details of the surface electronic structure. We constructed a spin-resolved potential for the Ni(111) surface following the receipt of Ref. [11]. In particular, the information from the DFT calculations [12-14] on the *s-p* bulk energy gap positions in both spin channels and the *s-p* surface state in the majority spin case were taken into account. Since the presence of the minority spin *s-p*

surface state in the Fermi level vicinity is not confirmed by the DFT calculations it was not taken into account in the model potential construction.

With this model potential we calculated the electronic structure of a slab consisting of 51 atomic layers. The resulting one-particle energies and wave functions where employed in the evaluation of the surface loss function. An important novel issue of this work is the inclusion of the electron temperature in its evaluation. Since the temperature in the experiments is comparable with the binding energy of the Ni(111) surface state, it may have an impact in the surface excitation spectra.

In the calculated surface loss function we find a peak ascribed to the acoustic surface plasmon. Its origin is ascribed to the partly occupied majority spin surface state. The resulting incomplete dynamical screening involving slow carriers in this surface state band and the faster ones in the bulk electron system is the origin of this mode. In this work we find that temperature introduces notable modifications in the calculated surface loss function at low energies and seriously affects the ASP properties on Ni(111). Nevertheless, even at such elevated temperature as 300 K, the ASP peak can be resolved at finite energy. Analysing the spatial charge density distribution corresponding to ASP, we find that its net charge is almost zero due to its quadruple nature, whereas the resulting spin of the oscillating charge related to the ASP should have excess of the majority spin type. Moreover, since in the vacuum side the majority spin surface state dominates, the oscillating charge related to the ASP should be mostly majority spin resolved.

[1] R. H. Ritchie, Phys. Rev. 106, 874 (1957)

[2] V. M. Silkin, A. García-Lekue, J. M. Pitarke, E. V. Chulkov, E. Zaremba, and P. M. Echenique, Europhys. Lett. 66, 260 (2004)

[3] B. Diaconescu, K. Pohl, L. Vattuone, L. Savio, P. Hofmann, V. M. Silkin, J. M. Pitarke, E. V. Chulkov, P. M. Echenique, D. Farías, and M. Rocca, Nature (London) 448, 57 (2007)

[4] K. Pohl, B. Diaconescu, G. Vercelli, L. Vattuone, V. M. Silkin, E. V. Chulkov, P. M. Echenique, and M. Rocca, EPL 90, 57006 (2010).

[5] S. J. Park and R. E. Palmer, Phys. Rev. Lett. 105, 016801 (2010)

[6] L. Vattuone, M. Smerieri, T. Langer, C. Tegenkamp, H. Pfnür, V. M. Silkin, E. V. Chulkov, P. M. Echenique, and M. Rocca, Phys. Rev. Lett. 110, 127405 (2013)

[7] J. Pischel, E. Welsch, O. Skibbe, and A. Pucci, J. Phys. Chem. C 117, 26964 (2013)

[8] X. Jia et al., Phys. Rev. Lett. 119, 136805 (2017)

[9] P. Alonso-Gonzalez et al., Nat. Nanotechnol. 12, 31 (2017)

[10] A. Politano, H. K. Yu, D. Farías, and G. Chiarello, Phys. Rev. B 97, 035414 (2018)

[11] E. V. Chulkov, V. M. Silkin, and P. M. Echenique, Surf. Sci. 437, 330 (1999)

[12] L. Magaud, A. Parturel, P. Mallet, S. Pons, and J.-Y. Veuillen, Europhys. Lett. 67, 90 (2004)

[13] J. Lobo-Checa, T. Okuda, M. Hengsberger, L. Patthey, T. Greber, P. Blaha, and J. Osterwalder, Phys. Rev. B 77, 075415 (2008)

[14] L. V. Dzemiantsova et al., Phys. Rev. B 84, 205431 (2011)

Fs timescale Charge Carrier Dynamics in organic Photovoltaics

F.Roth,[1] M.Borgwardt[2], L.Wenthaus[3], J. Mahl[2],S. Palutke[4], G.Brenner[4], S. Molodtsov[1,5], W. Wurth[3,4], O.Gessner[2], and W. Eberhardt[3*]

[1]*Institute of Experimental Physics, TU Bergakademie Freiberg, D-09599 Freiberg, Germany*

[2]*Chemical Sciences Division, Lawrence Berkeley National Laboratory, Berkeley, California 94720, USA*

[3]*Center for Free-Electron Laser Science / DESY, D-22607 Hamburg, Germany*

[4]*Deutsches Elektronen-Synchrotron DESY, Notkestraße 85, 22603 Hamburg, Germany*

[5]*European XFEL GmbH, Holzkoppel 4, 22869, Schenefeld, Germany*

(corresponding author W. Eberhardt; email wolfgang.eberhardt@cfel.de)

Charge carrier excitation, transport and recombination is very important for the design and performance of photovoltaic cells. Especially on the fs and ps time scales these dynamics are far from being completely understood. New analytical characterization tools at synchrotrons and FEL's such as time resolved core level photoemission spectroscopy (tr-XPS) have been developed recently allowing to investigate these ultrafast dynamical processes. Here, we present such a study for a prototype system for organic photovoltaics, the interface between CuPc and C_{60} using femtosecond time-resolved X-ray photoemission spectroscopy (tr-XPS) at the free-electron laser FLASH. These time resolved XPS spectra provide unique site-specific information about the location of electron in this blend of organic functional materials.

This interface is especially important, since organic photovoltaics are typically based upon a blend between an organic chromophore, in this case CuPc, where the light absorption and initial charge carrier generation occurs, and an electron acceptor, C_{60}, where the electron is captured and collected to prevent direct recombination of the initially excited excitonic like state. At the excitation wavelength of 775 nm, the experiment specifically addresses the relaxation of the interfacial charge-transfer (ICT) states, which are the crucial "gateway" for the generation of separate charges. Their dissociation efficiency is a central factor for controlling the overall photon-to-current conversion capability of a heterojunction at these low excitation energies. The initial excitation decays rapidly on the fs timescale either into an interface excitonic state or through direct recombination and emission of a photon [1,2] as previous studies with fs optical lasers have shown.

Here, we use femtosecond time-resolved X-ray photoelectron spectroscopy (tr-XPS) at the free electron laser FLASH to study the charge generation in a planar heterojunction consisting of a copper-phthalocyanine (CuPc) and a C_{60} acceptor phase.

Fig. 1 shows the time-resolved C 1s XPS spectrum of a planar heterojunction consisting of 1 – 2 ML of CuPc atop a thin film of C_{60} at three different pump-probe delays as indicated. At negative delays the probe pulse arrives prior to the excitation and accordingly shows the unexcited system. The intensity of the red C 1s component associated with negatively charged C_{60} directly and quantitatively shows the amount of C_{60} that has collected an extra free electron.

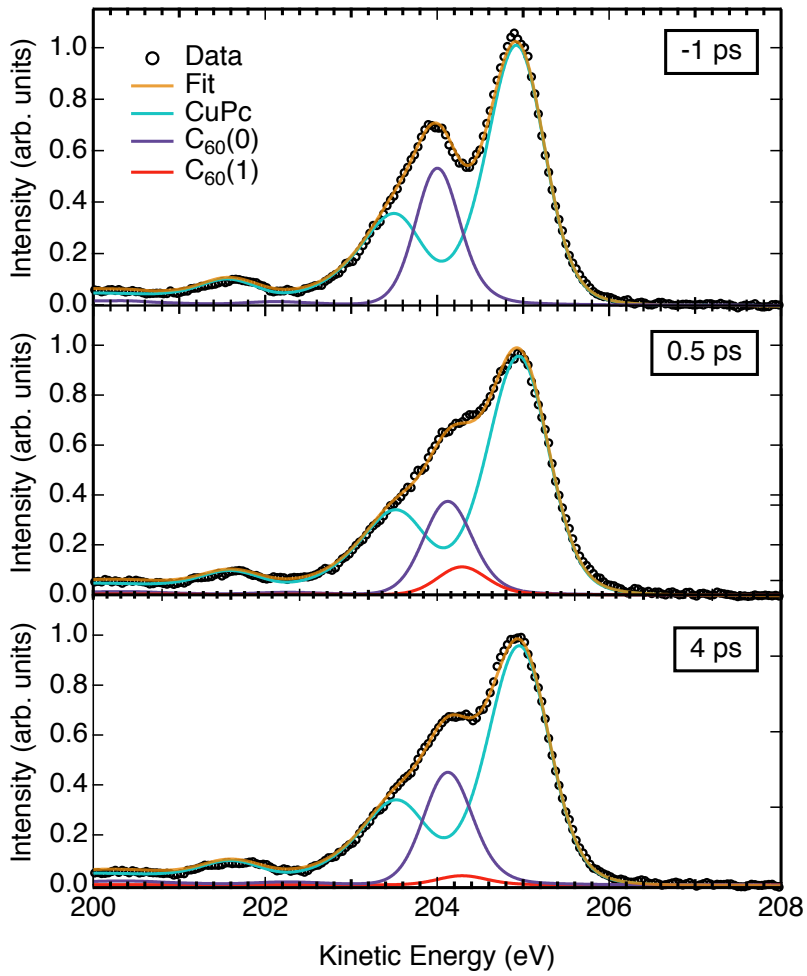

Fig. 1: Tr-XPS sepctra and their decomposition via a fitting procedure into the components of CuPc in green, C_{60} (0 or neutral) in black and C_{60} (1 or negatively charged) in red. Black symbols represent the measured C 1s spectra of the CuPc – C_{60} heterojunction, and the line through the data points the composite fit.

With our quantitative data on the charge separation we show that two channels contribute to the 1ps lifetime of the ICT states. The majority (78%) of the ICT states decays via recombination while about 22% result in charge separated states, that are essential for the function of the OPV structure.
These results just pertain to the fate of the lowest excited states of the heterojunction. At higher excitation energies (532 nm excitation wavelength) we have shown previously that a conversion from the triplett exciton in the chromophore to charge separated states is the major charge generation channel for the photovoltaic process which yields about an order of magnitude more separated charges than the singlet exciton channel [3].

We gratefully acknowledge the contribution of the late Prof. Wilfried Wurth to this work. We would like to thank the staff at FLASH at DESY for their excellent support during the experiment. These investigations were supported by the Helmholtz Association under the program ‘structure of matter’ and the Chemical Sciences Program at LBL Berkeley supported by DOE. F.R. acknowledges financial support from DESY. M.B. acknowledges support by the AvH Foundation.

.References:

[1] A.E. Jailaubekov et al, Nature Mater. **12**, 66 (2013)
[2] G. J. Dutton and S.W. Robey J. Phys. Chem. **C116**, 19173 (2012)
[3] T. Arion et al. Phys. Rev. B**99**, 020303 (2019)

Thermodynamic Stability of 2-D WO_3 Nanosheets: Growth on a Ag Foil

M. Mohammadi, S. Hasenauer, Falko P. Netzer, S. Surnev

Surface and Interface Physics, Institute of Physics, Karl-Franzens University, A-8010 Graz, Austria (corresponding author: falko.netzer@uni-graz.at)

Tungsten trioxide, WO_3, is a very flexible material with attractive properties for a wide range of physical and chemical applications, ranging from chromogenic devices, chemical sensoring to photoelectrochemical cells and catalysis. It is of fundamental scientific interest due to its complex structural phase diagram, its rich defect chemistry and its electronic behavior, which can be modified and activated upon doping. In particular, WO_3 nanosheets – free-standing materials at the 2-D limit of one-to-several unit cells thick – have shown great promise with novel functionalities that render them useful for advanced nanotechnologies. Recently, a crystalline 2-D WO_3 phase on an Ag (100) single crystal surface has been described [1], which features a structure that is not related to the bulk WO_3 crystal lattice, but akin to a sheet of the α-MoO_3 layered structure. This structure may be regarded as a combination of two layers of WO_6 octahedra linked by sharing corners and edges in a staggered square arrangement. The WO_3 sheets extend virtually defect-free over mesoscopic distances (μm), are incommensurate with rotational disorder on the Ag (100) surface and thus are only weakly coupled to the substrate. DFT calculations have suggested that this WO_3 double layer structure is thermodynamically very stable and it has been argued that the proposed structure should be a general model for WO_3 nanosheets [1]. The latter implies that the atomic structure of the growth substrate should have little influence on the WO_3 layer growth and structure.

Here we follow up on this work and report the growth of 2-D WO_3 layers on a polycrystalline Ag foil. The Ag foil substrate serves a dual purpose: i) it should contain a variety of low-index and high-index facets thus allowing us to study the structural influence of the substrate on the formation of the WO_3 overlayer structure, and ii) it is cheap, so that it may eventually be suitable for the removal of the substrate by etching, if the 2-D WO_3 nanosheets should have sufficient environmental stability.

The WO_3 overlayers have been grown in UHV via an MBE approach, using $(WO_3)_3$ clusters from the gas phase, which self-assemble on the Ag surface into a compact 2-D layer at elevated temperature. LEED, STM and XPS have been applied to probe the structure and morphology and the chemical composition of the oxide layer. Our present STM results (Fig. 1) confirm that the 2-D WO_3 nanosheets can indeed be grown with crystalline order on the various facets of the Ag foil, with a structure identical as established on the Ag (100) surface [1]. It appears that the Ag substrate serves merely as a planar structureless platform for the kinetics of the self-assembly of the W-oxide clusters. We conjecture that the thermodynamic stability of the WO_3 nanosheet structure provides the driving force for the condensation of the $(WO_3)_3$ clusters into a 2-D sheet geometry.

The further growth of WO_3 on the bilayer nanosheet surface follows an anisotropic uniaxial needle growth pattern (Fig. 2), both on Ag (100) [2] and on the foil support. The uniaxial growth direction is tied to the atomic lattice of the WO_3 overlayer (not related to substrate crystallographic directions). This uniaxial growth pattern is strange, since the surface lattice of the WO_3 layer has a square symmetry, and a symmetry break is thus required.

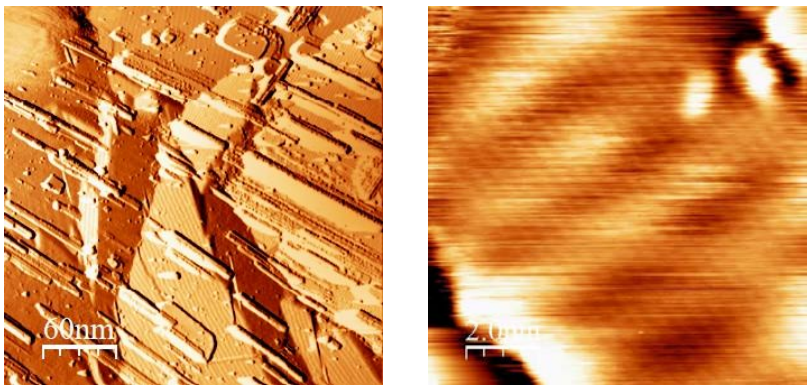

Figure 1: STM images of a 2-D WO_3 bilayer grown on a Ag polycrystalline foil (left). The high-resolution image (right) shows a Moiré pattern (bright and dark stripes) as a result of the superposition of the square overlayer lattice and a (111) substrate facet.

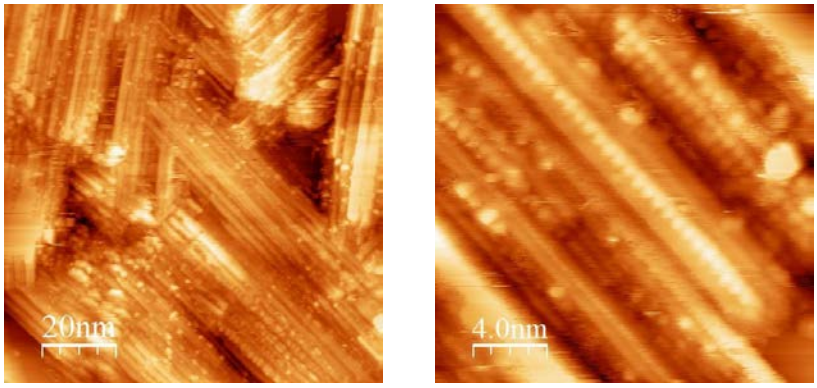

Figure 2: STM images of WO_3 needles grown on a Ag polycrystalline foil.

[1] F.R. Negreiros, Th. Obermüller, M. Blatnik, M. Mohammadi, A. Fortunelli, F.P. Netzer, S. Surnev, J. Phys. Chem. C 123 (2019) 27584

[2] Th. Obermüller, N. Doudin, D. Kuhness, S. Surnev, F.P. Netzer, J. Mater. Res. 32 (2017) 3924

SurfaceNet

Crystals

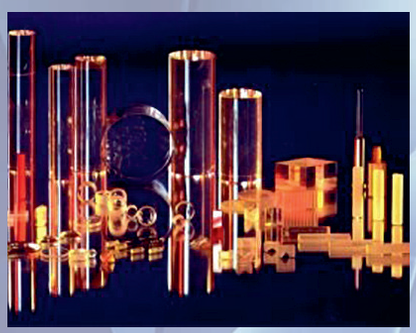

Crystal Puller

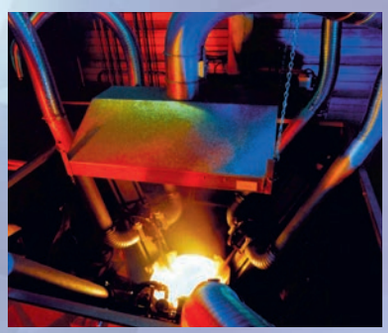

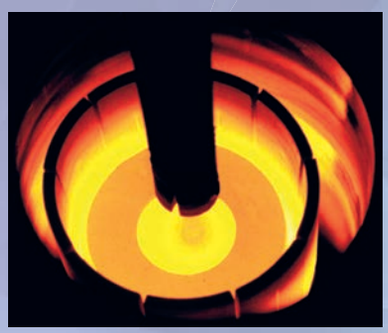

Wafers

Substrates
Custom Parts

Analytical Services

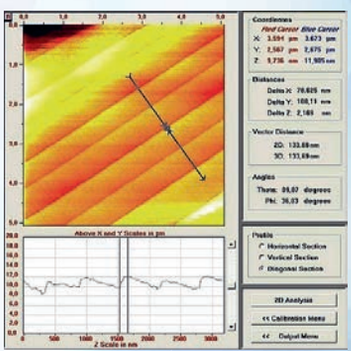

Sputter Targets
PLD Targets
Custom Crystal Growth

SurfaceNet GmbH
Oskar-Schindler-Ring 7 · 48432 Rheine – Germany
Fon +49 (0)5971 4010179 · Fax +49 (0)5971 8995632
sales@surfacenet.de · www.surfacenet.de

Friday

Insight into the Structural Evolution of Working IrO_2 Catalysts in Proton-Exchange Membrane Electrolyzers

K. Reuter

Chair for Theoretical Chemistry and Catalysis Research Center
Technische Universität München, Lichtenbergstr. 4, D-85747 Garching, Germany
(corresponding author: K. Reuter, e-mail: karsten.reuter@ch.tum.de)

Proton-exchange membrane (PEM) electrolyzers promise to overcome the power-density limitations of established alkaline electrolysis technology and could thereby pave the road towards a scalable energy storage from sustainable power sources. A key limiting issue is the very small materials base for oxygen evolution reaction (OER) catalysts that are both active and stable under the harsh acidic PEM operating conditions. Presently, the primary catalyst with a reasonably small overpotential for cost-efficient OER current densities is IrO_2, reaching ~2 A/cm^2 at cell voltages around 1.7 V vs. the reversible hydrogen electrode (RHE) [1]. Notwithstanding, under such conditions even this material seems to undergo a hitherto only incompletely characterized transformation from its rutile crystalline to some amorphous hydrous state with Ir in higher oxidation states [2]. The nature of the active sites in this new state is thereby presently as unclear, as is the compatibility of such a strong compositional and morphological transformation with the requirement of a long-term stability for economically viable PEM electrolysis.

In-depth characterization and mechanistic work on model systems has hitherto almost exclusively focused on low operating potentials. Under such potentials at maximum up to the onset of the OER, the integrity of the IrO_2 crystalline form was generally assumed. Even more so, advanced first-principles calculations have unanimously been based on the active site motifs offered by the rutile IrO_2(110) facet – in the understanding that this facet is the lowest-energy facet of rutile crystals at 0K and that this facet was indeed repeatedly found as dominant in *ex situ* characterization of synthesized IrO_2 particles. While substantial insight has been built up in these studies, it is unclear how much of this transfers to the above described working catalysts at cell voltages far beyond the OER equilibrium potential at 1.23 V.

In this work [3] we therefore conduct *ab initio* thermodynamic calculations to specifically address this higher potential range. Constructing the surface phase (Pourbaix) diagrams for all low-index surfaces of rutile IrO_2, we find the stabilization of highly oxidized superoxo (OO) species at the surface to induce a general thermodynamic instability of the rutile structure already at potentials not much above the OER onset. While this concurs with the experimentally observed transformation to the amorphous state, we find this instability to be preceded by a general shape transformation already at much lower potentials. Combining the

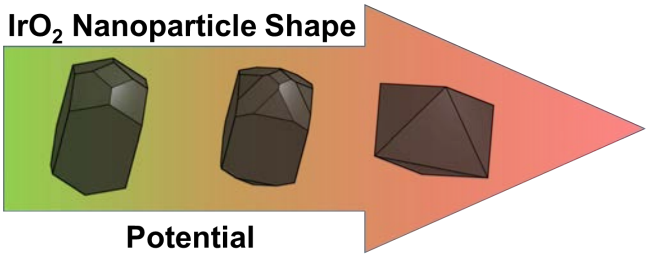

first-principles surface free energy data into a Wulff construction, this equilibrium shape exclusively exhibits hitherto not considered IrO_2(111) facets already at OER onset potentials. These first insights into the structural evolution of working IrO_2 catalysts highlight the urgent need to extend systematic characterization and mechanistic endeavors to higher potentials to identify the true active sites governing the OER at technologically relevant current densities.

Explicitly addressing the structural evolution of the IrO_2 nanoparticle into the suspected hydrous amorphous state would require full *ab initio* molecular dynamics (MD) simulations of the reactive processes at the electrified nanoparticle surface. As this is computationally not tractable for a foreseeable time, MDs based on machine-learned interatomic potentials are an appealing alternative. We are currently undertaking first steps in this direction using a Gaussian Approximation Potential (GAP) for IrO_2 combining two-body and smooth overlap of atomic positions (SOAP) descriptors to capture the atomic environment. The potential is trained with density-functional theory data comprising IrO_2 bulk, various surface slabs, Wulff shape nanoparticles, as well as semi-amorphous structures iteratively obtained from short MD trajectories based on the developing GAP. MD simulations based on a thus optimized GAP already provide first insight into stability and special OER active sites offered by nanoparticles of varying size and shape.

This research was supported by the Kopernikus/P2X programme (Cluster FC-A1) of the German Federal Ministry of Education and Research and the DFG Cluster of Excellence *e*-conversion.

[1] M. Bernt and H.A. Gasteiger, J. Electrochem. Soc. 163, F3179 (2016)
[2] E. Willinger, C. Massué, R. Schlögl and M.G. Willinger, J. Am. Chem. Soc. 139, 12093 (2017)
[3] D. Opalka, C. Scheurer, and K. Reuter, ACS Catal. 9, 4944 (2019)

Supported catalytically active liquid metal solutions: A new concept in single-site catalysis explored by surface science and operando methods

M. Kettner[1], C. Hohner[1], D. Blaumeiser[1], S. Maisel[2], M. Schwarz[1], C. Schuschke[1], J. Vecchietti[3], N. Taccardi[4], C. Stumm[1], H. Wittkämper[5], M. Grabau[5], Y. Lykhach[1], T. Bauer[1], C. Papp[1], A. Bonivardi[3], H.-P. Steinrück[5], P. Wasserscheid[4], A. Görling[2], and J. Libuda[1]

[1]*Lehrstuhl für Katalytische Grenzflächenforschung, ECRC, Friedrich-Alexander-Universität Erlangen-Nürnberg (FAU), D-91058 Erlangen, Germany*
(corresponding author: J. Libuda, e-mail: joerg.libuda@fau.de)
[2]*Lehrstuhl für Theoretische Chemie, FAU, D-91058 Erlangen, Germany*
[3]*Instituto de Desarrollo Tecnológico para la Industria Química, Universidad Nacional del Litoral and CONICET, 3000, Santa Fe, Argentina*
[4]*Lehrstuhl für Chemische Reaktionstechnik, FAU, D-91058 Erlangen, Germany*
[5]*Lehrstuhl für Physikalische Chemie 2, FAU, D-91058 Erlangen, Germany*

Recently Taccardi et al. proposed a new concept in single atom catalysis (SAC), the so-called *Supported Catalytically Active Liquid Metal Solution* (SCALMS). SCALMS consist of active species (Pd, Pt, Rh) dispersed in a low-melting-point metal matrix such as Gallium.[1] Typically, SCALMS show high selectivity and excellent resistance to coking. The operation principle is illustrated in Figure 1. It is believed that the active sites appear dynamically at the surface of the liquid metal droplet in form of isolated atoms, being more resistant to coking as the formation of larger carbon aggregates is suppressed.

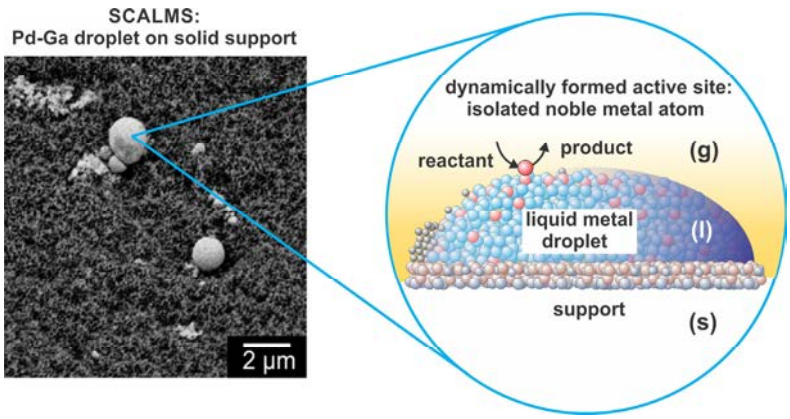

Figure 1: Real SCALMS and schematic representation of their operation principle.

Here, we summarize our latest work by surface science methods and operando spectroscopy, in which we aim to proof the single-atom nature of the active sites in SCALMS.[2-5]
Under ultrahigh vacuum (UHV) conditions, we prepared model systems for Pt-Ga and Pd-Ga SCALMS by physical vapor deposition (PVD) of Pd/Pt and Ga onto highly oriented pyrolytic graphite (HOPG, see Figure 2a) and characterized these by atomic force microscopy (AFM). The surface sites were probed systematically as a function of noble metal concentration and temperature by infrared reflection absorption spectroscopy (IRAS) using CO as a probe

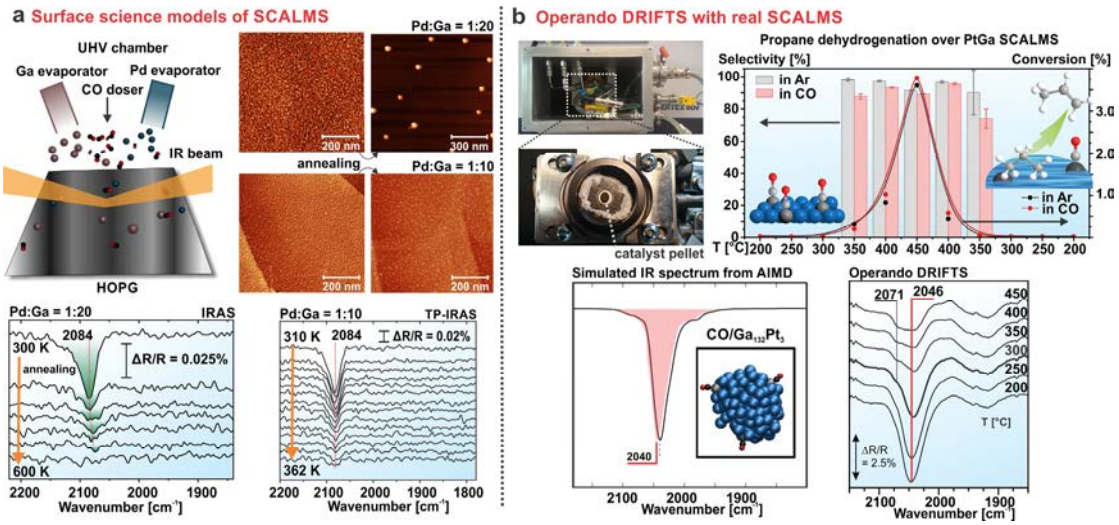

Figure 2: (a) Model systems for SCALMS prepared under UHV conditions by PVD of Ga and Pd onto HOPG. The model catalysts are characterized by AFM and CO adsorption is studied by IRAS; (b) Operando DRIFTS studies on real Pt-Ga SCALMS. The DRIFT spectra are compared to simulated spectra from AIMD.

molecule. Furthermore, we performed studies with polarization modulation IRAS (PM-IRAS) and near-ambient pressure X-ray photoelectron spectroscopy (NAP-XPS). In the limit of low metal concentration, adsorbed CO shows no dipole coupling effects which proves the isolated nature of the active sites. Both for Pd-Ga and for Pt-Ga SCALMS, we determined the characteristic vibrational frequencies for adsorbed CO and the corresponding adsorption energies.

In addition, we studied real Pt-Ga and Rh-Ga SCALMS by operando DRIFTS (diffuse reflectance infrared reflection absorption spectroscopy, see Figure 2b). Both SCALMS show high activity and selectivity for alkane dehydrogenation.[3,4] Using CO as a probe under reaction conditions, we identify characteristic IR bands for CO adsorbed on surface Pt atoms. By comparison with simulated spectra from ab-initio molecular dynamics (AIMD) calculations, we assign these bands to CO adsorbed on isolated Pt atoms at the surface of the supported liquid Ga droplets.

This project was financially supported by the Deutsche Forschungsgemeinschaft (DFG). In particular we acknowledge support by the DFG from the Excellence Cluster 'Engineering of Advanced Materials' (Bridge Funding). T.B. gratefully acknowledges financial support from the 'Fonds der Chemischen Industrie'. P.W. gratefully acknowledges funding through the ERC Advanced Investigator Grant No. 786475. In addition, we acknowledge additional travel support through the CONICET/BAYLAT. We would like to thank the HIPPIE beamline staff at MAX IV (Lund, Sweden) for the technical assistance during the experiments.

[1] N. Taccardi, M. Grabau, J. Debuschewitz, M. Distaso, M. Brandl, R. Hock, F. Maier, C. Papp, J. Erhard, C. Neiss, W. Peukert, A. Görling, H.-P. Steinrück, P. Wasserscheid, Nat. Chem. 9, 862 (2017)

[2] M. Kettner, S. Maisel, C. Stumm, M. Schwarz, C. Schuschke, A. Görling, J. Libuda, J. Catal. 369, 33 (2019)

[3] T. Bauer, S. Maisel, D. Blaumeiser, J. Vecchietti, N. Taccardi, P. Wasserscheid, A. Bonivardi, A. Görling, J. Libuda, ACS Catal. 9, 2842 (2019).

[4] N. Raman, S. Maisel, M. Grabau, N. Taccardi, J. Debuschewitz, M. Wolf, H. Wittkamper, T. Bauer, M.J. Wu, M. Haumann, C. Papp, A. Görling, E. Spiecker, J. Libuda, H.-P. Steinrück, P. Wasserscheid, ACS Catal. 9, 9499 (2019)

[5] C. Hohner, M. Kettner, C. Stumm, M. Schwarz, C. Schuschke, H. Wittkämper, M. Grabau, Y. Lykhach, C. Papp, J. Libuda, submitted.

The brightest Au(111) surface

W. Linpé[1], J. Evertsson[1], G. Abbondanza[1], A. Larsson[1], G. Harlow[1], J. Zetterberg[2], L. Rämisch[2], S. Pfaff[2], L. Jacobse[3], A. Stierle[3] and E. Lundgren[1]
[1]*Division of Synchrotron Radiation Research, Lund University, SE-221 00, Sweden*
(corresponding author: W. Linpé, email: weronica.linpe@sljus.lu.se)
[2]*Division of Combustion Physics, Lund University, SE-221 00 Lund, Sweden*
[3]*Photon Science, DESY, Notkestrasse 85, Hamburg 22607, Germany*

In situ studies of surfaces during a reaction are essential for the understanding the interaction between the surface and the surrounding environment. Cyclic Voltammetry (CV) has been extensively and successfully used to understand reactions occurring at the surface during electrochemical reactions. The measurements provides information on the overall reaction between the sample surface and the liquid electrolyte but contains little information on structural changes occurring on the sample surface during the CV. To characterize the surface changes during the reaction, *in situ* tools which can penetrate the liquid environment and probe the electrode surface are required [1, 2] Recently, we have used 2D Surface Optical Reflectance (2D-SOR) to follow the surface changes of a model catalyst during a catalytic reaction [3, 4]. We have also demonstrated that 2D-SOR provides information about the surface changes of the electrode during a CV measurement [5], however no atomistic changes can be obtained from 2D-SOR. To this end, we have combined 2D-SOR and High Energy Surface X-Ray Diffraction (HESXRD) at the Swedish beamline P21.2 at PetraIII, Desy, Hamburg, to study a Au(111) surface during CV in 0.1 M $HClO_4$ and 0.05 M H_2SO_4 electrolytes.

The Au(111) crystal is known to have a surface (Herringbone, HB) reconstruction [6,7]. In electrochemistry this reconstruction is observable with SXRD as a superlattice rod at low applied potentials [8], while only a (1x1) bulk terminated surface is observed by the presence of the Crystal Truncation Rods (CTRs) at higher potentials. In addition, the applied potential will induce different reactions on the surface, such as oxidation and reduction of the surface, and at higher and lower potentials the oxygen (OER) and hydrogen (HER) evolution reactions, respectively [9-11]. A better understanding of these reactions may promote more efficient electrolyzers and fuel cells, essential devices for a future sustainable society.

The CV for Au(111) from the present measurements, using a 0.1 M $HClO_4$ electrolyte, is shown in Fig. 1a), and is in good agreement with previous CVs. In a first experiment we selected a position in reciprocal space at which both the CTR and the HB rods where present. At this position we started the CV, collected HESXRD images with a time resolution of 1 second, and recorded the 2D-SOR. In Fig. 1b), the correlation between the measured intensities of the 2D-SOR, CTR and the HB during 10 CV cycles is shown.

The measurements show that the 2D-SOR reflectance decreases as the potential is increased and oxide formation starts, shown as peak 3 in the CV. As the potential reaches the reduction peak, number 2 in the CV, the reflectance once again increases as the oxide is reduced. The HESXRD measurements showed that the HB signal appeared at low potentials when the oxide was reduced and was present when the 2D-SOR intensity was highest. The appearance of the HB could also be shown to correlate to a decrease in the CTR intensity, which is attributed to the mixed FCC and HCP sites in the HB reconstruction, inducing destructive interference. The CTR signal could be shown to follow the 2D-SOR and CV quite well, except for the period when the HB reconstruction is present. This indicates that HESXRD and 2D-SOR can both detect the surface changes of the sample as a CV is scanned, but with the difference that the 2D-SOR images the overall surface changes and the HESXRD investigating the change at an atomistic scale.

In a second set of experiments, using a 0.1 M $HClO_4$ electrolyte, we increased the potential in steps, and at each step we performed a full rotational scan. The detector images in such a scan can be combined into a single image depicting a large part of reciprocal space. In this way, new structures such as surface reconstructions or oxide formation can be detected. Such images at different potentials are shown in Fig. 1c). From these images, we can conclude that the HB is lifted at potentials above 0.5 V, and that the CTRs becomes increasingly weaker at higher potentials, indicating roughening of the surface. At the highest potential (2.2V) above the onset of the OER, clear Au powder rings can be observed suggesting either an extremely rough powder-like surface or re-

deposited Au from dissolved Au in the electrolyte. A closer inspection of the images in Fig. 1c) demonstrate that no new scattering features are observed, thus no Au oxide formation or any chloride induced structure can be detected. Finally, we will also report on the usefulness of 2D-SOR to detect X-ray induced beamdamage, which may be significant in a water environment [12].

We have shown that the Au(111) surface is brightest when the HB is present on the surface. Further, the HESXRD data reveals no oxygen or chloride induced structures indicating that additional experiments with surface chemical sensitivity should be performed.

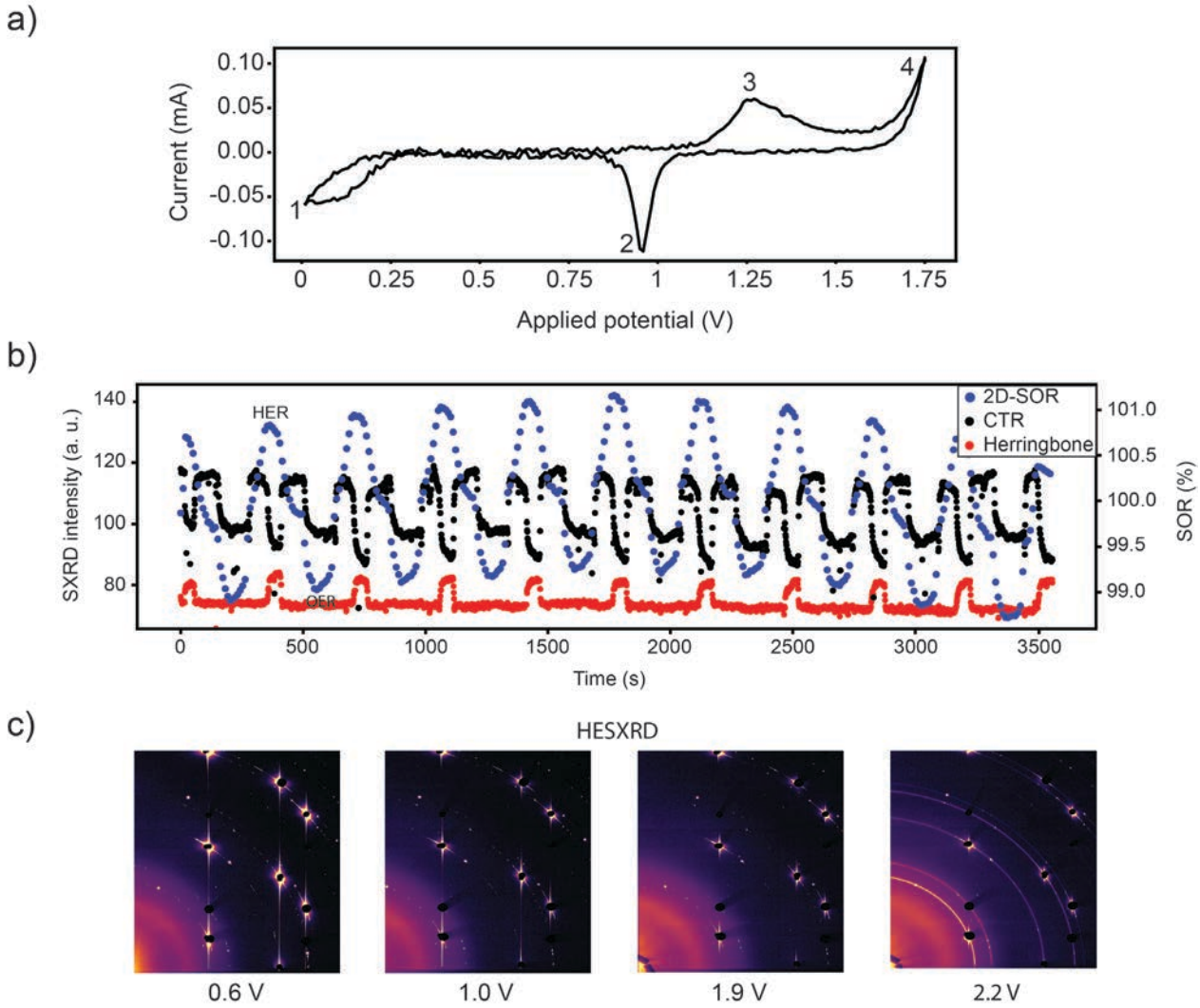

Figure 1: a) The CV of the measurements in 0.1M $HClO_4$ electrolyte, the numbers indicate the different reactions occurring, 1 being the lowest applied potential and close to the HER, 2 being the oxide reduction, 3 the oxidation and 4 the OER. b) The intensity of the 2D-SOR, CTR and HB as a function of measurement time. The position of the OER and HER are indicated in the plot. c) HESXRD images of the sample at certain applied potentials. Except for a continuous weakening of the CTRs and the formation of Au powder rings at 2.2V, no additional features are observed.

References

[1] S. Axnanda et al., Sci. Rep. **5** (2015) 9788
[2] M. J. Rost et al., Nat Commun **10** (2019) 5233
[3] J. Zhou et al., J. Phys. Chem. **121** (2017) 23511
[4] S. Pfaff et al.,Rev. Sci. Instrum. **90** (2019) 033703
[5] W. Linpé et al. Submitted.
[6] J. V. Barth et al., Phys. Rev. B **42**, (1990), 9307
[7] C. Wöll et al., Phys. Rev. B Condens. Matter **39(11)**, (1989), 7988
[8] Y. Grunder et al, Surf. Sci. **680** (2019) 113
[9] O- Diaz-Morales et al., Chem. Sci **4**, (2013), 2334
[10] L.D. Burke et al., Gold bulletin **30**, (1997), 43
[11] J. Perez et al., J. Phys. Chem. B, **102**, (1998), 10931
[12] J. Drnec et al., Electrochim. Acta, **224**, (2017) 220

In-situ electrochemical STM imaging of Cu(111) under reaction conditions

Andrea Auer, Eva-Maria Wernig, Nicolas Hörmann,[1] Karsten Reuter[1] and Julia Kunze-Liebhäuser

Institute of Physical Chemistry, University of Innsbruck, Innrain 52c, Innsbruck, 6020, Austria (corresponding author: A. Auer, e-mail: andrea.auer@uibk.ac.at)

[1] *Theoretical Chemistry, Technical University of Munich, Lichtenbergstr. 4, 85747 Garching, Germany*

The development of low temperature fuel cells for clean energy production is an attractive alternative to fossil-fuel technologies. Carbon monoxide (CO) is a key intermediate in the electro-oxidation of energy carrying fuels and in the electro-reduction of carbon dioxide. Its electrocatalytic oxidation has been extensively investigated on different metals, particularly on platinum (Pt).[1] On Pt, however, CO often acts as a poison in the oxidation of small organic molecules (such as C_1 and C_2 species like methanol or ethanol) due to its strong adsorption, which causes high overpotentials and low energy efficiency of the reaction of interest.[1] Due to its band structure, Cu is expected to adsorb CO less strongly,[2] which makes it extremely well suited for use as electro-oxidation catalyst. This fact makes it ever more remarkable that little to nothing is known about the CO oxidation reaction on Cu in an electrochemical environment, although it has been thoroughly and successfully investigated in the gas phase.[3,4] Surface structure-activity relations play an essential role in heterogeneous (electro)catalysis. Electrochemical scanning tunneling microscopy (EC-STM) is one of the few techniques that enable *in-situ* imaging of the solid/liquid interface with a variable resolution ranging from micrometer to atomic scale in real space under full potential control.

In this work, the ability of Cu(111) single crystals to electrochemically oxidize CO at low overpotentials of 350 mV is reported for the first time. *In-situ* infrared spectroscopy confirms weak adsorption of CO on Cu(111) as well as its oxidation to carbon dioxide which directly reacts to carbonate in solution. EC-STM reveals that during CO oxidation the Cu(111) surface reconstructs and concomitantly adsorbs OH, while forming one- and two-dimensional Cu nanostructures that are effectively stabilized through the presence of CO. Therefore, CO itself activates the (111) surface of Cu and enhances its own oxidation. This self-activation makes it a promising candidate for the oxidation of small organic molecules, e.g. hydrocarbons or alcohols.

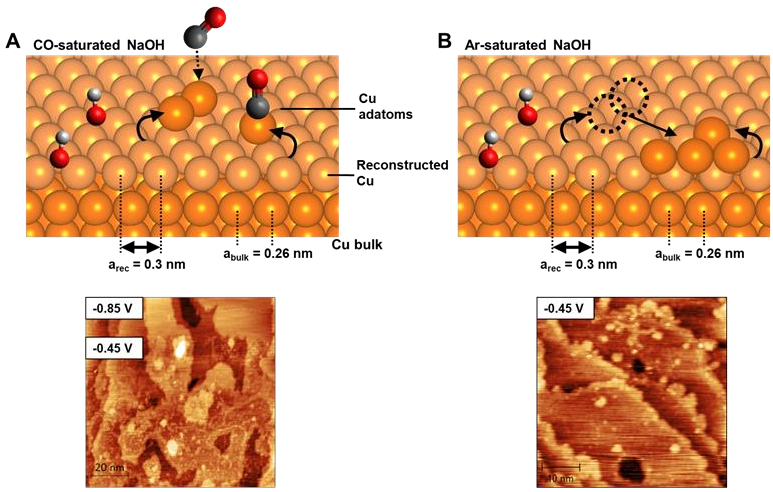

Figure: Schematic representation of the self-activation process. Reconstruction of the topmost layer and the different stabilization mechanisms of Cu adatoms with the corresponding in-situ STM image in (A) CO saturated and (B) Ar saturated NaOH.

Two different stabilization mechanisms of Cu adatom structures, formed upon reconstruction of the topmost Cu layer and ejection of the excess Cu, can be identified through EC-STM measurements in CO- and Ar-saturated NaOH (see Figure). Nanoscale ad-islands are formed and effectively stabilized in the presence of CO in solution. In the case of its absence and OH as a sole adsorbate, the excess Cu is quickly transported to the step edges, which results in their roughening and in less ad-island formation, i.e. less overall roughening of the surface, in the case of Ar-saturated electrolyte.

Density functional theory (DFT) calculations that include the effects of applied potential and solvent environment, confirm a difference in the diffusion barrier of Cu adatoms in the presence of adsorbed CO compared to OH. This effect can be correlated with the unequal binding characters of the two adsorbates. The CO promoted formation of one- and subsequently two-dimensional adatom islands was therefore found to be responsible for the enhanced activity of the electro-oxidation of CO on Cu(111). The observed high mobility of Cu atoms and the high tendency of Cu surfaces to reconstruct, can rationalize why Cu is one of the most unique metals in the field of electrocatalysis.

[1] W. Vielstich, H. A. Gasteiger, A. Lamm, H. Yokokawa, Ed., *Handbook of Fuel Cells* (Wiley 2010).

[2] S. Vollmer, G. Witte, C. Wöll, Determination of site specific adsorption energies of CO on copper, *Catal. Lett.* **77**, 97–101 (2001).

[3] G. G. Jernigan, G. A. Somorjai, Carbon Monoxide Oxidation over Three Different Oxidation States of Copper: Metallic Copper, Copper (I) Oxide, and Copper (II) Oxide – A Surface Science and Kinetic Study, *J. Catal.* **147**, 567–577 (1994).

[4] B. Eren, C. Heine, H. Bluhm, G. A. Somorjai, M. Salmeron, Catalyst Chemical State during CO Oxidation Reaction on Cu(111) Studied with Ambient-Pressure X-ray Photoelectron Spectroscopy and Near Edge X-ray Adsorption Fine Structure Spectroscopy, *J. Am. Chem. Soc.* **137**, 11186-11190 (2015).

Interactions between reactive mineral surfaces studied with the surface forces apparatus

J. Dziadkowiec[1,2], H.W.Cheng[1], A. Røyne[2], M. Valtiner[1]

[1] *Institut für Angewandte Physik, Technische Universität Wien, A-1040 Wien, Austria (corresponding author: J.Dziadkowiec, e-mail: joanna.dziadkowiec@tuwien.ac.at)*

[2] *NJORD Centre, Department of Physics, University of Oslo, Norway*

Spatial confinement is important in material engineering, geological environments, and biomineralization. Tiny spaces across which reactive mineral surfaces interact with each other can control the mechanical strength of rocks and materials or create special nucleation environments, in which the stability of certain mineral phases is favoured[1]. Such interactions between confined mineral surfaces are expected to be affected by the structure of aqueous ionic species on the surfaces, provided that the distance between solids is less than hundreds of nanometers. At such small separations, the electrical double layer, hydration, and electrostatic interactions will govern adhesion and repulsion between mineral surfaces in water[2]. As such, attractive and repulsive surface forces may influence the cohesion between mineral grains and are likely to affect the nucleation behavior of new phases within the interfacial region in disequilibrium conditions[3].

While extremely well-resolved information about molecular details, liquid structuring and heterogenous nucleation on isolated solid interfaces is available owing to the AFM imaging[4], less is known about these phenomena in tiny spaces. This is because the direct observation of a confined region between two mineral surfaces is experimentally challenging. One experimental method that can provide such information is the Surface Forces Apparatus (SFA). SFA combines optical white light interferometry technique with normal and shear force measurements. Owing to that, growth and dissolution processes can be monitored simultaneously with surface forces and any possible links between forces and surface reactivity can be elucidated.

In this work, we summarize our measurements of surface forces between two reactive mineral surfaces. The mineral of interest is calcite ($CaCO_3$) because of its high importance in dynamic geological environments and its major relevance in biomineralization. We explore the links between nucleation in confinement and mineral reactivity, based on SFA and AFM force measurements[5,6]. We present how these interactions change in asymmetric systems between two surfaces that differ in surface charge and zeta potential. We comment on the implications of these results for porous rocks and granular, mineral-based materials.

J.D. acknowledges support from The Research Council of Norway, grant nr 286733: 'Solid-solid interfaces as critical regions in rocks and materials: probing forces, electrochemical reactions, friction and reactivity'.

[1] Putnis, A., & Mauthe, G. (2001). The effect of pore size on cementation in porous rocks. Geofluids, 1(1), 37-41.

[2] Javadi, S., & Røyne, A. (2018). Adhesive forces between two cleaved calcite surfaces in NaCl solutions: The importance of ionic strength and normal loading. Journal of colloid and interface science, 532, 605-613.

[3] Røyne, A., Dalby, K. N., & Hassenkam, T. (2015). Repulsive hydration forces between calcite surfaces and their effect on the brittle strength of calcite-bearing rocks. Geophysical Research Letters, 42(12), 4786-4794.

[4] Söngen, H., Reischl, B., Miyata, K., Bechstein, R., Raiteri, P., Rohl, A. L., ... & Kühnle, A. (2018). Resolving point defects in the hydration structure of calcite (10.4) with three-dimensional atomic force microscopy. Physical review letters, 120(11), 116101.

[5] Dziadkowiec, J., Javadi, S., Bratvold, J. E., Nilsen, O., & Røyne, A. (2018). Surface Forces Apparatus measurements of interactions between rough and reactive calcite surfaces. Langmuir, 34(25), 7248-7263.

[6] Dziadkowiec, J., Zareeipolgardani, B., Dysthe, D. K., & Røyne, A. (2019). Nucleation in confinement generates long-range repulsion between rough calcite surfaces. Scientific Reports, 9(1), 8948.

All in One: N-Heterocyclic Carbenes for the Self-Assembly of Monolayers of Superior Quality and Stability

A. Krzykawska[1], M. Wróbel[1], K. Kozieł[2], and P. Cyganik[1]

[1]*Smoluchowski Institute of Physics, Jagiellonian University, Łojasiewicza 11, 30-348 Krakow, Poland (corresponding author: P. Cyganik, e-mail: piotr.cyganik@uj.edu.pl)*

[2]*Faculty of Chemistry, Jagiellonian University, Gronostajowa 2, 30-387 Krakow, Poland*

Self-assembled monolayers (SAMs) form well-defined upright oriented monomolecular films on solid substrates and are considered one of the most prototypical systems for molecular nanostructurs formation [1]. Among numerous applications SAMs become particular attractive in the area of molecular and organic electronics playing fundamental role in the analysis of conduction mechanism, controlling injection barrier between metal and organic semiconductors in OLED, OPV and OFET devices, as well as providing an active element in molecular diodes, transistors, switches and memory devices [2]. All these versatile applications are related to the charge transport across the molecule-metal interface and for realistic applications demand optimization of two very basic parameters which are the defects concentration and thermal stability. Low defects concentration is crucial both for achieving sufficiently high stability of the vertical junction (limited by the short-circuiting problem) [2] and for high-resolution lithography of SAMs [3] which is essential for successful design of the device [2]. The importance of the thermal stability is related to the heat transport at the molecule-metal interface, which is a key problem in electronic devices based on organic-inorganic interfaces, where the mismatch between the vibrational density of states of the organic and inorganic parts leads to weak thermal conductivity and thus to overheating problems [4]. Since the heat transport at the molecule-metal junction increases with the strength of the chemical bonding and the packing density of SAMs [4], densely packed, strongly bonded, thermally stable and highly ordered SAMs are urgently needed.

The structure and properties of SAMs are the result of the rather complicated interplay of different interactions, out of which the chemical bonding between the molecule and the solid substrate is one of the most important. For more than thirty years, the majority of SAM research and applications have been based on systems using sulfur (thiols) as bonding molecules with a gold substrate [1]. However, sulfur as a chemical anchor suffers from relatively low thermal and oxidative stability. Recently, N-heterocyclic carbene (NHC) has been proposed as an extremely interesting alternative to form SAMs on gold through the C-Au bonding [5-7]. It has been demonstrated experimentally [5,6] and supported by theoretical calculations [8] that due to the higher stability of the Au-C bond compared to the Au-S the NHC based SAMs on gold substrate can exhibit significantly higher thermal and chemical stability from standard SAMs based on thiols. However, as pointed above in addition to high

thermal stability an equally important parameter that makes SAMs suitable for different applications, such as those related to molecular electronics or nanolithography, is the ability to form highly ordered and dense two-dimensional (2D) structures characterized by low defects concentration. The NHC SAMs developed to date do not meet this important criterion and form either ordered but very-low-density (flat lying, with an area per molecule ~ 0.90-1.80 nm^2) structures via vacuum-based preparation [9,10] or dense (standing up with an area per molecule ~ 0.25 nm^2) but disordered structures via preparation from solution [5,6].

By the current study [11] we overcome all above obstacles and demonstrate formation of model NHC SAMs on Au(111) substrate that simultaneously exhibit exceptionally high degree of 2D order, surface packing close to highest known for SAMs on Au(111) surface, as well as the highest thermal stability reported for SAMs on Au(111). Finally, we also demonstrate that our structural optimization of NHC SAMs substantially improves the quality of the electronic junctions formed by these molecules. The self-assembly of such dense, highly crystalline and extremely stable structures is associated with the strong C-Au bonding and the rational design of assembled molecules, which result in a high mobility of both adsorbate and substrate atoms, as confirmed by the size of the molecular domains and the adsorbate-driven modification of the Au(111) substrate, respectively. The structural analysis of the NHC SAMs was based on combination of spectroscopic, mass spectrometric and high resolution microscopic analysis by using XPS, SIMS, and STM, respectively. The thermal stability of the BIM/Au(111), including desorption energy analysis, was conducted in situ using temperature programmed SIMS (T-SIMS). The conductance of the system was statistically analyzed (>1600 traces) using large area molecular junction based on liquid metal electrode.

This work was supported financially by the National Science Centre Poland (grant DEC-2018/31/B/ST5/00057). The XPS and SIMS equipment was purchased with the financial support of the European Regional Development Fund (grant POIG.02.02.00-12-023/08).

[1] J. C. Love et al. Chem. Rev. 105, 1103 (2005)
[2] A. Vilan et. al. Chem. Rev. 117, 4248 (2017)
[3] R. K. Smith et al. Prog. Surf. Sci. 75, 1, (2004)
[4] M. D. Losego et al. Nat. Mater. 11, 502 (2012)
[5] C. M. Crudden et al. Nat. Chem. 6, 406 (2014)
[6] C. M. Crudden, et al. Nat. Commun. 7, 12654 (2016)
[7] C. A. Smith et al. Chem. Rev. 119, 4986 (2019)
[8] K. Chang, et al. J. Phys. Chem. A 121, 2674 (2017)
[9] C. R. Larrea et al. ChemPhysChem 18, 3536 (2017)
[10] G. Wang et al. Nat. Chem. 9, 152 (2016)
[11] A. Krzykawska, M. Wróbel, K. Kozieł and P. Cyganik submitted

Coordination controlled electrodeposition of metal nanostructures on top of self-assembled monolayers

Zhen Yao,[1] Stephen M. Francis,[1] Andrea diFalco,[2] Michael Bühl,[1] Manfred Buck[1]

[1]*EaStCHEM School of Chemistry, University of St Andrews, St Andrews, KY16 9ST, UK*
corresponding author: M. Buck, e-mail: mb45@st-andrews.ac.uk
[2]*SUPA, School of Physics and Astronomy, University of St Andrews, St Andrews, KY16 9SS, UK*

Monolayers of organic molecules are widely studied as templates in area selective deposition which encompasses a range of rather different schemes such as atomic layer deposition (ALD), electroless and electrochemical deposition, or growth of films of metal organic frameworks (MOFs). With advanced manufacturing moving towards the bottom end of the nanoscale, the variability in dimensions of the deposited structures due to the limited control of the underlying processes such as diffusion and nucleation becomes a major bottleneck. Accordingly, there are increasingly stringent requirements as regards the structural quality, precision in patterning, and control of chemical functionality of the templating monolayers.

Focusing on the generation of ultrasmall metal structures we have been investigating a coordination controlled electrodeposition scheme as illustrated in Fig. 1a. A crucial point of this scheme is the reduction of metal ions coordinated to the outer surface of a self-assembled monolayer (SAM) [1-3], which not only results in metal deposition on top of the organic layer but also provides an active control of the deposition by a molecular property, in contrast to a complementary approach where deposition is controlled by defects in a SAM [4]. Originally devised for the deposition of coordinated metal only, the scheme has recently been extended to the electrodeposition of metal from the bulk electrolyte [5], which offers the possibility to generate bimetallic systems and affords the deposition of continuous layers, thus, overcoming a major limitation of the coordination-only approach. Lateral resolution is straightforwardly achieved by a SAM pattern consisting of coordinating and non-coordinating molecules (SAM-1 and SAM-2 in Fig. 1a). This can be either a binary mixture of different molecules or, as exemplified in Fig. 1b/c, a single component aromatic SAM which, similar to other systems [6,7], is locally modified by electron irradiation, in the present case rendered chemically passive.

Enabling metal patterns with lateral features in the 10-15 nm range and a thickness of less than 3 nm (Fig. 1c), further reduction in dimensions and their variability will require a better understanding of a number of factors ranging from the details of the coordination chemistry to the nucleation and growth of the metal deposits. As regards the former, STM and XPS studies of Pd coordination to SAMs of 3-(4-(pyridine-4-yl)phenyl)propane-1-thiol (PyP3, see Fig. 1a for structure) reveal that only a fraction of the molecules coordinate Pd. Surprisingly,

the amount of coordinated Pd increases when the density of the pyridine moieties is lowered by diluting PyP3 with a structurally analogous but chemically inert thiol, which suggests that single component layers might not be the optimal choice. This also extends to the control of nucleation. DFT calculations yield a substantial driving force for the formation of Pd dimers with one atom interacting with the π-systems of the pyridine moieties. Thus informing experiments on mixed monolayers, the average size and size distribution of the metal nanoparticles are found to be substantially dependent on both the combination of molecules and their ratios, again highlighting the opportunities for SAMs beyond single component systems.

[1] T. Baunach, V. Ivanova, D. M. Kolb, H. G. Boyen, P. Ziemann, M. Buttner, P. Oelhafen, Adv. Mater. 16, 2024 (2004).

[2] O. Shekhah, C. Busse, A. Bashir, F. Turcu, X. Yin, P. Cyganik, A. Birkner, W. Schuhmann, C. Wöll, Phys. Chem. Chem. Phys. 8, 3375 (2006).

[3] C. Silien, D. Lahaye, M. Caffio, R. Schaub, N. R. Champness, M. Buck, Langmuir 27, 2567 (2011).

[4] Z. She, A. DiFalco, G. Hähner, M. Buck, Beilst. J. Nanotechnol. 3, 101 (2012).

[5] Z. She, Z. Yao, H. Ménard, S. Tobish, D. Lahaye, N. R. Champness, M. Buck, Nanoscale 11, 13773 (2019).

[6] A. Turchanin and A. Gölzhäuser, Prog. Surf. Sci. 87, 108-162 (2012).

[7] C. Yildirim, E. Sauter, A. Terfort, M. Zharnikov, J. Phys, Chem. C 121, 9982 (2017).

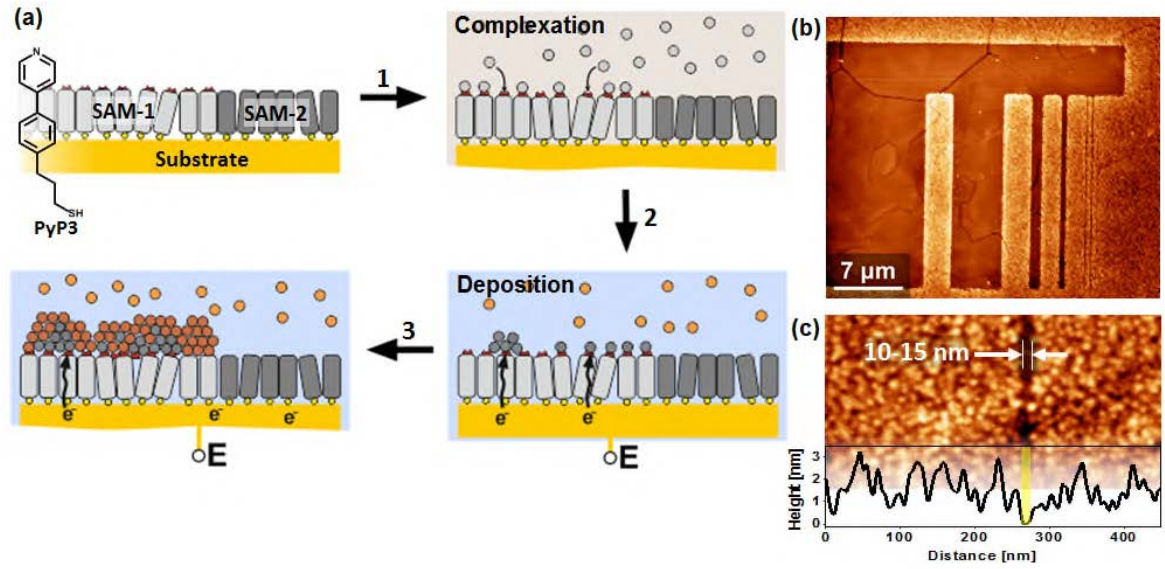

Figure 1: (a) Scheme of coordination controlled electrodeposition with deposits confined to areas of a self-assembled monolayer (SAM-1) which is functionalized and able to coordinate metal ions. After complexation of one metal (step 1) electrochemical deposition is performed in an electrolyte containing another metal (steps 2/3). After reduction of the coordinated metal (step 2) and formation of clusters, these act as seeds for the deposition of metal from the bulk electrolyte (step 3). (b,c) AFM images of area selective electrodeposition of Cu/Pd templated by a PyP3 SAM which has been patterned by electron beam lithography.

Epitaxial Cobalt Oxide Films with Wurtzite Structure Grown on Au(111)

Maximilian Ammon[1], Lutz Hammer[1], Sara Baumann[1], Andreas Raabgrund[1], Tilman Kisslinger[1], Josef Redinger[2], and M. Alexander Schneider[1]

[1] *Lehrstuhl für Festkörperphysik, Universität Erlangen-Nürnberg, D-91058 Erlangen, Germany (corresponding author: M. Ammon, e-mail: maximilian.ammon@fau.de)*

[2] *Institut für Angew. Physik & CMS, TU Wien, Technische Universität Wien, A-1040 Wien, Austria*

The existence of wurtzite (w)-CoO was already suggested in 1962 by Redman and Steward [1], but it took 40 years for an unambiguous verification by Risbud et al. [2] as nano-crystalline powder. In recent times, w-CoO has attracted much attention due to its special catalytic [3], semiconducting [4], and antiferromagnetic [5] properties. Beyond nanoparticles, several publications mention recipes for reactive growth of w-CoO on various surfaces [4, 6-10]. However, none of them demonstrate the growth of a well-oriented and closed film of w-CoO beyond the ultra-thin 2-bilayer (BL) limit [10].

In this work we present a route to grow several nanometer thick w-CoO films on Au(111), which are closed, well-ordered and epitaxially oriented (Fig.1). Thus, these films can be regarded as prototypical for (non-existing) bulk w-CoO material. We characterize the films

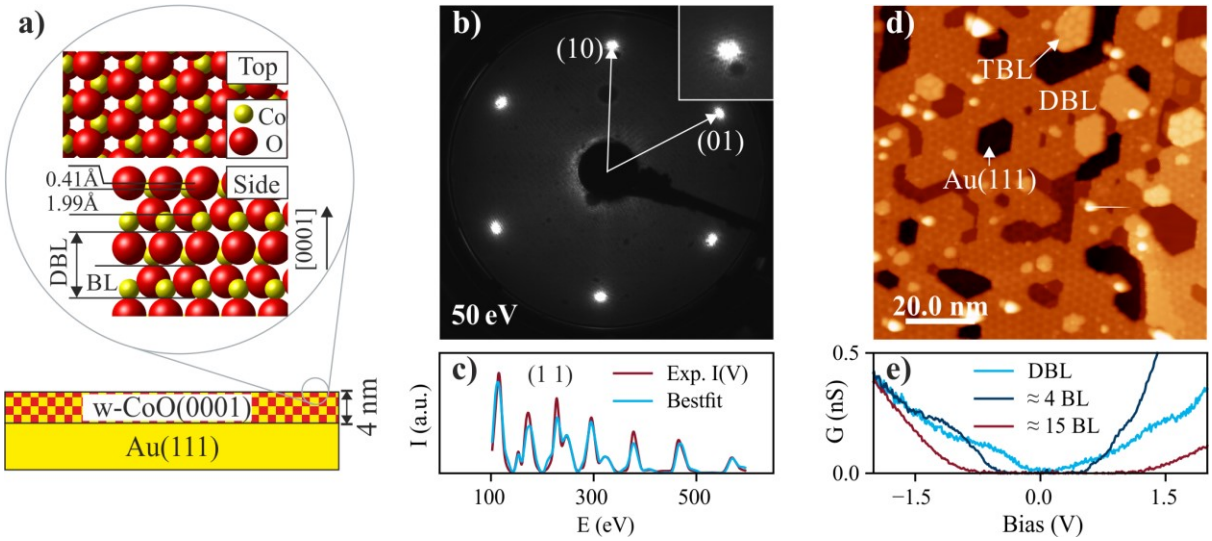

Figure 1: (a) Ball model of a w-CoO (0001) film on Au(111). Wurtzite-CoO(0001) is made up of closed packed CoO bilayers (BL). The complete w-CoO unit cell contains two of these layers, called a double bilayer (DBL). The top layer distance is found to be strongly contracted by the LEED analysis and DFT. (b) LEED shows the single crystallographic orientation of a 15 BL thick film. (c) IV-spectrum of the (11)-beam and its bestfit ($R_{p,11} = 0.100$) as a representative example of the LEED-IV analysis (total $R_p = 0.112$). d) STM image of a nearly closed DBL film (STM: +3.0 V, 0.1 nA): The films predominantly consist of DBLs, but also patches of the Au(111) substrate and of the next layer (TBL) can be found. The strong moiré on the DBL shows a similar unit cell as described by Walton et al. [8] for DBL islands. e) STS measurements for different film thicknesses show the opening of the bandgap with increasing thickness. For closed films, the nominal thickness is given.

experimentally by quantitative low energy electron diffraction (LEED), scanning tunneling microscopy (STM) and spectroscopy (STS) as well as theoretically by density functional theory (DFT) calculations based on hybrid functional or LDA+U schemes.

Wurtzite CoO films were grown via deposition of Co from an electron beam evaporator in ~5×10^{-7} mbar oxygen on the substrate held at room temperature and subsequently were annealed to 200°C. The resulting films have sharp LEED spots and at sufficient thickness (here 4 nm, Fig.1b) the spots of the underlying bulk structure have vanished completely. This demonstrates the well-defined crystallographic orientation and the closure of the hexagonal w-CoO film over the entire area of the electron beam (~ 1 mm^2). The films grow rather flat with terraces of up to $(10\ nm)^2$ size as determined by STM.

A LEED-IV analysis ($\Delta E = 2118$ eV, $R_p = 0.112$) proves the crystallographic structure to be oxygen terminated w-CoO(0001) ($a = 3.26$ Å, $c = 5.22$ Å) with a strong surface-induced contraction of the outermost oxygen layer distance (see Figs.1a,c). These structural parameters are quantitatively reproduced by DFT in all details. In addition, we ascertain a clear energetic preference for an oxygen termination at the interface to the substrate in the calculations. Therefore, the total film contains slightly more oxygen than the expected 1:1 stoichiometry of the single unit cell.

We also characterize the electronic properties of the w-CoO films by STS and DFT. Thick w-CoO films (15 BL ≈ 4 nm) exhibit a bandgap of 1.8 ± 0.2 eV (see Fig.1e). This result is comparable to the optical bandgap quoted in literature for random nano-crystalline films [4]. With decreasing film thickness the bandgap is found to shrink continuously until it eventually vanishes for a minimal thickness of a double bilayer film (see Figs.1d,e).

Annealing to 600°C in UHV induces a phase transition to closed rocksalt (rs-)CoO(001) films. Experiments with ultrathin films (≤ 4 BL) show that rs-CoO forms with a minimum thickness of three cubic lattice constants (≈ 1.2 nm), which may lead to extremely flat and homogeneous films. The conversion is further found to be sensitive to the initial preparation conditions of the w-CoO(0001) suggesting a relation to the quality of the oxygen terminated substrate interface. The additional oxygen can help to counterbalance oxygen desorption and keep the 1:1 stoichiometry of rs-CoO(001) during annealing.

[1] M. J. Redmen and E. G. Steward, Nature **193**, 867 (1962).
[2] A. S. Risbud et al., Chem. Mater. **17**, 834 (2005).
[3] J. Fester et al., Nat. Commun. **8**, 14169 (2017).
[4] Y. Wang et al., Chem. Commun. **54**, 13949 (2018).
[5] A. G. Roca et al., Small **14**, 1703963 (2018).
[6] J. Alaria et al., J Phys D Appl. Phys. **41**, 135004 (2008).
[7] H. L. Meyerheim et al., PRL **102**, 156102 (2009).
[8] A. S. Walton et al., ACS Nano **9**, 2445 (2015).
[9] J. Fester et al., Top. Catal. **60**, 503 (2017).
[10] M. De Santis et al., PRB **84**, 125430 (2011).

Growth and atomic-scale characterization of ultrathin silica and germania films: The crucial role of the metal support

A. L. Lewandowski, W.-D. Schneider, M. Heyde, and H.-J. Freund

Fritz-Haber-Institut der Max-Planck-Gesellschaft, Faradayweg 4-6, 14195 Berlin, Germany,
(corresponding author W.-D. Schneider, e-mail: wolf-dieter.schneider@epfl.ch)

Recently, we reported on the preparation and atomic-scale characterization of ultrathin films of the glass-forming materials silica and germania [1]. To this end state-of-the-art surface science techniques, in particular scanning probe microscopy, and density functional theory calculations have been employed. The investigated films range from monolayer to bilayer coverage where both, the crystalline and the amorphous films, contain characteristic XO_4 (X=Si,Ge) building blocks. A side-by-side comparison of silica and germania monolayer, zigzag phase and bilayer films supported on Mo(112), Ru(0001), Pt(111), and Au(111) leads to a more general comprehension of the network structure of glass former materials. This allows us to understand the crucial role of the metal support for the pathway from crystalline to amorphous ultrathin film growth.

Here, we address specifically the film-substrate interaction in germania films on a herringbone reconstructed Au(111) surface on which purely amorphous germania bilayer films are grown [2]. The presence of the film affects the native configuration of the Au soliton walls, as observed with scanning tunneling microscopy. They partly avoid the film islands, and partly penetrate under film patches. This behavior indicates a weaker film-substrate interaction than the one reported for other oxide films on reconstructed Au(111) where the reconstruction is lifted [3–6]. Moreover, this new system highlights the impact of the metal support on the structure of ultrathin films of germania: With decreasing film-substrate interaction the amorphous phase is promoted. Density functional theory calculations confirm and rationalize the experimental observations. This work provides a useful generalization of the relationship between film structure and adhesion energy [2].

The preparation procedure of the films follows the steps reported previously for germania films supported on Ru(0001) and Pt(111) [7–9]. The Au(111) single crystal surface is cleaned by several cycles of sputtering and annealing at 820 K for 15 min. The cleaning process stops when a clear herringbone reconstruction is observed with the STM. Next, germanium is evaporated from a graphite crucible using an electron-beam evaporator. The deposition and the subsequent annealing step are carried out in 2×10^{-6} mbar pressure of oxygen. Remarkably, well-defined films are obtained at annealing temperatures (~ 580 K), much lower than the one employed to grow germania films on Ru(0001) and on Pt(111) (~ 820 K) [7–9]. The amount evaporated onto the surface is inferred from previous experiments and based on the STM image features [7–9].

To summarize the results for ultrathin germania films on Au(111), in contrast to earlier observations for oxide films on reconstructed Au(111) [3–6], for germania on Au(111)

several soliton walls penetrate below the germania bilayer film patches. This behavior indicates a weaker film-substrate interaction than the one observed for other oxide films. In other words, the changes in the soliton wall behavior of the Au(111) reconstruction upon film coverage yield a qualitative measure for the interaction strength. For the present ultrathin GeO_2/Au(111) system, the consequence of the observed weak film-substrate interaction is an amorphous germania film growth. Our experiments and the theoretical modeling with DFT calculations highlight quantitatively the impact of the metal support on the oxide film structure concerning strain, adhesion energy, charge transfer, and, most importantly in the present context, crystalline versus amorphous growth.

This project has received funding from the European Research Council (ERC) under the European Unions Horizon 2020 Research and Innovation Program (Grant Agreement No. 669179).

[1] A. L. Lewandowski, S. Tosoni, A. Fuhrich, L. Gura, M. J. Prieto, Z. Yang, D. Usvyat, W.-D. Schneider, T. Schmidt, M. Heyde, G. Pacchioni, and H.-J. Freund, submitted.

[2] A. L. Lewandowski, F. Stavale, S. Tosoni, W.-D. Schneider, M. Heyde, G. Pacchioni, and H.-J. Freund, Phys. Rev. B (R) (2019), in press.

[3] C. Wu, M. S. J. Marshall, and M. R. Castell, J. Phys. Chem. C 115, 8643 (2011).

[4] D. Ragazzon, A. Schaefer, M. H. Farstad, L. E. Walle, P. Palmgren, A. Borg, P. Uvdal, and A. Sandell, Surf. Sci. 617, 211 (2013).

[5] F. Stavale, L. Pascua, N. Nilius, and H.-J. Freund, J. Phys. Chem. C 117, 10552 (2013).

[6] S. Y. Quek, M. M. Biener, J. Biener, C. M. Friend, and E. Kaxiras, Surf. Sci. 577, L71 (2005).

[7] A. L. Lewandowski, P. Schlexer, C. Büchner, E. M. Davis, H. Burrall, K. M. Burson, W.-D. Schneider, M. Heyde, G. Pacchioni, and H.-J. Freund, Phys. Rev. B 97, 115406 (2018).

[8] A. L. Lewandowski, S. Tosoni, L. Gura, P. Schlexer, P. Marschalik, W.-D. Schneider, M. Heyde, G. Pacchioni, and H.-J. Freund, Angew. Chem., Int. Ed. 58, 10903 (2019).

[9] A. L. Lewandowski, P. Schlexer, S. Tosoni, L. Gura, P. Marschalik, C. Büchner, H. Burrall, K. M. Burson, W.-D. Schneider, G. Pacchioni, and M. Heyde, J. Phys. Chem. C 123, 7889 (2019).

Author Index

PFEIFFER VACUUM

VACUUM SOLUTIONS

A one stop source for the highest standard in vacuums

No two vacuum processes are alike since individual requirements are what matters. Together with our customers, we obtain a vacuum solution based on their specific needs. This process includes all steps in creating a perfect vacuum condition. Besides best-in-class products for vacuum generation, measurement and analysis, we also offer accessories, application training programs and worldwide service.

See for yourself what Pfeiffer Vacuum solutions are about at:

www.pfeiffer-vacuum.com

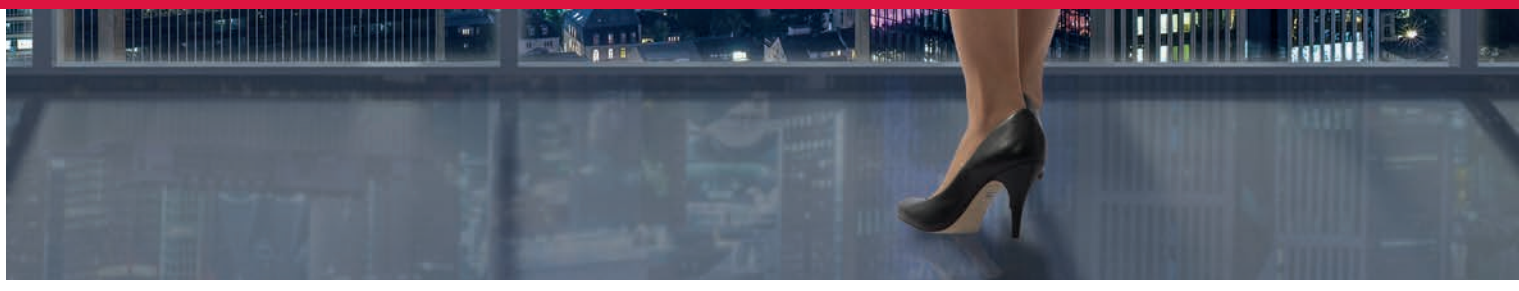

Company Information

Investing in the Success of the Scientist

scientaomicron

Scienta Omicron has acquired the complete SPM and XPS business from Sigma Surface Science.

A new Scienta Omicron business unit has been formed consisting of Scienta Omicron and Sigma Surface Science staff. Sigma has invested significantly into new lines of SPM and XPS products. These, together with the Scienta Omicron products represent a world-class range of UHV surface science instrumentation and will be offered and serviced through the global Scienta Omicron Sales and Services organisation. In the future, our customers can expect new technology breaking barriers within the world of surface science.

For further information on the acquisition please contact:
Henrik Bergersen, COO Scienta Omicron and
Managing Director, Scienta Omicron Technology
Tobias Persson, Vice President Sales & Service, Scienta Omicron

SYMPOSIUM ON SURFACE SCIENCE 2020
St. Christoph am Arlberg, Austria
March 1 - 7, 2020

Friedrich Aumayr und Ulrike Diebold, organizers
Institute of Applied Physics, TU Wien (Vienna University of Technology)

Sunday, 01 Mar. 2020

16:00 - 18:30	REGISTRATION
18:30 - 19:30	DINNER
20:00 - 20:20	OPENING

chair: AUMAYR

20:25 - 20:45	RUPPRECHTER
20:45 - 21:05	HEINRICH
21:05 - 21:25	JELINEK

Monday, 02 Mar. 2020

07:15 - 08:00	BREAKFAST

chair: IBACH

08:00 - 08:20	WÖLL
08:20 - 08:40	RAMESHAN
09:15 - 12:00	SKIING INSTRUCTIONS
12:00 - 13:00	LUNCH
13:30 - 15:30	SKIING INSTRUCTIONS

chair: DIEBOLD

16:40 - 17:00	MORGENSTERN
17:00 - 17:20	LUNDGREN
17:20 - 17:40	SHIPILIN
17:40 - 18:00	EDSTRÖM
18:00 - 18:20	SUCHORSKI
18:30 - 19:30	DINNER

chair: KOCAN

19:30 - 19:50	HAMMER
19:50 - 20:10	LINSMEIER
20:10 - 20:30	ORTEGA
20:30 - 20:50	DIL

Tuesday, 03 Mar. 2020

07:15 - 08:00	BREAKFAST

chair: ECHENIQUE

08:00 - 08:20	SETVIN
08:20 - 08:40	OBERHOFER
09:15 - 12:00	SKIING INSTRUCTIONS
12:00 - 13:00	LUNCH
13:30 - 15:30	SKIING INSTRUCTIONS

chair: MESSING

16:40 - 17:00	ARNAU
17:00 - 17:20	VINOGRADOV
17:20 - 17:40	BRANDIMARTE
17:40 - 18:00	SANCHEZ-PORTAL
18:00 - 18:20	RENAUD
18:30 - 19:30	DINNER

chair: FÖRSTER

19:30 - 19:50	GÖLZHÄUSER
19:50 - 20:10	SCHWESTKA
20:10 - 20:30	LEMELL
20:30 - 20:50	SIKOLA

Wednesday, 04 Mar. 2020

07:15 - 08:00	BREAKFAST

chair: NETZER

08:00 - 08:20	GIESSIBL
08:20 - 08:40	BARTH
09:15 - 12:00	SKIING INSTRUCTIONS
12:00 - 13:00	LUNCH
13:30 - 15:30	SKIING INSTRUCTIONS

chair: BERGHAUS

16:40 - 17:00	MAIER
17:00 - 17:20	STEMPEL

chair: LUNDGREN

17:25 - 18:25	POSTER INTRODUCTION
18:30 - 19:30	DINNER
19:30 - 21:30	POSTERSESSION

Thursday, 05 Mar. 2020

07:15 - 08:00	BREAKFAST

chair: KUNZE-LIEBHÄUSER

08:00 - 08:20	WIDMER
08:20 - 08:40	MAGNUSSEN
09:15 - 12:00	SKIING INSTRUCTIONS
12:00 - 13:00	LUNCH
13:30 - 15:30	SKIING INSTRUCTIONS

chair: RIVA

16:40 - 17:00	STIERLE
17:00 - 17:20	JAKUB
17:20 - 17:40	VONK
17:40 - 18:00	STERRER
18:00 - 18:20	ROCCA
18:30 - 19:30	DINNER

chair: SEITSONEN

19:30 - 19:50	MITTENDORFER
19:50 - 20:10	SILKIN
20:10 - 20:30	EBERHARDT
20:30 - 20:50	NETZER

Friday, 06 Mar. 2020

07:15 - 08:00	BREAKFAST

chair: STARKE

08:00 - 08:20	REUTER
08:20 - 08:40	LIBUDA
09:15 - 12:00	GIANT SLALOM RACE
12:00 - 13:00	LUNCH
13:30 - 15:30	SKIING INSTRUCTIONS

chair: VALTINER

16:30 - 16:50	LINPE
16:50 - 17:10	AUER
17:10 - 17:30	DZIADKOWIEC
17:30 - 17:50	CYGANIK
17:50 - 18:10	BUCK

chair: ROCCA

18:30 - 18:50	AMMON
18:50 - 19:10	SCHNEIDER
19:10 - 19:40	GIANT SLALOM RACE AWARD CEREMONY
20:00	CONFERENCE DINNER